2016

Development of magnetorheological elastomer technologies for protecting structures from seismic events

Jian Yang
University of Wollongong

UNIVERSITY OF WOLLONGONG

Department of Mechanical, Materials & Mechatronic

Development of magnetorheological elastomer technologies for protecting structures from seismic events

Jian Yang

This thesis is presented as part of the requirement for the

Award of the Degree of Doctor of Philosophy

of the Engineering

University of Wollongong

October 2016

ABSTRACT

Protecting civil engineering structures from uncontrollable events such as earthquakes while maintaining their structural integrity and serviceability is very important. Various methods have been developed to either reinforce the protected structures or isolate the seismic motions. Passive aseismic methods and active aseismic methods used to be attractive methods, however, their respective inherent drawbacks limit their wide acceptance. Semi-active methods, which synergize the advantages of both passive and active methods, have been popularly and widely accepted since their emergence. One of the many ways to implement semi-active devices based on magnetorheological elastomers (MREs).

This thesis first provides a literature review on the recent progress of MREs and their applications. The investigations into the mechanical property, the ingredients, the preparation process, the modelling of MREs as well as the internal and external factors that influence their properties have been the research hotspot during the past decades. Then research interests arose in the implementation and development of smart devices using MREs, including MRE isolators, MRE tuned mass damper, and MRE absorbers. For the purpose of protecting buildings from seismic motions, base isolation and tuned mass damper are two major technologies. MRE base isolation aims to decouple the protected structures from the ground motions once earthquakes happen by being installed between them, while MRE tuned mass damper intends to track and identify the vibration frequency so that the vibration energy can be transferred to the tuned mass damper leaving the structures undamaged. In order to lay the groundwork for the new designs of MRE base isolator and MRE tuned mass damper in the following chapters, comprehensive reviews on their development evolutions are also included.

In the following chapters, a modelling study aiming to describe the unique characteristics of MRE isolator is conducted. The resemblance between the predicted and measured response verifies that the newly proposed model is competent to model the MRE seismic isolator. To further improve the base isolator technology so that it can more effectively isolate ground motions, a stiffness softening MRE isolator is designed and presented. An obvious reduction of the effective stiffness and natural frequency of the proposed MRE isolator can be observed when the current is continuously adjusted. This device can also work as a conventional MRE isolator as

its effective stiffness and natural frequency increase when a negative current is applied. To evaluate the capability of dealing with seismic vibrations, this stiffness softening MRE isolator is applied on a scaled three story building. A closed-loop system, including a scaled three story building, four MRE isolator prototypes, and a controller, subjected to the scaled El Centro earthquake record, was built. The simulation and experimental results showed that the stiffness softening MRE isolator controlled by fuzzy logic is effective to suppress any structural vibration.

An attempt is also made to develop a tuned mass damper (TMD) using MREs. This semi-active tuned mass damper incorporates four multi-layered MRE structures. A wide frequency shift range from 3Hz to 7.5Hz proved that this new design is feasible and controllable. In order to verify the capability of the MRE based TMD (MRETMD) of protecting the building from earthquake, extensive simulation work and experimental testing were conducted. Adequate illustrations and analyses have verified that the semi-active MRETMD outperformed all other passive TMDs under either swept sinusoidal or seismic motion.

To further make a TMD more useful in reducing vibrations, an effective way is to increase the number of its natural frequencies so that it can handle with complicated vibrations with multiple frequencies. In this regard, a MRE-based TMD with two natural frequencies is designed, tested, and evaluated. The experimental results demonstrate that the as-designed MRE TMD has two natural frequencies and it can more effectively reduce vibrations.

ACKNOWLEDGEMENTS

First of all, I would like to express my deepest gratitude to my three supervisors: Professor Weihua Li, Professor Haiping Du, and Professor Gursel Alici, for their enthusiastic support, professional direction and constant encouragement that inspired me to get through the tough times and kept my research in the right track. Particular gratitude goes to my principal supervisor, Professor Weihua Li, who acts as not only an excellent academic supervisor but also a wonderful life guider. His inspirational guidance, unselfish help and academic support through these last few years have significantly broaden my horizon and nurtured me to be a young researcher. His spirit of dedication towards his research sets me a role model and his life wisdom as a modest and nice person is also a valuable virtue to learn.

Then I would like to give my deep gratitude to my beloved husband and working partner, Dr Shuaishuai Sun, who fights together with me from the very beginning of my PhD journey. Without his consistent encouragement and company, I would not have been able to persist to the end. It is really appreciated that I have such a wonderful companion in my life and work, who strives for the common dream with me.

I would also like to express my gratitude to my colleagues, Mr Donghong Ning, Mr Xin Tang, Dr Jun Zhang, Dr Gangrou Peng, and my close friends, Miss Dan Yuan and Miss Xinxin Shao. They not only share their practical research experience and instructions with me, but also kindly provided emotional support. Their presence infuses too much joy and laughter to my study and life. It is worth to spend a whole life time to cherish the friendship and emotional bonds built with them. Special thanks also go to the administration staffs of faculty, technicians of Engineering Workshop and ITS, and staffs of SMART building.

It is an honour for me to acknowledge the greatest financial support from the China Scholarship Council (CSC) and IPTA scholarship from University of Wollongong.

Last but not least, I am deeply indebted to my parents. Their unconditional love, support and encouragement always inspired me to pursue my dreams.

TABLE OF CONTENTS

LIST OF FIGURES

LIST OF TABLES

1 INTRODUCTION

1.1 Background and motivation

The aim of this thesis focuses on exploring scientifically innovative and effective ways to protect buildings from devastating seismic events (or earthquakes). According to literature recordings, considerable efforts have been conducted in the last decades to implement and develop structural control devices, especially for the mitigation of seismic responses of buildings. Passive, active, and semi-active strategies are the most common means to protect buildings from seismic events. Passive control strategies, including base isolation systems, viscoelastic dampers, and tuned mass dampers, are well understood and widely accepted by the engineering community as attractive means to help the buildings against the impacts of dynamic loadings from earthquakes. However, these passive devices are unable to adjust their parameters to adapt to loading variations or building changes [1, 2]. For several decades, researchers have endeavoured to figure out the possibility of using active control techniques to improve upon passive approaches to mitigate the effects of damaging earthquakes on buildings [3-9]. Even though they are more complicated, active systems have superior advantages over passive systems in terms of achieving a higher level of performance. Despite of that, more impediments exist to the general acceptance and wide practical applications of active control systems, including: (1) high capital cost and maintenance, (2) large reliance on external power, and (3) potential threat to system reliability and robustness.

In order to address these above challenges, the concept of semi-active is introduced as a technology that fills the gap between the passive system and active system. Semi-active systems have advantage of offering the reliability of passive systems, yet maintaining the versatility and adaptability of fully active systems without requiring high cost and large power consumption. Studies have shown that appropriately implemented semi-active systems perform significantly better than passive devices and have the potential to achieve, or even surpass, the performance of fully active systems. One popular means of achieving semi-active devices is to use controllable smart materials. In recent decades, numerous efforts have been conducted to the possibility of incorporating smart materials into the semi-active devices for vibration reduction. Magnetorheological elastomers (MREs) are one of the most attractive

choice recently. Typical MREs consist of three components named polarized particles, matrix, and additives. These polarized particles are suspended in a non-magnetic solid or gel-like matrix. The most attractive property of MRE is that it can change its elastic modulus or stiffness monotonically as the magnetic field increases [10, 11], and then reclaim its original property immediately when the magnetic field is removed. Therefore, the physical status of MRE can be switched from soft to semi-solid elastomers or reversely with the presence of magnetic field. This enables MRE to overcome such disadvantages as liquid leakage, sedimentation issue, sealing, and environmental contamination and meanwhile empowers MRE the superiorities to be a favorable candidate for vibration control applications.

Generally, the most common semi-active devices using MRE as controllable stiffness component for vibration reduction include absorbers and isolators, in particular, base isolators are usually implemented for aseismic applications. Base isolations are one of the most adopted and effective means of mitigating unwanted and harmful vibrations to protect buildings, bridges, and other key civil infrastructure from seismic events[12-14]. They isolate vibration sources by being installed between ground and superstructures. However, because it is inherently passive, traditional base isolations cannot adapt to changes in the environment or source vibrations, which, as a consequence, compromises their efficiency and robustness and in some cases, cause adverse effects [15].

In an attempt to address the challenges faced by the current base isolation design/practice, Behrooz *et al*. incorporated a MRE into a base isolator and then succeeded in protecting a scaled three storied building from seismic motions using a Lyapunov algorithm [16, 17]. The unique property of MRE brings new possibilities to implement adaptive base isolators with real-time controllability that could overcome the shortcomings inherent in traditional base isolation systems. Inspired by the commercialised traditional base isolator utilising natural rubber, Li *et al.* developed a large capacity adaptive base isolator [18, 19] which is the first adaptive base isolator utilising stiffness hardening MRE. The results obtained from testing the characteristics of this MRE adaptive base isolator showed it can increase lateral stiffness by up to 18 times [19]. However, the principle of an effective base isolation relies on decoupling a structure from its source of vibration by softening (decreasing the lateral stiffness of) the isolators. Although hardening the isolator makes it possible to shift the entire structural frequencies away from the resonant frequencies

of the sources of vibration, this is not as effective as decoupling the structure from the source of vibration. Fortunately, Yang *et al*. have found a solution to this problem; they developed a stiffness softening MRE base isolator by adopting two permanent magnets [20, 21] that can energise the MRE continuously without consuming power, while the solenoids produces an electromagnetic field that is opposed to the permanent magnetic field, so the lateral stiffness of the MRE isolator can be lowered. In order to further evaluate its ability to protect structures from seismic motions, this newly developed MRE isolator was used to isolate a scaled three story building from earthquake motions [22].The simulation and experimental results showed that the stiffness softening MRE isolator controlled by fuzzy logic proved to suppress any structural vibration. Upon the successful development of MRE isolators, one key challenge inserted in MRE isolation technology is its complicated nonlinearity. This issue has produced impedance to its access to controllability, which limits its practical applicability seriously. To this end, an appropriate phenomenological model which can accurately describe its nonlinear property is needed.

Tuned mass damper (TMD) using multilayered MRE as stiffness component is a new attempt in this thesis. This inspiration is from the powerful capability and wide acceptance of MRE as a stiffness-adjustable material as well as the existed challenges of the current TMD designs that controllable TMDs are in urgent need. TMDs protect the primary structure from undesired vibration through the absorption and dissipation of energy by matching their natural frequency to the vibration frequency. However, the inherent passive nature causes a series of problems such as a narrow band of effective frequency, ineffective reduction of frequency changing vibration, and detuning, and these factors limit their effectiveness [23]. For the purpose of overcoming the passivity, many active TMD designs have been developed [24, 25], but the high power consumption, high cost and difficulty of maintenance of active TMDs limit their practical usage despite of their better vibration suppression response [26, 27]. In order to overcome these drawbacks but still keep the benefits of both the active TMD and the passive TMD, semi-active technology has emerged. For example, shape memory alloys, piezo stacks, and piezo-electrics were used to implement semi-active TMDs.

1.2 Objectives

The ultimate goal of this thesis is to explore aseismic technologies for buildings using MREs technology. Specifically, this thesis, on one hand, is oriented to solve some problems existed in current aseismic technology, while at the same time, aims to develop new designs and makes some certain creative ideas into practice. The content of this thesis involves two major aseismic technologies: base isolation and tuned mass damper (TMD). For each of them, creative innovation and reasonable improvements are included in terms of modelling, structural design, material choice, and magnetic circuit design.

Modelling is always an essential step between the practical device prototype and control theory, especially for an MRE isolator with complicated nonlinear characteristics. Without an accurate model, the device would not have access to advanced control algorithms, which significantly reduces its practical applicability. For the current base isolation practice, MRE has been adopted into the implementation of stiffness hardening isolator, which is already a great improvement upon the traditional base isolation technology. However, the principle of an effective base isolation relies on decoupling a structure from its source of vibration by softening (decreasing the lateral stiffness of) the isolators. Therefore, exploring innovative approaches to achieve stiffness softening isolators is a significant task to be achieved.

As for the TMD technology, its working mechanism aims to shift the natural frequency of the protected building away from the earthquake frequencies. With more natural frequencies, the TMD will be more effective on dealing with vibrations with multiple frequencies. In this regard, the key challenge is to figure out a kind of material that is capable of adjusting the natural frequency of TMD. Additionally, the corresponding structural design and the magnetic circuit design occur to be new challenges as well. This thesis aims to find solutions to solve the above issues or at least bring out creative and original ideas to update and improve the current aseismic technology.

1.3 Thesis outline

The outline of this thesis is shown in Figure 1.1.

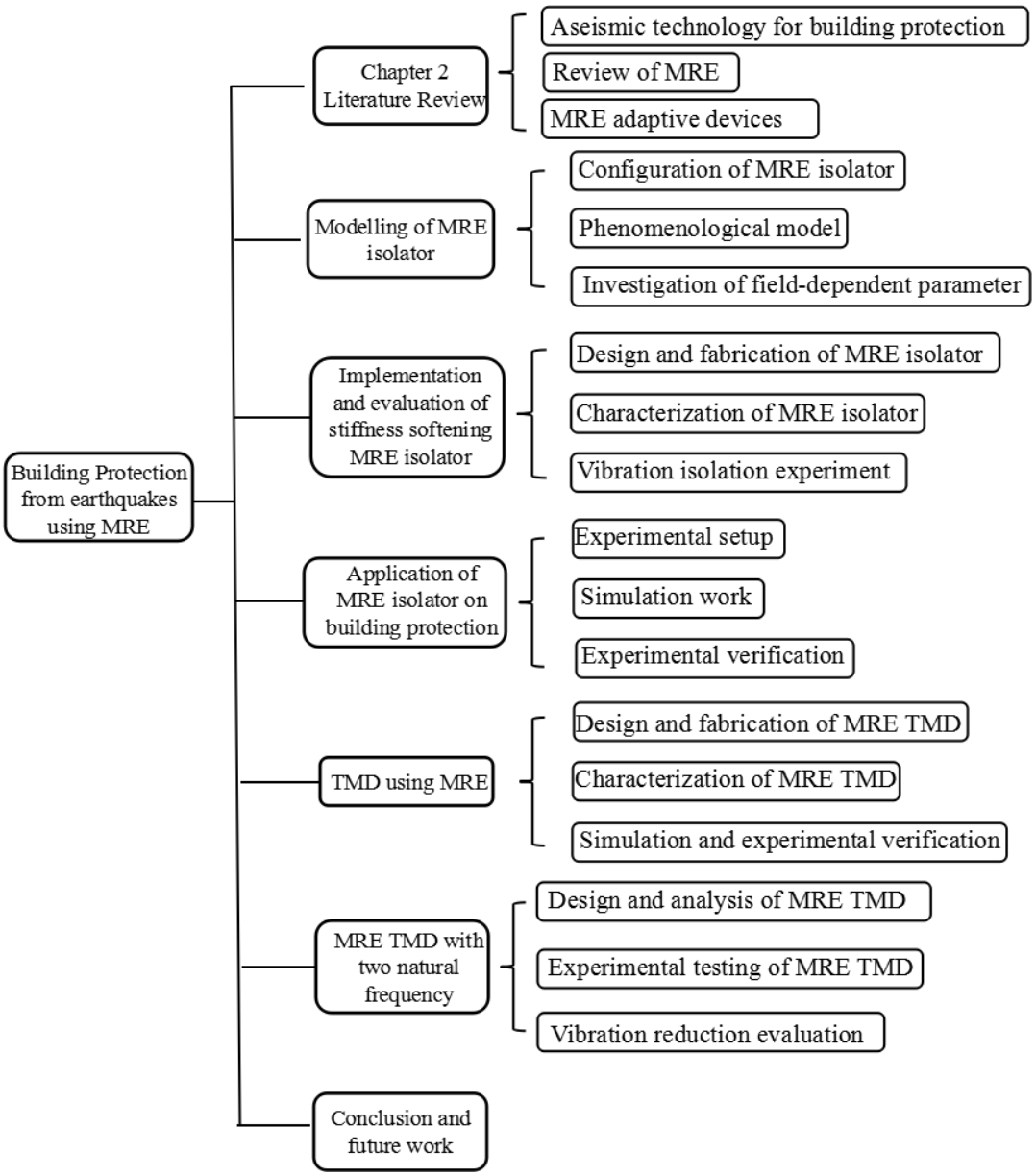

Figure 1.1 Thesis outline

Chapter 2 starts with a review on aseismic technology which can be catagorized into three groups: passive control systems, active control systems, and semi-active control systems, with extra attention to the semi-active aseismic technology using MREs. Research activities on studying the mechanical properties and engineering applications of MREs have achieved fruitful results, though, the potentials of MREs still need to be further explored and their applications need expanding. Challenges faced with MRE in terms of expanding its application range need to be overcome so that applications of MRE will not mainly limit to vibration reduction and isolation. Opportunities emerge along with challenges as research on MRE technology has

advanced, resolving these challenges will lead to improvement and new developments in the field.

In Chapter 3, a phenomenological model was proposed to reproduce the dynamics of the MRE isolator [21]. Based on the experimentally obtained relationships between force and amplitude or velocity, a Bouc-Wen component and a Viogt element were used to produce hysteresis loops and describe solid-material behaviors, respectively. Then a parameter was used to balance the proportion of linearity and nonlinearity. Extensive simulations including restoring force tracking, force-amplitude relationship fitting, and parameter dependence investigation were conducted and verified that this model is effective on portraying the MRE isolator behaviors.

In Chapter 4, a base isolation design with a hybrid magnetic system, which achieves the property of softening stiffness, was proposed. The advantage of this seismic isolator is that an obvious reduction on its effective stiffness can be achieved when the applied current was increasingly adjusted. On the other hand, this device could also work as a stiffness hardening MRE isolator as its effective stiffness and natural frequency also increased when an opposite current was applied. Further testing was carried out on a 1-degree-of-freedom system to assess how effectively this device isolated vibration. In this experiment, two cases were considered, and in each case vibration of the primary system was obviously attenuated under ON-OFF control logic, thus demonstrating the feasibility of this novel design as an alternative adaptive vibration isolator.

In Chapter 5, this paper describes the performance of a stiffness softening MRE isolator in a scaled three story building. In order to construct a closed-loop system, a scaled three story building was designed and built according to the scaling laws, and then four MRE isolator prototypes were fabricated and utilised to isolate the building from the motion induced by a scaled El Centro earthquake. Fuzzy logic was used to output the current signals to the isolators, based on the real-time responses of the building floors, and then a simulation was used to evaluate the feasibility of this closed loop control system before carrying out an experimental test. The simulation and experimental results showed that the stiffness softening MRE isolator controlled by fuzzy logic proved to suppress any structural vibration.

In Chapter 6, a semi-active MRE TMD is another highlight in this thesis. The creativity of this TMD is not only the incorporation of four multi-layered MRE structures but also the design of these four structures in a square layout. This design

obviously increases the TMD stability, yet more importantly eliminates the magnetic flux leakage because of the formed four closed magnetic circuit. A wide frequency shift range from 3Hz to 7.5Hz proved that this new design is feasible and controllable. In order to verify the capability of this MRE TMD of protecting a three story building from earthquake, the swept sinusoidal signal and the scaled 1940 El Centro earthquake record were used as ground motions. Both simulation and experiment verified that the semi-active MRETMD outperformed all other passive TMDs under either swept sinusoidal or seismic moves.

Chapter 7 presents a new design of MRE-based TMD with two natural frequencies by attaching an eccentric mass on the multilayered MRE structure. The experimental testing results have verified that the designed MRE TMD has two natural frequencies from two vibration modes: one in the torsional direction and the other in translational direction. With the two natural frequencies, the designed MRE TMD is more effective on reducing vibrations, which has been verified by experiments.

Chapter 8 finishes with conclusions on this thesis, and summaries the major findings and contributions of my PhD research, as well as pointing out the potential possibilities and future direction of this area.

2 LITERATURE REVIEW

2.1 Structural control

Because of the potential benefits either in minimizing catastrophic failure or in increasing structural safety, intensive research efforts have been made for the development and exploration of aseismic technology to civil engineering structures [6, 27-42]. It has been a truth that buildings at present are much taller and more flexible than ever before, for those modern buildings to function safely under hostile environments, e.g., strong earthquakes or wind loads, appropriate control systems may conceivably become an integral part of the building. The goal of the involvement of structural control is to increase the survivability of the building in the presence of extraordinary excitations from winds and earthquakes. Additionally, structural control can be an important part of designing new structures and retrofitting existing structures for earthquakes. Therefore, it seems necessary to promote the structural control research and applications. The control methods of structural vibrations induced by earthquake or wind can be various such as modifying stiffness, masses, damping, or shape. It has been documented that even though some methods of structural control have been used in practice successfully, the newly proposed approaches are still expanding and developing for the purpose of extending applications and improving efficiency.

Since the initial concept of structural control by Yao in 1972 [43], the field has continued to grow. Over the past few decades, the evolution of structural control has been rapid, attracting the interest and attention of scores of researchers. As a result, a wide variety of control methods has sprung up. The control methods for mitigating structural vibrations are generally categorized into three types: passive control system, active control system, and semi-active control system. Passive control systems are such systems that do not require an external power source while can impart forces that are developed in response to the motion of the structure; however, they cannot increase the energy in a passively controlled structural system including the passive devices themselves. On the contrary, active control systems are those in which external sources are needed to power control actuators that apply forces to the structure in a specified manner. Those forces can be used to either add or dissipate energy in the structure. In an active feedback control system, the signals sent to the

control actuators are dependent on the immediate responses of the system measured with physical sensors. With respect to semi-active control systems, on one hand, they can be called a class of active control systems with exception that the external energy requirements are orders of magnitude smaller than typical active control systems, and that typical semi-active devices do not add mechanical energy to the structural systems, which guarantees the bounded-input bounded-output stability [6]. On the other hand, semi-active control devices can be viewed as controllable passive devices for the reason that they can work normally as passive devices when the power is unavailable.

2.1.1 Passive control systems

Passive control systems are well understood and widely accepted by structural engineering community because of advantages in terms of high reliability, low cost, easy maintenance, etc. Unfortunately, all these advantages cannot neutralize their inherent passive nature: passive control systems cannot adapt to changes in the environment or source vibrations, which as a consequence compromises their efficiency and robustness and in some cases, cause adverse effects. For example, passively isolated structures in one region of Los Angeles that survived the 1994 Northridge earthquake [1], may well have been damaged severely if they were located elsewhere in the region [2]. Even though passive control systems may give way to more advanced control systems, it cannot be denied that they had undergone years of improvement and evolution before they became popular research topics. From the very first, passive energy dissipation systems were widely used for natural hazard mitigation [44, 45], such as metallic yield dampers [46-49], friction dampers[50-54], viscoelastic dampers[48, 55, 56], passive tuned mass dampers [57-62], passive tuned liquid dampers [63-65], etc. They are generally characterized by a capacity to enhance energy dissipation in the structural systems, the larger the energy dissipation capacity the smaller the amplitude of vibration. Even though all these passive methods of dissipating energy are very effective in reducing the amplitudes of vibration, no one particular damper is best for all design circumstances, and the biggest limitation is the lack of adaptability. In this regard, adaptable and controllable devices which are likely to find application in civil engineering structures should be explored and proposed. Anyway, the design and utilization of

this entire technology of passive dissipating system is a positive step forward in promoting the development of advanced control systems.

2.1.2 Active control systems

Active vibration control is the active application of force in an equal and opposite fashion to the forces imposed by external vibration. Attracted by its powerful capability to achieve vibration-free, researchers from all over the world have undertaken considerable efforts to develop the active structural control into a workable technology. However, it is noticeable that it really is a challenge to carry on experimental confirmation of the feasibility and implementability of active control devices in practice [42]. A collaborative experimental study [66] for the active control of model buildings subjected to earthquake excitations reported that the analytical results of active control laws available in the literature are quite limited for seismic applications. The first full-scale application of active control to a building was accomplished by the Kajima Corporation in 1989 [67]. From then on, a large body of literature related to the development of feasible active control algorithms emerged in large numbers. Despite the intensive research efforts made for the possible application of active control systems to civil engineering structures, the practical applicability of active control systems is significantly limited due to its inherent drawbacks in terms of high power and cost requirements.

2.1.3 Semi-active control systems

The attention semi-active devices received in recent years can be attributed to their advantages of offering the versatility of fully active control and reliability of passive control. They are both cost and energy efficient compared to the active dampers whilst providing the comparable performance. As a matter of fact, battery power is enough to start up many semi-active devices, which is a critical benefit because the main power source to the structure may fail during seismic events. A more convincing truth is that semi-active control systems based on semi-active devices combine the best features of both passive and active control systems and consequently they can offer the greatest likelihood to be accepted as a viable means of protecting civil engineering structures against earthquake and wind loading. It has been acknowledged that appropriately implemented semi-active control systems can perform significantly better than passive systems and has the potential to outperform

the fully active control systems [68-70]. Such devices include variable-orifice fluid dampers, variable-stiffness devices, controllable friction devices, smart tuned mass dampers and tuned liquid dampers, controllable fluid dampers, and controllable impact dampers.

Over the past decades, the development of smart materials brought new possibilities for the semi-active devices to evolve significantly and expand their applications. The media commonly used to implement semi-active devices can be field dependent fluids, such as the electrorheological fluids (ERF) and the magnetorheological fluids (MRF), which will undergo obvious changes in their rheological properties in response to the variations of the electric and magnetic and all of the alterations is completely reversible [71, 72]. Many applications use their varying viscosity in either damping or torque transfer scenarios [73, 74]. ERF damper and MRF damper, for example, change their damping and force characteristics under the action of electric and magnetic fields, respectively. In addition to those above mentioned field dependent fluids, there are some other smart materials which are semi-solid. Such material refers to magnetorheological elastomers (MREs). MRE and MRF constitute the key members of MR family. Their common feature is that both of their mechanical property is magnetic field dependent, while their mechanisms are significantly different. MRF aims to damp vibrations by dissipating vibration energy and MRE works on reducing the transmissibility via changing its stiffness at the present of magnetic field.

2.2 MRE materials

2.2.1 MR effect

The MR effect was firstly discovered by Rabinow in 1940s [75, 76] by operating on the magnetic fluid clutch. The clutch was composed of two parallel plates with finely divided iron filled in the space between those two parallel surfaces. The magnetic fluid clutch works on the basic principle that the magnetized iron binds the plates together against movement parallel to their surfaces with the establishment of a magnetic field between the two plates. The finely divided iron was mixed with a kind of liquid such as oil to prevent packing and to afford smoother operation of the clutch. An attractive feature happened to the mixture when it was acted on by a magnetic field that the mixture seemingly “solidifies”, where the MR effect was the most

initially demonstrated and the mixture was the archetype of what is now called magnetorheological fluids (MRFs). Since then, from the first moment the MR effect was discovered, its advantages had been obvious and recognized: (1) the clutch is easy to control and requires very small amount of electrical power; (2) the new clutch exhibits the square law to a markedly less degree or even the torque-versus-current curve is almost a straight line below saturation; (3) no discontinuities in torque exist at the instant of initiation of slip for the reason that the value of static friction does not differ measurably from kinetic friction. Figure 2.1 shows the first demonstration of MR effect.

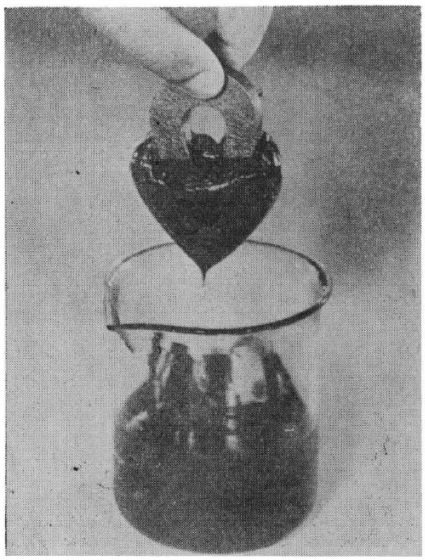

Figure 2.1 First demonstration of MR effect [76]

It was almost 40 years since the discovery of MR effect that Rigbi and Jilken [77, 78] reported their pioneering work on the magnetically sensitive elastomer. The first attempt to use the elastomer filled with soft ferrites was to use these in the design of certain medical and measuring appliances by Rigbi [77]. Then the attractive experimental findings drew the attention of hese two scientists. Then a decade later, Jolly et. al. conducted the first comprehensive investigation on MRE [78]. Their experimental data showed that a 30-40% change in modulus of the materials tested was observed as a response to the applied magnetic field for a composite containing 30% (volume%) iron particles. The original comment about MRE from the authors is "such elastomer composites hold promise in enabling variable stiffness devices and adaptive structures". Since then, MRE have been increasingly popular in engineering and become a well research topic.

2.2.2 MRE materials components

As a polymer composite, MRE typically consists of three basic components: polarized magnetic particles, an elastomer/rubber matrix, and additives [79, 80]. All these components are mixed thoroughly to form a compound and they have either zero or limited mutual solubility or compatibility, even if they can be totally distributed in each other. The polarized particles can be homogeneously dispersed inside the elastomer or gel or they can be grouped to form chain structures. It is the scattered manner of the polarizable particles that determines the mechanical property of MRE. External magnetic acts as a trigger to the change of magnetic interaction between the polarized particles and thus the field-dependent shear modulus of MRE can be observed. Figure 2.2 presents the typical MRE.

Figure 2.2 Typical MR elastomer

(A) Polarizable particles

The polarizable or magnetizable particles are typically dispersed in a non-magnetic solid or gel-like medium. Before choosing the favourable particles, their size, geometry, particle wetting, distribution must be taken into serious consideration. For example, particle size can range from several micrometers to hundreds of micrometers, which has a significant impact on the functionality of the material. Structure reinforcement can be easily obtained with sizes smaller than 100 nm. In addition, factors of magnetic permeability, levels of remnant magnetization and saturation magnetization are also key features to determine the mechanical behaviour of the composite [78]. It is easy to understand that particles with high magnetic permeability are recommended because magnetic interaction between those particles

can readily take place and thus maximum MR effect can be induced [81]. A low remnant magnetization is preferred because particles can separate from each other more easily after the magnetic field is turned off, which therefore makes reversible MR effect possible [82]. The most commonly used polarized particles are spherical carbonyl iron. The reasons of choosing it are that the general size of each particle is a few microns, and that iron has high permeability, low remnant magnetisation and high saturation magnetisation.

(B) Matrix

The existence of matrix material or host material in MRE overcomes some disadvantages, such as liquid leakage, container corrosion problem, particle aggregation, etc. Despite that difference matrix materials will not affect the rheological property of a MRE significantly; appropriate selection of host material can become a crucial factor in certain applications especially when it comes to the long term stability of MRE [83]. Therefore, the selection of host materials is adjusted according to need though the most commonly chosen matrix material is natural rubber [84-88] or silicon rubber [87-92].

(C) Additives

The functionality of additives is mainly to adjust the mechanism properties of MREs. Generally, silicone oil is chosen as the additives for MRE fabrication. In addition, the additives can also average the distribution of internal stress in the materials, which makes them crucial components for fabricating MRE [93]. Some other additives are also favourable for some specific applications. For instance, MREs become electro-conduction by choosing the graphite microparticles as the additives [94]; and by introducing carbon black into the matrix, the mechanical behaviour of MRE is improved and the damping ratio is reduced [95].

2.2.3 Fabrication of MRE

MRE can be categorized into two groups: isotropic MRE and anisotropic MRE, due to different ways of curing. The difference between the fabrication procedures of isotropic and anisotropic MRE lies in that if the mixture is cured under a magnetic field. As the name implies, isotropic MRE means having identical values of a property in all directions. This is because the particles of isotropic MRE are

homogeneously distributed inside the matrix. As opposed to isotropic MRE, anisotropic MRE has directionally dependent property because of the regular particle chains formed at the presence of a magnetic field. Figure 2.3 shows the phenomenon of magnetic particle displacements under the action of a magnetic field in a thin film of composite with the use of metallographic optical microscope as well as optical microscopy [96]. It is seen in Figure 2.3 (a, c) that the particles in anisotropic form chained structures under the influence of the magnetic field; while in Figure 2.3 (b, d) the particles are distributed randomly in the absence of the field. It should be noted that the particle displacement is completely reversible, i.e. the particles in Figure 2.3 (a) will return to their initial positions when the magnetic field is turned off. Figure 2.4 shows the major steps of fabrication of these two MREs [82, 94, 97-102].

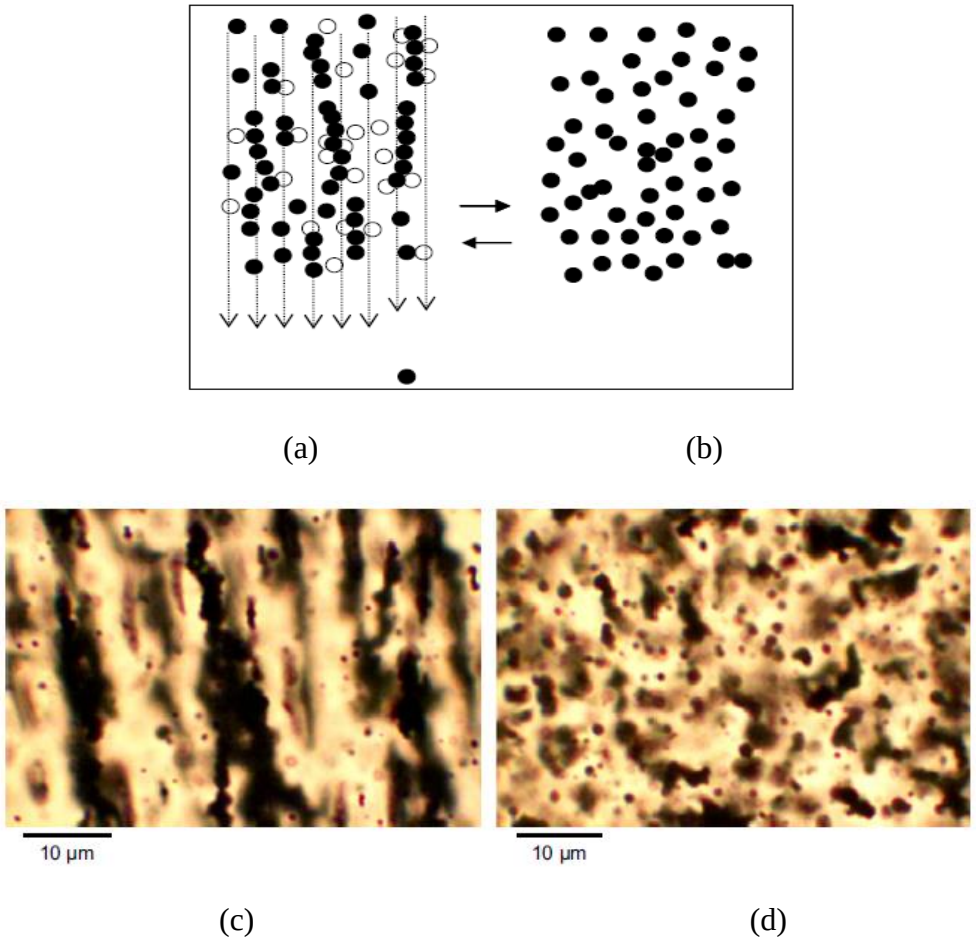

(a) (b)

(c) (d)

Figure 2.3 Phenomenon of magnetic particle displacements under the action of a magnetic field in a thin film of composite with the use of metallographic optical microscope as well as optical microscopy: (a) chained structure under magnetic field; (b) randomly dipersed particles without magnetic field; (c) aligned particles with magnetic field; (d) randomly distributed particles without magnetic field [96]

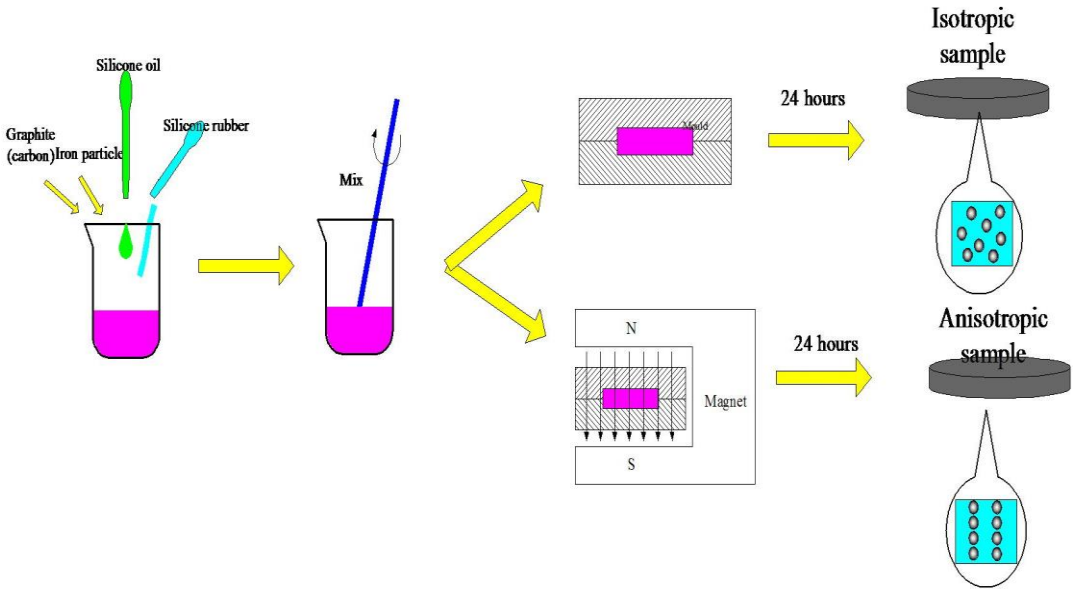

Figure 2.4 Fabrication of conventional anisotropic and isotropic MRE

The general procedure for fabricating an MR elastomer includes material preparation, mixing, curing, and polymerization. Normally, three basic ingredients are silicon rubber, silicon oil, and iron particles. After all ingredients are thoroughly mixed at room temperature into a homogenous mixture, a special treatment is needed before the mixture is cured, i.e. air bubbles or moisture inside of the mixture have to be removed in a vacuum chamber [81, 103] or by heat treatment [104]. The purpose of such treatment is to enhance the compatibility and permeability as well as uniformity of MRE material. Then it's the curing process where the fabrication of isotropic MRE and anisotropic MRE gets to be different. The isotropic MRE is cured at room temperature for 24 hours without the presence of a magnetic field, while the anisotropic MR elastomer is cured with the action of a strong magnetic field, usually above 0.8T [104-106], to form chained structures of magnetic particles in the matrix along the direction of the magnetic field. It should be noted that for some matrixes, a constant temperature (usually above 120℃) is required to maintain the flexibility of the magnetic particle for both isotropic and anisotropic materials [104, 105] during curing. After curing, the magnetic particles are locked in the matrix instead of moving around freely [107]. Following the curing process, a further chemical process called polymerization [81] or vulcanization [104] is conducted to modify the polymer by forming cross-links between the individual polymer chains, thus creating a more durable and stable material. This process will make the material less sticky and give

it a superior mechanical property for engineering applications. It has been documented that the anisotropic MREs have a larger MR effect than that of isotropic MREs [108]. Gong *et al*. have did research on the determining factor in the formation of ordered microstructures in anisotropic MREs and the relation between their microstructures and viscoelastic properties. The results show that the field-dependence of MREs' viscoelastic properties increases with the applied magnetic flux densities. MREs prepared under high magnetic fields have a large field-induced shear modulus and high MR effect [109].

2.2.4 Mechanical property of MRE

MRE materials generally operate at the pre-yield region and behave the same as material with viscoelastic properties [78, 80, 108, 109]. Its smart property of controllable stiffness has attracted considerable research studies [110-114]. Yet, it is stated in some studies that the damping property of MRE is also dependent on the applied magnetic field; other studies concluded that the changes induced by the magnetic field to the damping parameter of MRE can be neglected [19, 79, 82, 84, 108, 115-117]. As such, the MR effect of MRE is normally evaluated by the ratio of modulus increase ΔG at the measured magnetic field to the initial storage modulus G_0 at the zero magnetic field. The first investigation to this type of material was started by Jolly *et al* [78]. They provided the field-dependent property of the MRE by building double-lap shear specimens and then shearing the outer and inner board under different frequencies. Subsequently, Ginder et. al. [82, 115] also studied the field-dependent mechanical property of MRE by using column-like shear equipment. In their pilot work in [87], Ginder et. al. found a substantial MR effect over the entire frequency range (not just within 1 to 20 Hz). The increase in the shear modulus changed initially with the strength of the magnetic field but saturated at higher strength fields. Figure 2.5 shows the stress-strain relationships of the MRE sample at a constant strain amplitude of 10% but at various magnetic fields from 0 to 440 mT [118]. It can be seen that all stress-strain relationships form nice elliptical shapes, the areas of which increase steadily with the increment of the magnetic fields. The slope of the main axis of the elliptical loops varies with the magnetic field, which means that the modulus of MREs varies with the magnetic field. Therefore, MREs exhibit variable stiffness and damping properties. Along with this finding, the potential of MRE to implement tuned vibration absorbers was validated. Motivated by this, a

series of research in terms of MRE modelling [80, 105, 110, 119-125], materials development and property testing [71, 93, 96, 103, 109, 114, 118, 126-144], new device design and characterization [18, 145-162] and performance evaluation has been conducted. The wide recognition and acceptance of MRE is largely attributed to its field dependence on changing modulus. Zhou et. al. [115] stated that the changes of dynamic storage modulus can be over 50%, while Gong et. al. [163] concluded that it can be over 100%. Additional advantages brought by the unique properties include fast response time, high stability, compatibility to mechanical components and reasonably low power requirement. In particular, a wide range of adjustable moduli provides a more effective manner for vibration mitigation [19]. Such superiorities have progressed the applications of MRE to wider prospects including aeronautic engineering, mechanical engineering, automobile engineering and civil engineering. Implementation of controllable devices based on MRE has been reported for vibration absorbers [146-149, 151-155, 164], vibration isolators [104, 165-167], adaptive base isolators [16, 18, 19, 161], a vibration mount [159] and a sandwich beam [168-179].

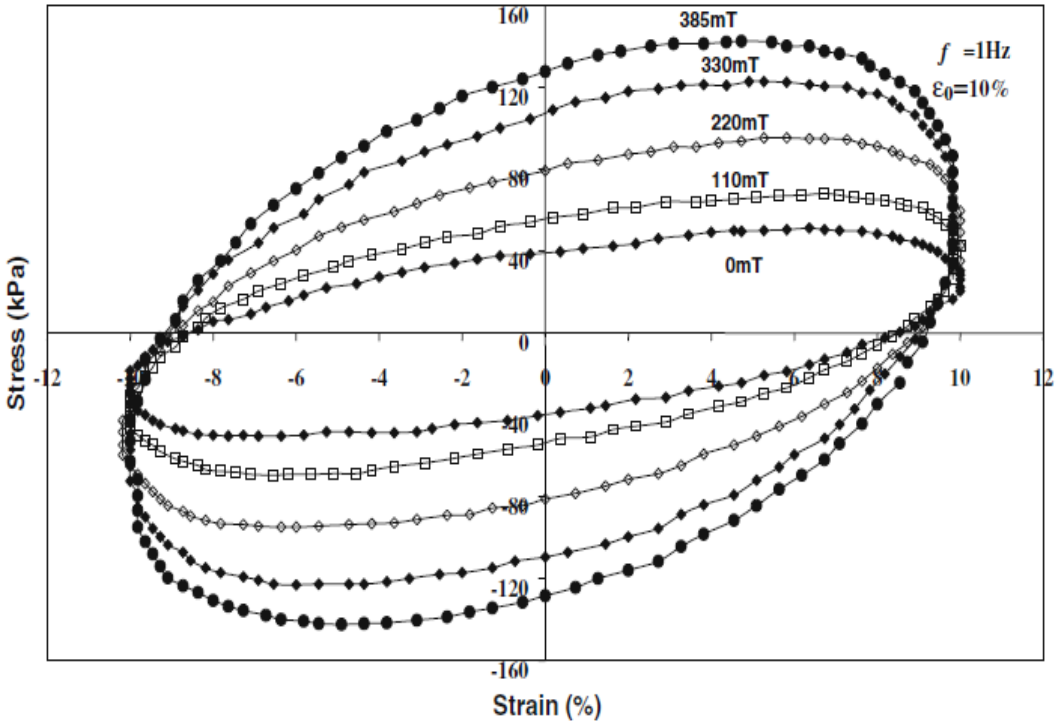

Figure 2.5 Stress-strain relationships with various magnetic fields at a constant strain amplitude of 10% [118]

The factors influencing the mechanical properties of MRE are various. Apart from the influence of the inherent components, i.e. the filler particles, the additives, and the matrix materials [82, 111], external loading conditions should also be taken into account. The study by Lokander et. al. [111] showed that the MR effect of MRE worked as a function of the amplitude of strain with special emphasis on that the MR effect decreases rapidly with increasing strain within the measured range, while the MR effect is not relevant to the loading frequency. The MR effect of MRE is sourced from the field dependence of the polarized particles, i.e. the magnetic interaction forces between these particles. To be precise, it is said that the behaviour of MRE is a combination of the properties of the matrix and the internal magnetic network of the polarized particles. Therefore, it is believed that the application of magnetic field is another indispensable condition to the appearance of MR effect of MRE. When it comes to the influence of the matrix material, the permeability of matrix material should be considered. According to the literature, the addition of magnetically active material in the matrix will decrease the MR effect of MRE [82, 180]. Additionally, experimental results by Lokander et. al. [111] showed that the filler particles with appropriate shape and size contribute significantly to enhancing the MR effect of MRE. They found that the MR effect was more obvious for materials with ASC300 iron (particle size<60um) than for materials with carbonyl iron (particle size 3.9-5.0um). For particles larger than 60um, the MR effect tended to be slightly poorer. On the other hand, Demchuk and Kuzmin [128] found that with the presence of a magnetic field the modulus for MRE with smaller particles was smaller than for larger particles, while the situation reversed when the magnetic field was removed. This is because the increased modulus difference of the MRE with larger particles exceeded that of MRE with fine particles. According to Lokander et. al. [82], the particle concentration actually plays an important role in demonstrating the MR effect. As the benchmark, the term of critical particle concentration should be defined as that at which the particles are in touch with each other and the voids between them are completely filled with the elastomer. For particle concentrations larger than critical particle concentration, the MR effect of MRE will be weak because of the limited room for elastomer to fill all the voids between the particles. Another reason is that larger particle concentration increases the initial stiffness of MRE substantially, therefore, the increase of stiffness will be largely limited.

2.2.5 Modelling studies of MRE

Considerable ongoing research activities are mostly focused on the mechanical properties and engineering applications of MREs. As a matter of fact, modelling the complicated nonlinear behaviors of MRE is an essential step toward the deep understanding of its nonlinear viscoelastic characteristics and engineering applications. According to the literature, a limited work on the modelling MRE can be referenced [181-183].

A point-dipole model was proposed by Jolly *et al* in [79], where the MR effect was studied as a function of particle magnetization. The dipolar model is augmented with a proposed mechanism of how magnetic flux density distributes itself with the particle network. The schematic is shown in Figure 2.6. It is assumed that the uniform saturation occurs in each particle in region (s). Furthermore, distance s decreases from r to zero as average composite flux density increases from zero to some large level.

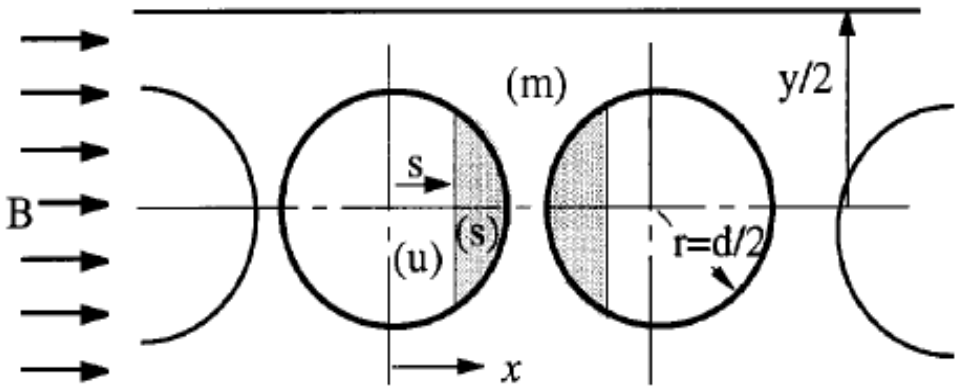

Figure 2.6 particle saturation model [79]

The viscoelastic behaviour of a rubber material is normally described using a three-parameter model which is a combination of a stiffness element and a classical Kevin model. The Kevin model is a stiffness element and a damping element in parallel and its efficiency can be improved by adding the stiffness element. Building on this model, Li et. at. [118] developed a four-parameter model, as is shown in Figure 2.7. This four-parameter model is designed by adding a stiffness element parallel to the classical three-parameter model and its efficiency in describing the behaviour of MRE is proven. A dynamic model which is a combination of

Ramberg-Osgood model and a Maxwell model was proposed by Eem et. al. [142]. The Ramberg–Osgood model is used to describe the nonlinearity of the material, while the Maxwell model is used to introduce a viscoelastic element into the model. The fitting results also show good agreement with the experimental data. Chen and Jerrams [137] proposed a rheology model that takes the viscoelasticity of the polymer composite, the magnetic field-induced properties and the interfacial slippage into consideration, see Figure 2.8. A standard linear solid model which contains two spring elements and a damping element was used to describe the viscoelasticity, a variable stiffness spring was chosen to model the field-dependent stiffness property, and a spring-Coulomb was used to model the interfacial slippage between the matrix and particles.

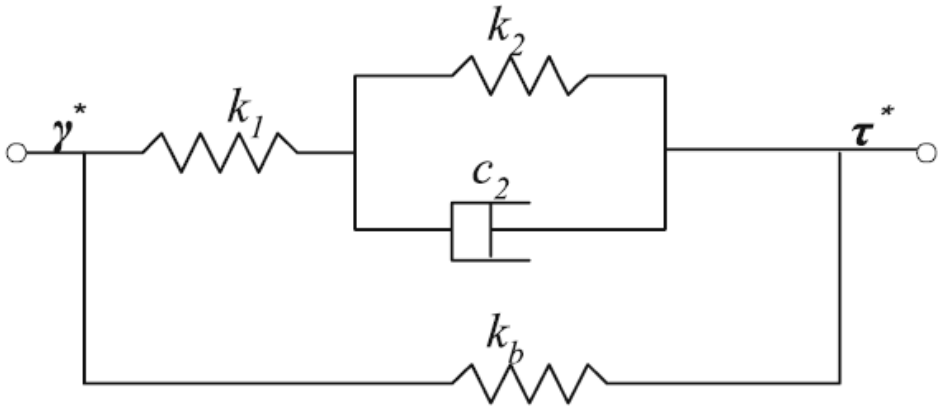

Figure 2.7 Four-parameter viscoelastic model proposed by Li *et al* [118]

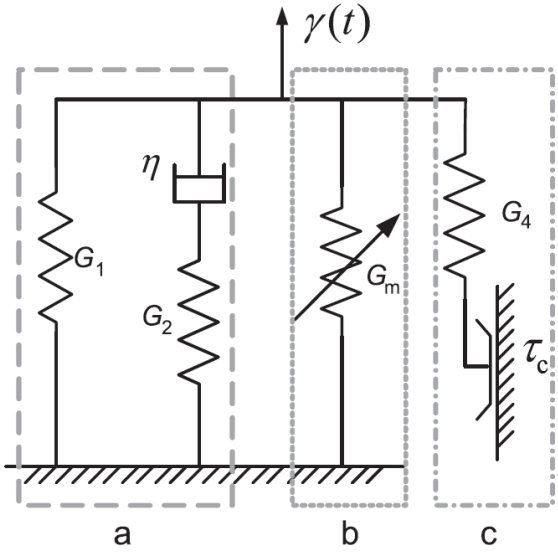

Figure 2.8 A rheological model proposed by Chen and Jerrams [137]

2.3 MRE Adaptive Devices

Elastomers with field responsive rheology hold promise in enabling simple variable stiffness devices. Among these are adaptive tuned vibration absorbers (TVAs) [23, 184], stiffness tunable mounts and suspensions [185], and variable impedance surfaces.

2.3.1 MRE working modes

The possession of variable stiffness and damping when subjected to a magnetic field makes MRE a natural candidate to be developed into smart devices such as vibration absorbers, vibration isolators, base isolators and sandwich beams. An important prerequisite toward the design of MRE devices is to well understand the working modes of MRE materials. For the reason that iron particles in MRE are locked within the matrix material and the external excitations can only lead to local movement around the original locations, the direction of the formed chain structures under a magnet field does not align with the direction of magnetic field. Operation modes for MRE are basically two types: shear mode and squeeze mode, as shown in Figure 2.9. Those operation modes are applicable for either isotropic MRE or anisotropic MRE. Devices using shear mode MRE include vibration absorbers [146-154], vibration isolators [104, 155, 167, 186], and base isolators [19, 20].

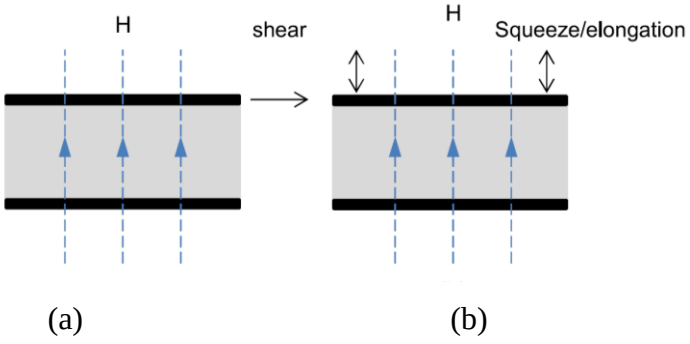

Figure 2.9 Basic operation modes for MRE: (a) shear mode; (b) squeeze mode

2.3.2 MRE based isolators

Base isolation is a particular technology of isolating vibrations for civil structures [12, 14, 187]. A seismic base isolation system decouples structures and their contents from potentially dangerous ground motions and deflects the energy emanating from earthquakes, especially in those frequency ranges where structures are most

vulnerable [188], by installing between them. To this end, base isolators require flexible lateral stiffness while high vertical stiffness to carry large vertical loading. For a base isolator, displacement transmissibility and force transmissibility are generally the references used to evaluate the system performances. Figure 2.10 shows the simple principle schematic of a passive base isolator. Because it is inherently passive (the stiffness and damping parameters cannot be changed once the device is designed), traditional passive base isolations cannot adapt to changes in the environment or source vibrations, which as a consequence compromises their efficiency and robustness and in some cases, cause adverse effects [15]. For example, traditional elastomeric bearings are vulnerable when coping with earthquakes with characteristics different from the particularly designed characteristics. An effective base isolation system is basically a trade off in design based on the estimated properties of a structure and the magnitude and frequency range of an expected earthquake [189]. Essentially then, a base isolation system can be effective against designated earthquakes but be ineffective when encountering different types of earthquakes [15, 188]. Therefore, it is concluded that effective base isolators should be those that can deal with different earthquakes. To overcome the shortcomings of traditional passive base isolations, recent and emerging research has been exploring various options such as adding supplementary energy-dissipating members with a magnetorheological damper, or a friction or hydraulic fluid damper, to reduce the seismic response of building structures [189, 190, 191-193]. Yoshioka *et al*. [15] and Ramallo *et al*. [188] proposed a combination of conventional base isolators and controllable dampers to compensate for a traditional base isolation system in extreme earthquakes. Wongprasert *et al*. [191] experimentally evaluated a combined spherical sliding bearing and variable fluid damper system for a multi-story building frame. These methods are classified as hybrid base isolation systems that offer a possible solution for improving the adaptability of traditional base isolation systems under certain types of earthquakes. However, in addition to the inherent limitations in a hybrid solution, simply adding supplementary devices to passive systems may cause additional problems; for example, adding a passive or controllable damper can reduce displacement at the top of the isolators but also increase the floor accelerations of the isolated structure as higher vibration modes are passed to the superstructure. Moreover, hybrid base isolation systems increase the complexity of a

design and implementing a base isolation system is not only costly, it also potentially compromises the reliability of these systems [194].

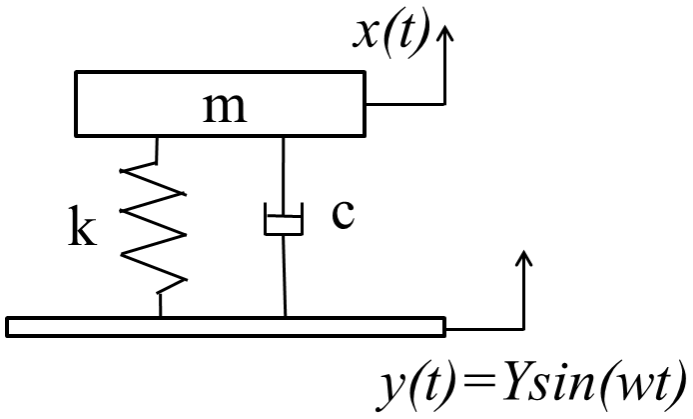

Figure 2.10 Principle of passive base isolation

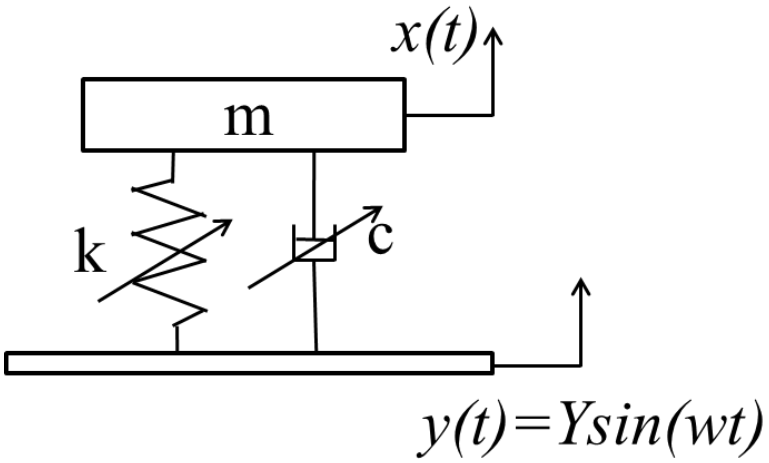

Figure 2.11 Principle of MRE base isolation

In an attempt to address the challenges faced by the current base isolation design/practice, a great deal of efforts has been expended on investigating and developing a highly adjustable MRE isolator [11, 18]. The reason is that base isolators incorporating MRE is adaptable, which can be simply shown by Figure 2.11 in which the stiffness and damping are controllable. Despite the fact that Figure 2.11 only shows an MRE base isolator of vertical direction, MRE base isolators can work in both lateral and vertical directions in terms of isolating vibrations, especially for building protection. Hwang et al [195] conducted a conceptual study on using MRE

on a base isolation system for building structures. Usman et al [196] numerically evaluated the dynamic performance of a smart isolation system using MRE and validated the feasibility of isolating unwanted vibration using a structure with five degrees of freedom. The results showed that an MRE isolation system outperformed a conventional system by reducing the response of a structure under various seismic excitations. A vibration isolation system which used four MRE elements as a tunable spring was reported in [104], and in this study, the proposed MRE isolator successfully suppressed the response of the payload. Behrooz et. al. [16, 17] designed an MRE-based variable stiffness and damping isolator (VSDI) and four prototypes of the isolator were built and utilized in a scaled three-story building. Figure 2.12 shows its cross section view and prototype photo. It includes two steel caps each embedded with two coils. Two MRE layers and one elastomer layer on each side are placed on the top of each cap such that the MREs are placed on the top plate. Positive and negative power cords are configured so that a closed-loop magnetic field is guaranteed in the device to generate the highest possible magnetic field in the MREs. The transmissibility performance of the device under different current levels from 0A to 3 A is shown in Figure 2.13. An obvious frequency shift property is found in the transmissibility. The experimental results demonstrate that the VSDIs are capable of simultaneously increasing their dynamic stiffness and damping by 30% and 10%, respectively. However, the potential concerns for this design for the seismic protection of civil structures is the limited vertical support capacity and the related problems such a bulging and limited lateral flexibility because of the limited layers of MRE.

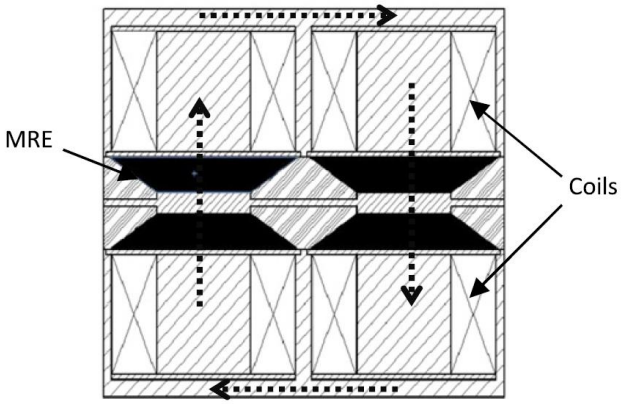

Figure 2.12 Schematic of the cross section of the VSDI [17]

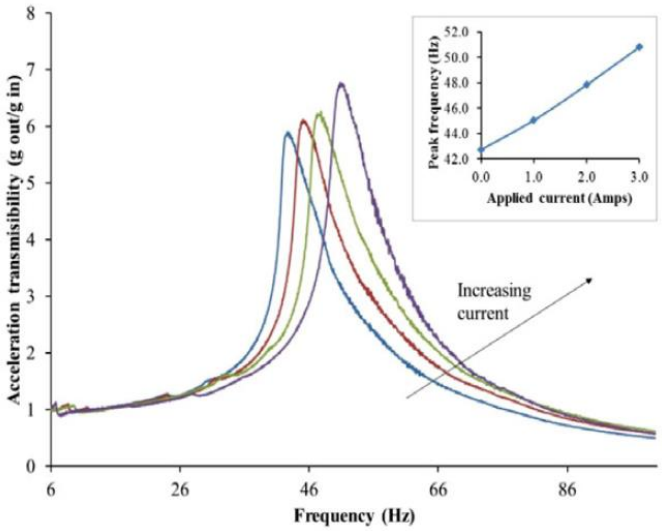

Figure 2.13 Transmissibility of VSDI under different currents [16]

Li et al presented the development and experimental evaluation of a smart base isolation utilising MRE in [18].The main contribution of the study is that the MRE isolator used a laminated structure for the traditional base isolator, where 47 layers of thin MRE sheets were bonded onto 46 thin steel plates, which enabled the isolator to maintain high vertical stiffness while simultaneously minimising lateral stiffness, see Figure 2.14. A hollow cylindrical coil was placed outside of the laminated structure. The steel plates at two ends, the hollow cylindrical steel yoke, the cylindrical steel block, and the laminated structure form an enclosed magnetic path. The results of this experiment showed that the force of the MRE isolator increased up to 45% and the stiffness increased up to 38%; thus demonstrating the potential of the proposed MRE isolator for smart base isolation applications. In order to achieve a larger range of increased stiffness under an applied magnetic field, a further effort has been conducted by Li and his group [19, 161], which also tried to find the optimal configuration for a magnetic circuit designed to provide a strong and uniform magnetic field in MRE. A new and highly adjustable MRE isolator was fabricated which increased the force by up to 1579% and the stiffness by up to 1730%. Eem et. al. also made an attempt to design a base isolator using four aluminium plates inserted in the MR elastomer compound [166]. However, the requirement for two large electromagnetic coils to energize such a small laminated structure largely limits its practical application in seismic isolation.

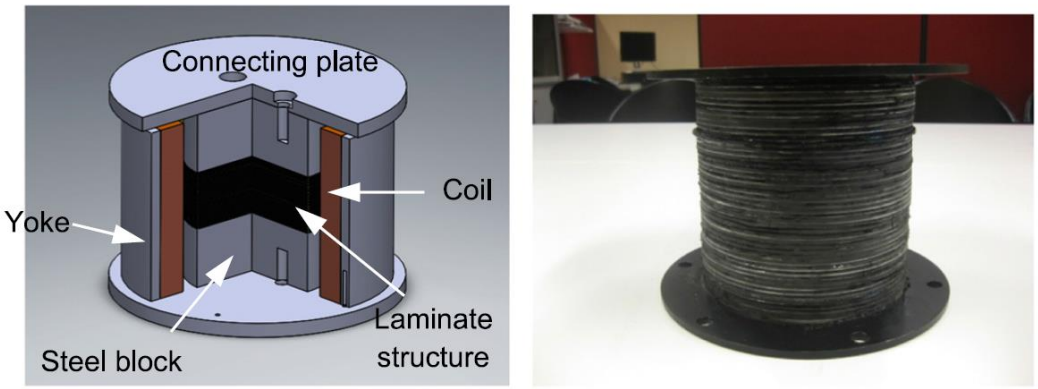

(a) (b)

Figure 2.14 Laminated MR elastomer base isolator [18, 161]: (a) cross section view of the base isolator and (b) the laminated MR elastomer and steel structure.

Despite the success and breakthrough on the development and proof-of-concept of the adaptive base isolator with stiffness hardening MRE, one critical challenge emerged as a result of the pilot research: an adaptive base isolator with stiffness hardening MRE may not be suitable for the practical implementation of seismic protection of civil infrastructures. This conclusion was based on the fact that the principle underlying the adaptability of a stiffness hardening MRE base isolator is its ability to increase lateral stiffness (i.e. the isolating frequency) away from damaging earthquake frequencies by magnetising MRE, but the effectiveness of base isolation relies on decoupling a structure from its source of vibration, i.e., decreasing the lateral stiffness of (softening) the isolators. Although increasing the isolation frequency makes it possible to shift the entire structural frequencies away from the resonant frequencies of the sources of vibration and therefore suppress vibration in the structure, this is not as effective as decoupling the structure from the source of vibration. In order to provide a softening lateral stiffness when an earthquake begins, stiffness hardening MRE isolators must be powered up for most of their operational time, which means these systems are not sustainable or reliable in practice. To overcome the drawbacks, MRE-based isolators that are stiffness softening is in urgent need.

To facilitate further application of MRE base isolator for structural vibration control, modelling work has to be done to make the MRE isolators accessible to advanced control algorithms. Due to the inherent hysteresis property and nonlinearity, modelling MRE isolators inevitably complicates. It is not expected that models for

MRF dampers can entirely work for MRE isolators for the reason that there are distinct differences between the MRF dampers and MRE isolators. However, the Bouc-Wen model, which is widely accepted in structure engineering and MR behavior for its mathematical simplicity and ability to represent a large class of hysteretic behavior, can be used to describe the hysteresis property of MRE base isolators [17, 21]. An example of using Bouc-Wen model is in [17], a phenomenological model with springs, viscous dampers and a hysteretic Bouc–Wen element is proposed, as shown in Figure 2.15. Eem *et al* used a combination of Maxwell and Ramberg–Osgood models as a phenomenological model for shear deformation of MREs [142] and Li *et al* used the standard three-parameter solid model and a modified Maxwell model to produce the strain stiffening property of MRE base isolator [197]. Yu *et al* [198] then conducted a series of modelling work for MRE base isolators.

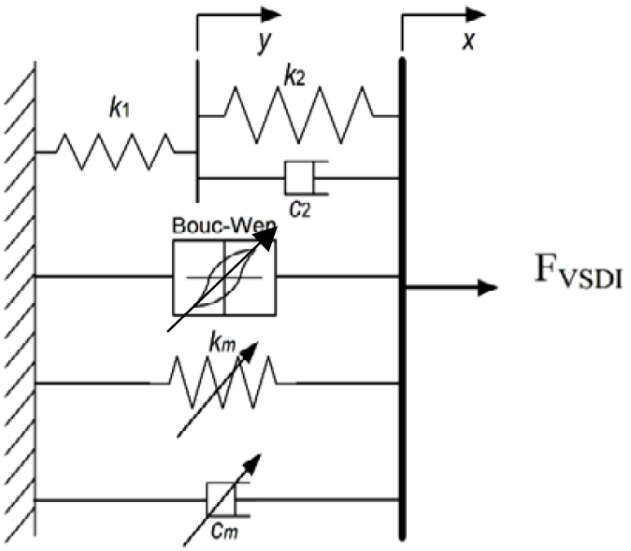

Figure 2.15 The proposed phenomenological model

2.4 Conclusions

This chapter presents a general review on the recent progress of aseismic technology for building protection, with special emphasis on the contributions of MRE technology to this area. To keep the integrity of the knowledge, this chapter includes an introduction of the discovery of MR effect and MR elastomers. Followed by a comprehensive review on the research progress of MRE, its composition, mechanical

property, modelling study, and its potential to be used for adaptive devices implementation are all involved. In the past few decades, adaptive devices using MREs have been blooming, with numerous ongoing research activities ranging from vehicle industry to civil area. For the innovative design of MRE devices, comprehensive understanding of the material property is a necessity. Despite the fact that the applications of MRE in the engineering fields are advancing rapidly, its potential are certainly not fully explored. At the same time, some challenges exit for both material science and engineering applications. For example, further efforts are needed to expand the knowledge on the combined operation mode; and it's necessary to find advanced and effective control algorithms to realize the real-time controllability of MRE devices.

3 EXPERIMENTAL STUDY AND MODELING OF A NEW MAGNETORHEOLOGICAL ELASTOMER ISOLATOR

3.1 Introduction

This chapter reports an experimental setup aiming at evaluating the performance of a newly designed MRE seismic isolator. As a further effort to explore the field-dependent stiffness/damping properties of the MRE isolator, a series of experimental tests were conducted. Based on the analysis of the experimental responses and the characteristics of the MRE isolator, a new model that is capable of reproducing the unique MRE isolator dynamics behaviors is proposed. The validation results verify the model's effectiveness to portray the MRE isolator. A study on the field-dependent parameters is then provided to make the model valid with fluctuating magnetic fields. To fully explore the mechanism of the proposed model, an investigation relating the dependence of the proposed model on every parameter is carried out.

3.2 Experimental Setup and Testing

3.2.1 Configuration of the MRE seismic isolator

A prototype of a new MRE base isolator was designed and fabricated [18]. The configuration of the MRE isolator, as shown in Figure 3.1, incorporates the laminated structural design of traditional laminated rubber bearing [19]. It consists of multilayer thin MRE sheets bonded onto multilayer thin steel plates. In this design, there are 26 layers of the steel sheet with a thickness of 1 mm and 25 layers of MRE sheets with a thickness of 1 mm being used. The diameter of the MRE and steel sheets is 120 mm.

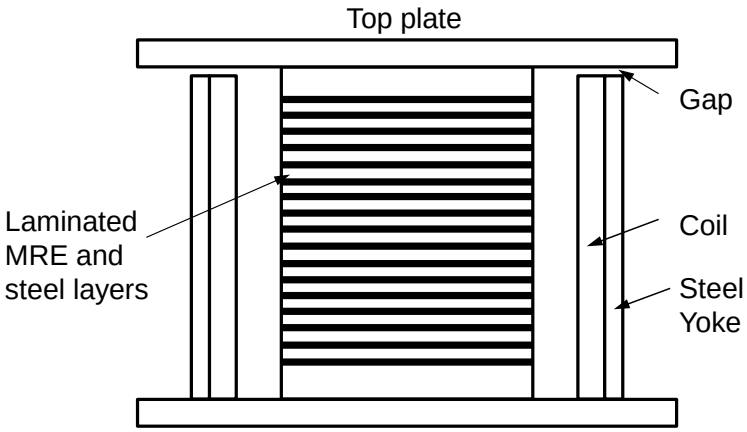

Figure 3.1 Cross section of the MRE seismic isolator

In the design, the laminated bearing element is placed inside of a solenoid, which generates magnetic field after it is energized with electric currents. The solenoid is made of electromagnetic coil and thin non-magnetic support as illustrated in Figure 3.1. The detailed dimensions can be referenced to [19]. The cylindrical shape non-magnetic support is made of epoxy material and has an inner diameter of 146 mm and a thickness of 2 mm. The cylindrical electromagnetic coil has an inner diameter of 150 mm and an outer diameter of 200 mm. The coil is firmly attached to the epoxy support. The diameter of the coil wire is 1.0 mm with a total winding number of 2900 turns. The wire made of copper has an electric resistance of 42.3 Ω. The space between the laminated MRE structure and the coil enables the MRE isolator to have a maximum deformation of 15 mm, equivalent to the maximum allowable shear strain of 60%.

3.2.2 Magnetic circuit design

In the design of the highly adaptive MRE isolator, one innovation is the laminated structure consisting of 25 layers of MRE sheets sandwiched between 26 layers of steel plates. As can been seen from Figure 3.2, the MRE material is placed inside of the magnetic coil, serving as the magnetic core of the magnetic circuit. Comparing with the weak and divergent magnetic field outside of the coil, the magnetic field inside the solenoid is strong and uniform. The major advantage of this design is that it creates a large effective area that is essential for MRE base isolator design. The MRE material inside the solenoid can be fully energized by a uniform magnetic field. However, due to the low permeability of the MRE material, the configuration needs

to be modified in actual design to increase the permeability of the magnetic coil for which MRE forms a part of it.

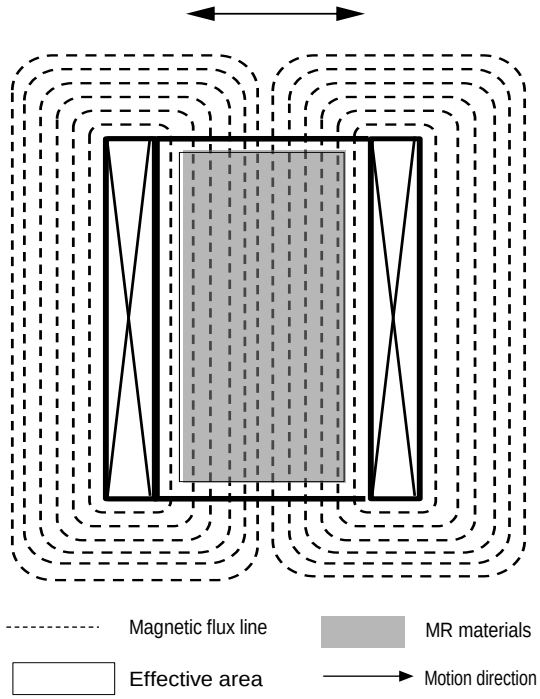

Figure 3.2 Invention design of magnetic circuit

3.2.3 Experimental setup

To evaluate and characterize the performance of the MRE base isolator prototype, a series of experimental tests were conducted. Figure 3.3 shows the schematic of the experimental set-up, where a shake table, which is available in the University of Technology, Sydney, was used to provide horizontal loadings to the isolator either in the quasi-static mode or in dynamic mode. The MRE base isolator was mounted on the shake table and moves along with the shake table motion. A load cell (Model No. STS-300-B10, Sun Scale INC) was installed to a fixed reaction rig to measure the lateral load applied to the isolator. During the test, the top plate of the MRE isolator and the load cell remain motionless thus eliminate the undesired inertia force in the measurements. A displacement sensor (MTS, USA) was used to measure provides the displacement. A DC power supply (DC Power Conditioner, SOLA Electric, Division of SOLA Basic Australia) with a capacity of 240V and 5.3A, as shown in Figure 3.4, provides DC current to energize the magnetic coil. A slider (Type: S-260-10, Yamabishi Electric Co. Ltd, Tokyo, Japan) was used to adjust the applied

current to the magnetic coil, also shown in Figure 3.4. A multi-meter (Model No. 115, Fluke) was also used to monitor the current output from the slider during the testing.

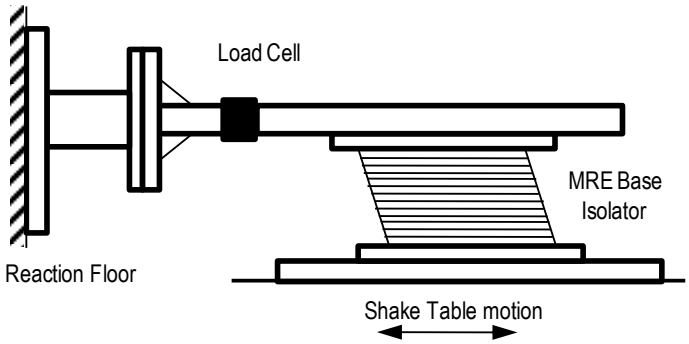

Figure 3.3 Sketch diagram of the experimental set-up

Figure 3.4 MRE seismic isolator during testing and equipment (power conditioner and the slider)

In this study, a series of preliminary tests were conducted to measure the response of the damper under various loading conditions. In each test, the MRE isolator was driven with a sinusoidal signal with a fixed frequency, and the current applied to the MRE isolator was held at a constant level. A wide range of frequencies (0.1Hz, 1.0Hz, 2.0Hz, and 4.0Hz), amplitudes (2mm, 4mm, and 8mm, corresponding to shear strain of 8%, 16%, and 32%), and currents (0A, 1A, 2A, and 3A) are considered. The sampling rate for the data acquisition was set at 256 Hz for capturing all test results including the dynamic tests. The velocity response was calculated from the measured displacements using a central difference method.

3.2.4 Testing results

Figure 3.5 shows the responses of force-displacement (Figure 3.5(a)) and force-velocity (Figure 3.5(b)) when the MRE isolator was loaded with the sinusoidal signal of three amplitudes (2 mm, 4mm and 8mm) at constant frequency (4 Hz) and current (2 A). The effects of changing the amplitudes are clearly observed. On one hand, it is observed from Figure 3.5(a) that the maximum force and the equivalent damping, indicated by the area enclosed by the force-displacement loop, gain a large increase with the increasing amplitude. Also it is noted that the nonlinear relationship between force and velocity appears much more obvious when the amplitude is large, as shown in Figure 3.5(b). On the other hand, a closer observation on the hysteresis loops reveals that the effective stiffness of the MRE isolator, represented by the slope of force-displacement loop, decreases slightly with ascending loading amplitudes. This physical phenomenon is called Mullins Effect, which was first studied by Holt [199] and further examined by Mullins [200, 201].

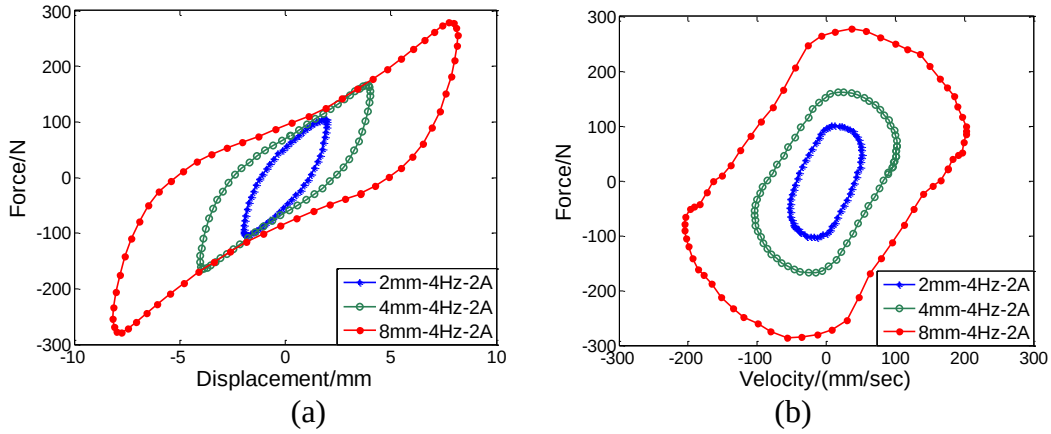

Figure 3.5 Experimental responses of the MRE isolator under sinusoidal inputs with different amplitudes: (a) Force vs. displacement; (b) Force vs. velocity

Mullins Effect is explained that if a rubber is stretched to a relative elongation and released, it will not follow the same stress-strain curve when it is stretched once again. Instead, the rubber appears to be much softer on the second stretch. The physical meaning of Mullins effect is the strain softening behavior of the elastomer when increase the loading amplitude, indicated by the descending stiffness for ascending amplitude cases [202].

The effects of changing frequencies on performance of the MRE isolator are presented in Figure 3.6. It is noticed from Figure 3.6 (a) that frequencies have a slight influence on the maximum force and effective stiffness. In particular, in the cases when the frequencies are above 0.1Hz the measured force and effective stiffness almost remain independent of frequency. Similar to amplitudes, the ascending frequencies induce an increasing nonlinearity of force-velocity relationship.

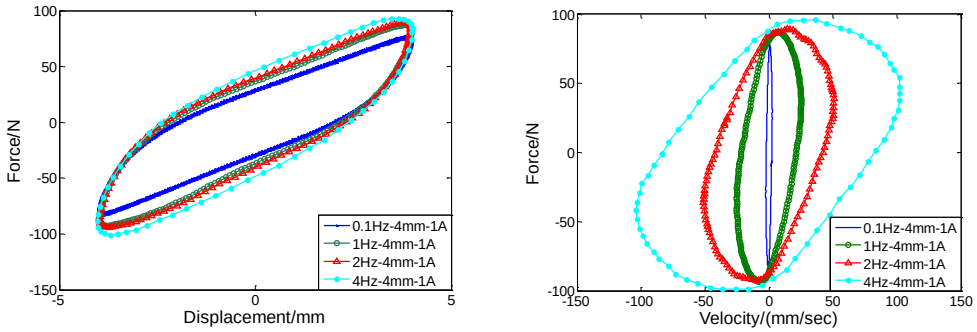

(a) (b)

Figure 3.6 Experimental responses of the MRE isolator under sinusoidal inputs with different frequencies: (a) Force vs. displacement; (b) Force vs. velocity

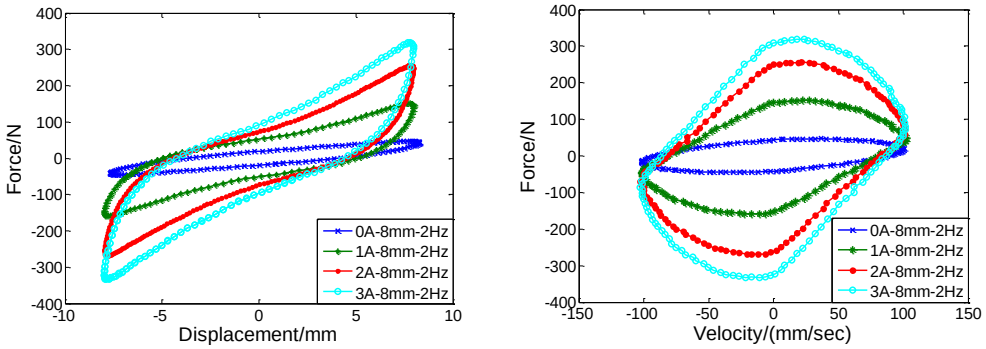

(a) (b)

Figure 3.7 Experimental responses of the MRE isolator under sinusoidal inputs with different currents: (a) Force vs. displacement; (b) Force vs. velocity

The response of the MRE isolator based on a 2 Hz sinusoid with an amplitude of 8mm is shown in Figure 3.7 for four constant current levels, 0 A, 1A, 2 A, and 3 A. At the 0 A level, the force-displacement relationship is approximately elliptical, and the force-velocity relationship is nearly linear. However, as the current level increases, the strain stiffening phenomenon shown in Figure 3.7(a) and the nonlinear

response of force-velocity illustrated in Figure 3.7(b) appear to be evident. Also, the increase in the force-displacement loop area and the effective stiffness demonstrates that the damping capacity and shear modulus of MRE are functions of the applied current.

Another property to be noted in the experimental data is strain stiffening which is obvious when the amplitude is large. The explanation for strain stiffening is attributed to the limited extensibility of the polymer chains [203] for normal rubber. However, for the field-dependent MRE cases, it is much more complicated. When a certain current level is applied to the MRE, in addition to the resistance of rubber matrix, the iron particles are also held by the magnetic force from the surrounding iron particle, which makes the extensibility of the chain structure even less. This explains some cases where the strain stiffening is minimal for zero field situations but is obvious for nonzero magnetic field, as illustrated in Figure 3.7(a).

3.3 Modelling and Validation

In modeling the MRE isolator responses, a major challenge is being able to capture the strain stiffening in force-displacement loops and the nonlinear relationship between force and velocity. To accurately portray these unique behaviors of the MRE isolator, a new phenomenological model is proposed in this section as shown in Figure 3.8. This model incorporates a Bouc-Wen component, which reproduces hysteresis loops, in parallel with a Viogt element, which describes solid-material behaviors. The Bouc-Wen component is described by the evolutionary variable z that represents a function of the time history of the displacement. It is widely accepted in structure engineering and MR behavior for its mathematical simplicity and ability to represent a large class of hysteretic behavior. In this work, the Bouc-Wen component combined with a spring and a damper is used to portray the unique field dependent stiffness/damping properties of MRE isolator. The force of this system is given by:

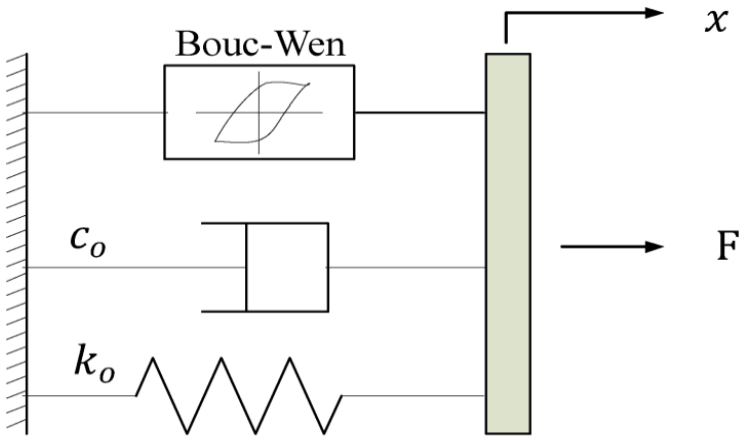

Figure 3.8 Schematic diagram of the proposed MRE isolator model

$$F = \alpha k_0 x + (1-\alpha) k_0 z + c_0 \dot{x} \ , \tag{3.1}$$

where the evolutionary variable z is described as:

$$\dot{z} = A\dot{x} - \beta|\dot{x}||z|^{n-1}z - \gamma\dot{x}|z|^{n}, \tag{3.2}$$

k_0 is the stiffness of the spring, and c_0 represents the viscous coefficient indicating the damping capacity of the system. The item of $c_0\dot{x}$ is a component of the total force. The rest part represents the restoring force as the summation of a linear component $\alpha k_0 x$ and a purely hysteretic component $(1-\alpha)k_0 z$, in which $\alpha \in (0,1)$ represents the linearity level of the hysteresis loops. In Eq. (2), A, n, β and γ, which are non-dimensional parameters, are responsible for the shape and the size of the hysteresis loops. The parameter A has a big influence on the maximum force, and n is recognized to control the transition from linear to nonlinear range. In this work, the value of $n = 1$ is considered for the purpose of reducing the overall number of system unknowns in the identification process on the ground that the chosen value satisfies the fitting requirements. β and γ mainly shape the hysteresis loops. Different combinations of the signs of $\beta + \gamma$ and $\beta - \gamma$ reproduce different shapes of hysteresis loops. A detailed investigation has been done in [204], where five kinds of hysteresis loops corresponding to five combinations of the signs of $\beta + \gamma$ and $\beta - \gamma$ have been presented.

To evaluate the model's effectiveness to predict the MRE isolator performances, a set of parameters are identified for the model to fit the experimental data shown in Figure 3.5 (8mm-amplitude, 4Hz-frequency, and 2A current). The identified values are listed in Table 3.1. In the identification process, there are in total 6 parameters to

be determined and a least-square method in combination with the Trust-region-reflective algorithm available in MATLAB (2011b) is employed to determine the appropriate values for them. The Trust-region-reflective algorithm refers to minimizing the value of a function, denoted as $g(x)$, by approximating $g(x)$ with a simpler function $p(x)$, which reasonably reflects the behavior of function $g(x)$ in a neighborhood N which is defined as the trust region. The key questions in defining a specific trust-region approach to minimizing $g(x)$ are how to choose and compute the approximation $p(x)$, how to choose and modify the trust region N, and how accurately to solve the trust-region problem. The objective herein is to minimize the root mean square, as indicated by Eq. (3.3).

$$J = \sum_{i=1}^{N} \sqrt{\frac{(F_{pi} - F_{ei})^2}{N}} \tag{3.3}$$

where N is the number of input-output pairs in each loop. F_p indicates the model-predicted output and F_e, the experimentally obtained output.

Table 3.1Parameter values of the proposed MRE isolator model

Parameters	A	α	β	γ	c_0	k_0
Values	0.62288	0.40962	0.30397	-0.47708	0.32774 N/(mm/sec)	14.542N/mm

Figure 3.9 shows the tracking process and relative errors of the predicted and measured forces with increasing time. It is observed that the relative error percentage is limited below 8%, which is acceptable in this modeling study. Figure 3.10 plots the comparison between the simulated and experimentally obtained responses. Figure 3.10(a) illustrates the force-displacement loop and Figure 3.10(b) describes the nonlinear relationship of force and velocity. It is obviously observed that the predicted behaviors resemble the experimental data very well, especially in the regions where the strain stiffening is obvious.

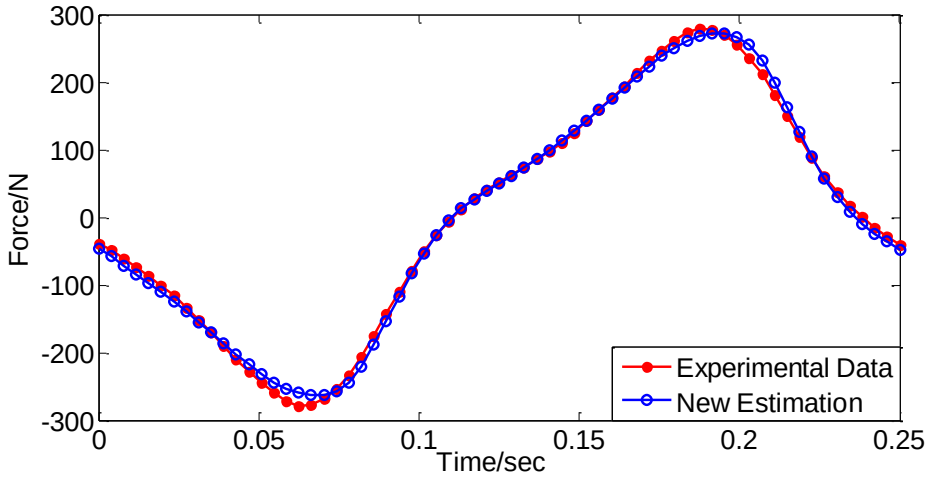

(a)

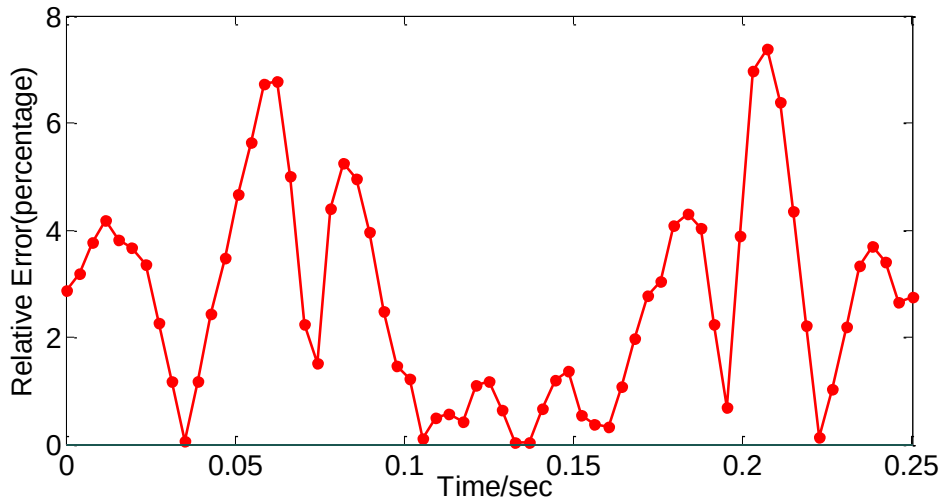

(b)

Figure 3.9 Force Tracking and Relative Error: (a) Force vs. time; (b) Relative error

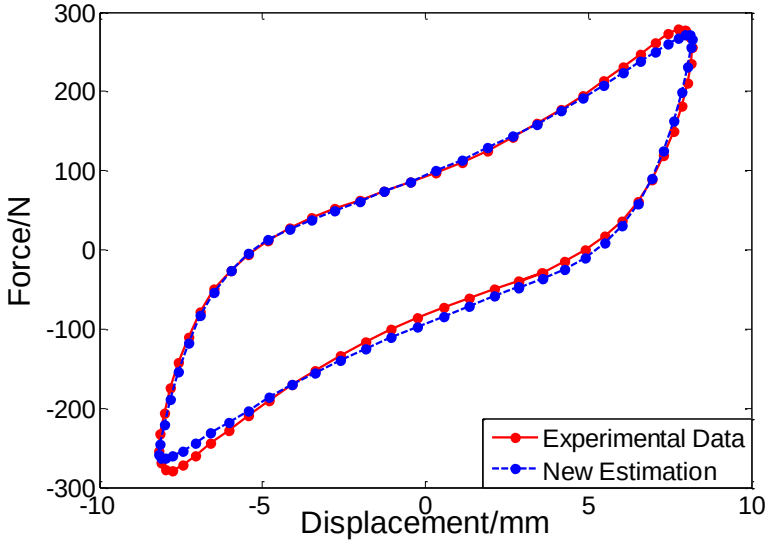

(a)

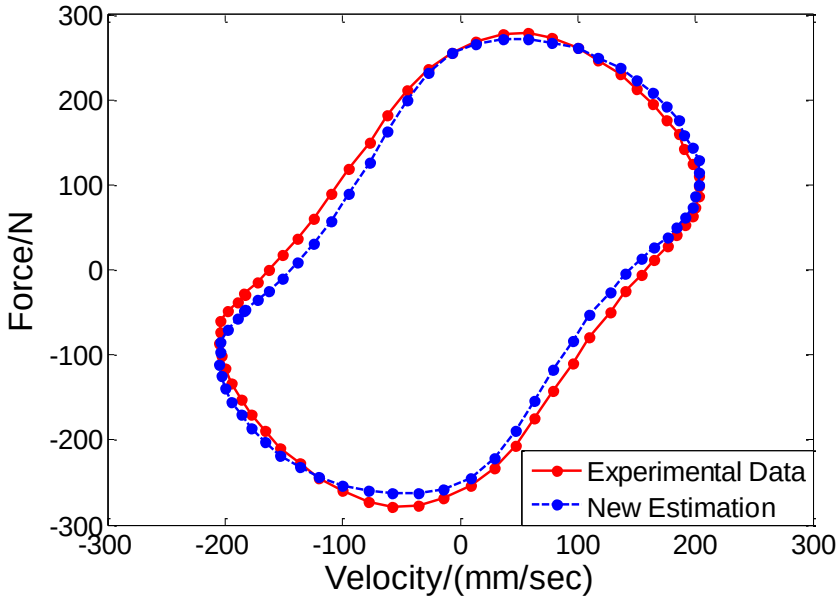

(b)

Figure 3.10 Comparisons between the model predictions and experimental responses: (a) Force vs. displacement; (b) Force vs. velocity

To further validate the capability of the model for portraying the behaviors of the MRE isolator, more sets of comparisons between the predicted and measured data corresponding to different loading conditions are given in Figure 3.11. The new estimations presented in Figure 3.11(a) are optimized to fit the experimental data of 2 A - current, 4 Hz - frequency for 2mm, 4mm, and 8mm amplitudes respectively. It is seen that the experimentally measured responses are reasonably modeled. A closer

look at the three predicted force-displacement loops illustrates that the effective stiffness reduces slightly as the amplitudes increases, demonstrating that the model is able to capture the Mullins Effect revealed in the experimental data. The measured force-displacement pairs shown in Figure 3.11(b) are obtained by loading the isolator with a 4 Hz sinusoid and an 8mm-amplitude at three current levels, 0 A, 1A, and 3 A, respectively. The three sets of comparisons verify the model's ability to describe the increasing nonlinearity of the hysteresis loops with the increasing currents. In particular, in each hysteresis loop, the predicted response resembles the unique behavior of straining hardening very well.

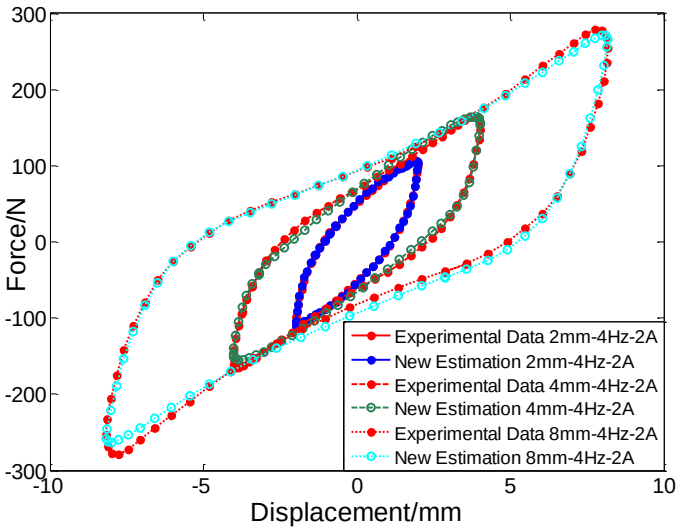

(a)

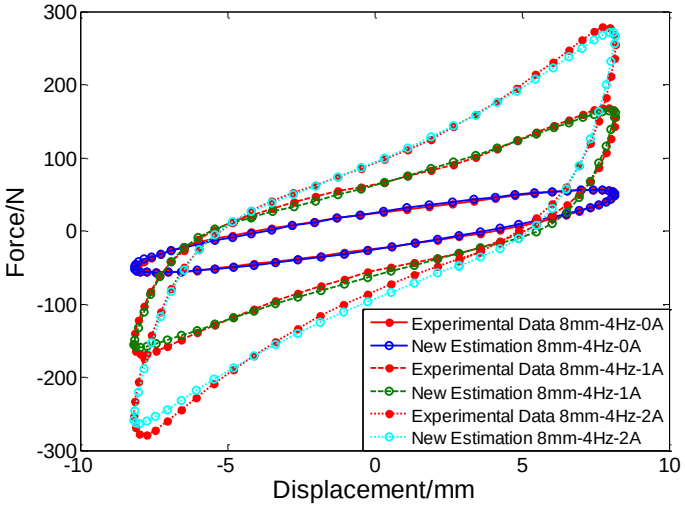

(b)

Figure 3.11 Validation responses of the proposed MRE isolator model: (a) Force vs. displacement; (b) Force vs. velocity

The predicted hysteresis loops change in the same regulation are summarized in Section 2.2. Besides some specific phenomena, for instance, strain stiffening, are captured, general rules are revealed in the figures as well. For example, the equivalent damping and maximum force change in an ascending way with the increasing amplitudes and currents, and also the increase in the current induces a large gain in the effective stiffness. All in all, Figure 3.11 further proves this proposed model is capable to accurately portray the MRE isolator's dynamics behaviors. Specifically, the predicted responses of the proposed model are matched the experimentally measured data of the MRE isolator when the current is in a constant level. Evidences provided verify the model's ability to accurately portray the behaviors of MRE isolator, especially in some specific regions. However, a versatile model is expected to achieve the unique performances of MRE isolator device when the fluctuating magnetic field is considered. To this end, a study on the field-dependent parameters is presented in the next section. Additionally, the effect of every single parameter on the sizes and shapes of hysteresis loops is discussed.

3.4 Field-Dependent Modeling and Discussion

In the proceeding section, the effect of fluctuating currents on the parameters in the proposed model is discussed and analyzed. Furthermore, the contribution of every parameter to the sizes and shapes of the predicted hysteresis loops is investigated.

Table 3.2 lists four groups of optimal values for the parameters of the proposed model described by Equations (3.1) and (3.2). These values are identified using the experimental data obtained by loading the isolator with an 8 mm and 4 Hz sinusoidal signal at four current levels of 0 A, 1A, 2 A, and 3 A respectively. Among the four columns, the first one is chosen as the initial guess for the other three optimization processes. In each process, only one parameter is identified for three current levels. It is therefore that 18 cases in total have been conducted.

Table 3.2 Identified values of parameters under different currents

	0 A	1 A	2 A	3 A
A	0.0014419	0.095326	0.17508	0.24699
α	0.9916	0.63032	0.32596	0.12973
k_0 (N/mm)	5.6994	14.792	24.913	31.494
c_0 (N/(mm/sec))	0.1246	0.38192	0.59138	0.69734
γ	-3.3327	-3.6512	-3.7028	-3.7239
β	2.6644	2.3265	2.2756	2.2351

Figure 3.12 shows the relationships between the parameters and the current based on the listed values in Table 3.2. It is seen that these four parameters of A, α, k_0 and c_0 appear to vary linearly with the current. Therefore, the following relations are proposed:

$$A = A_a + A_b I \quad , \quad \alpha = \alpha_a + \alpha_b I \quad , \quad k_0 = k_{0a} + k_{0b} I \quad \text{and} \quad c_0 = c_{0a} + c_{0b} I \tag{3.4}$$

The optimal parameters for relationships in Equation (3.4) are provided in Table 3.3. To validate the effectiveness of the field dependent parameters, comparison plots are presented in Figure 3.13, where the experimental data is from a loading of 4 mm and 4 Hz sinusoidal signal with the current of 1A. It can be seen from Figure 3.13 that the MRE isolator's behaviors are well captured.

Table 3.3 Identified values for field dependent parameters

Parameter	Value	Parameter	Value
A_a	0.80225	A_b	$1.5043I^{-1}$
α_a	0.15371	α_b	$0.28939I^{-1}$
k_{0a}	1.3103/(N/mm)	k_{0b}	3.322/(N*I/mm)
c_{0a}	0.044604/(N*sec/mm)	c_{0b}	0.087104/(N*sec*I/mm)
β	0.8549	γ	-0.91404

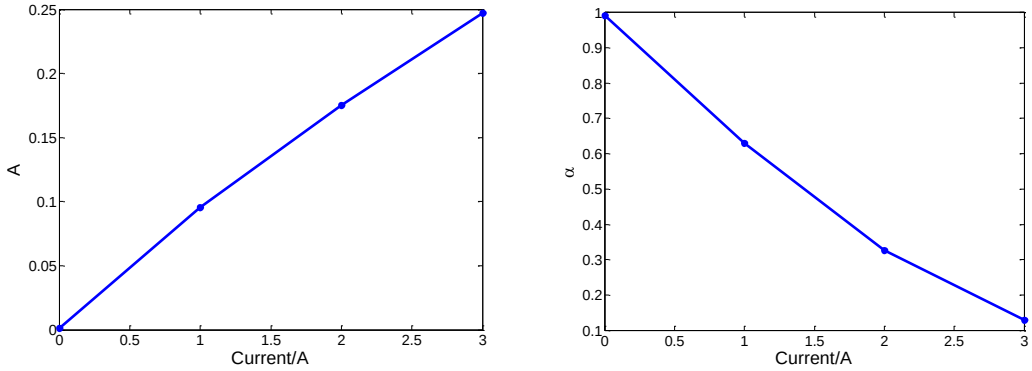

(a) (b)

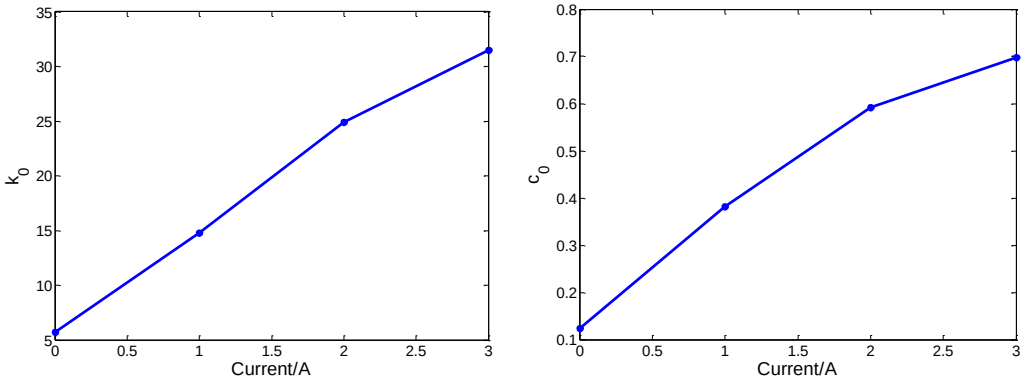

(c) (d)

Figure 3.12 Relationships between parameters and current：(a)A vs. current；(b) α vs. current； (c) $k_0$vs. current; (d) c_0 vs. current

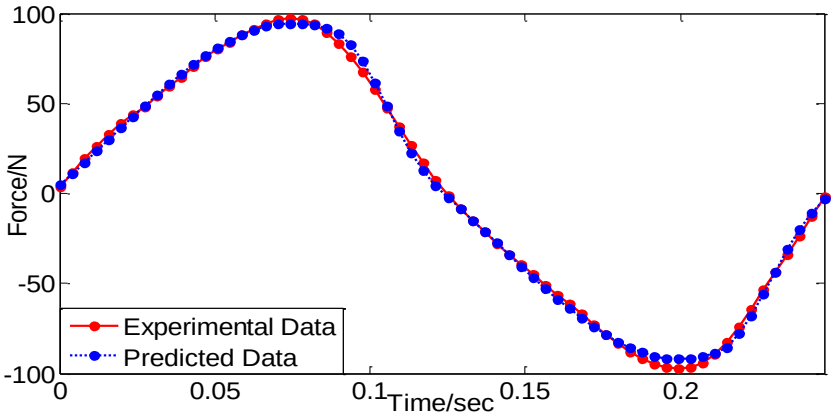

(a)

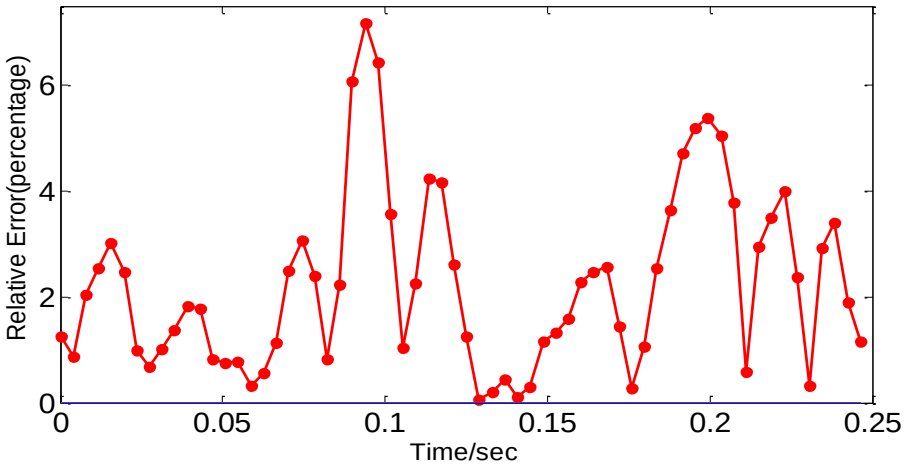

(b)

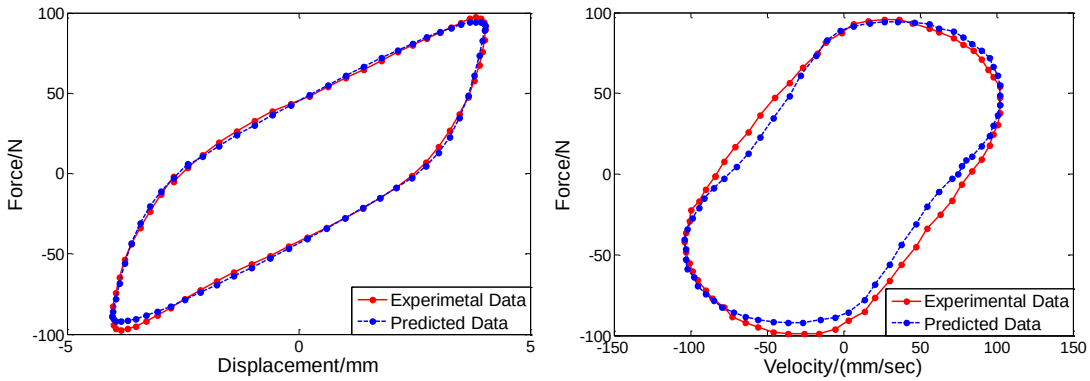

(c) (d)

Figure 3.13 Comparisons between the predicted and experimentally measured response: (a) Force vs. time; (b) Relative error vs. time; (c) Force vs. displacement; (d) Force vs. velocity

Taking the continuously varied currents into account makes this model more comprehensive for use, and meanwhile makes it easier to adjust parameters. Parameter adjustment after identification process helps improve the resemblance between the predicted and measured response, however, the influence of every parameter on the performances of the proposed model must be first investigated. In the following part, an effort to study the parameters' effects on the model output for the purpose of making it possible for the model to be easily controlled and adjusted is made. The optimized values listed in Table 3.1 are used as reference values. In each case among five cases, only one parameter is adjusted and the corresponding input-output pairs are collected and plotted to see variations of hysteresis loops.

As mentioned above, α indicates the linear degree of every hysteresis loop. For this reason, every value of α represents a hysteresis loop of different shape. Three sets of hysteresis loops corresponding to three α values, 0, 0.40962, and 1, respectively, are given, as shown in Figure 3.14.

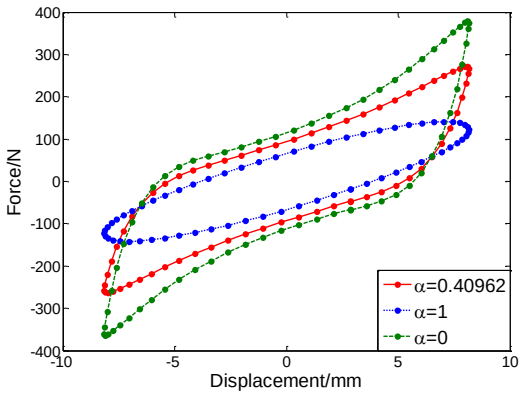

(a)

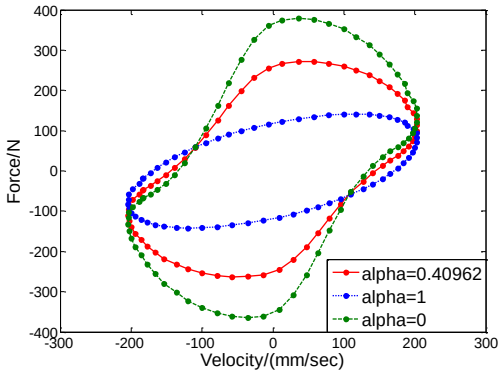

(b)

Figure 3.14 α dependent responses of the proposed MRE isolator model: (a) Force vs. displacement; (b) Force vs. velocity

When α equals to 1, the force function is simply represented in Eq. (3.5), it is observed from Figure 3.14 that the hysteresis loop is exactly an ellipse which presents a linear relationship. Instead, when α equals to zero corresponding to force function of Eq. (3.6), the nonlinearity of the hysteresis loop reaches the maximum degree. When α fluctuates in the range of (0,1), the nonlinearity degree varies between the two extreme situations, namely linearity and maximum nonlinearity.

$$F = k_0 x + c_0 \dot{x} \tag{3.5}$$

$$F = k_0 z + c_0 \dot{x} \tag{3.6}$$

Similar to the force-displacement responses, the force-velocity response shows the same rule, i.e. the hysteresis loops tend to be more nonlinear with the descending values of α.

As can be seen from the force-velocity relationships shown in Figures 3.5-3.7, the output forces almost reach its maximum when the velocity is zero and decrease to its minimum when the velocity equals to its maximum. It is concluded that the damping force, indicated by $c_0\dot{x}$ in the force function, contributes a small part to the total force. The identified values of c_0 being very small support this conclusion. It is therefore reasonable that c_0 varies in a small range. Figure 3.15 presents four sets of hysteresis loops of different sizes and shapes corresponding to four different values of c_0. As might be expected, the effect of changing c_0 on the maximum force is slight. The other effect to be noted is that the sizes of the force-displacement loops tend to be thinner when c_0 is fixed at a small value than when c_0 is assigned a bigger one. Since the areas enclosed by the force-displacement loops indicate the equivalent damping, the change in the graphical curves matches the numerical variations.

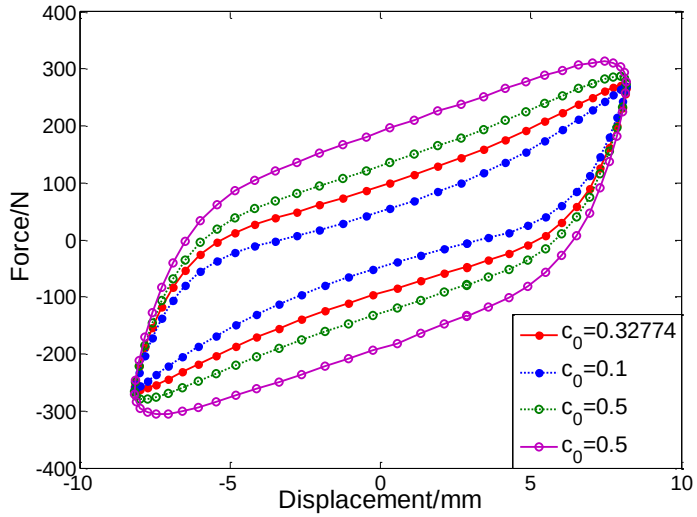

(a)

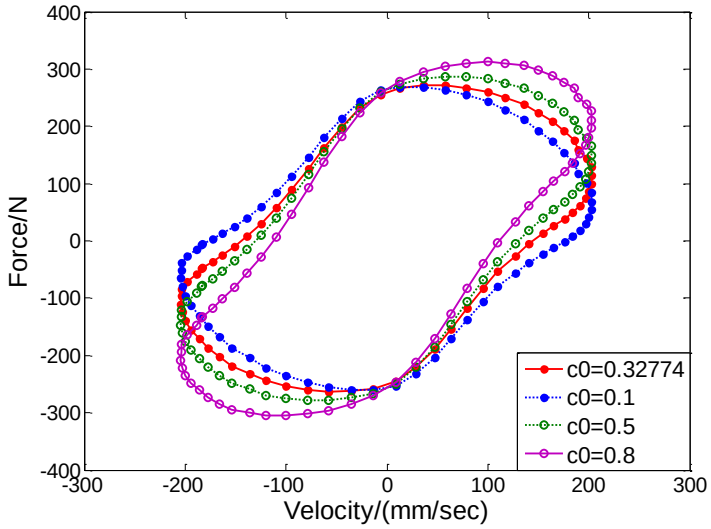

(b)

Figure 3.15 c_0 dependent responses of the proposed MRE isolator model: Force vs. displacement; (b) Force vs. velocity

Figure 3.16 presents the resultant hysteresis loops by changing the values of k_0. It is seen that the maximum force and effective stiffness change almost linearly with k_0. Another phenomenon worth noting is that all the loops intersect at two points, as highlighted by M and N in Figure 3.16(a), from which the system stiffness under different k_0 becomes different. Furthermore, the two points indicate the critical points of strain stiffening, as observed in each loop strain stiffening tends to be obvious from these two points. In order to provide a more detailed explanation, the hysteresis loop can be divided into two parts, separated by the solid line. Take only

the upper section for an example, as the force-displacement loops follow clockwise paths, it is noticed that the system stiffness of the left part of point M decreases as the hysteresis loop progresses, while the system stiffness of the right part tends to increase. It is therefore reasonably inferred that strain stiffening starts from point M. Additionally, the horizontal axis range for strain stiffening is from -2 mm to 8 mm. The same rule applies to point N and the strain stiffening range of the lower section is from 2 mm to -8 mm.

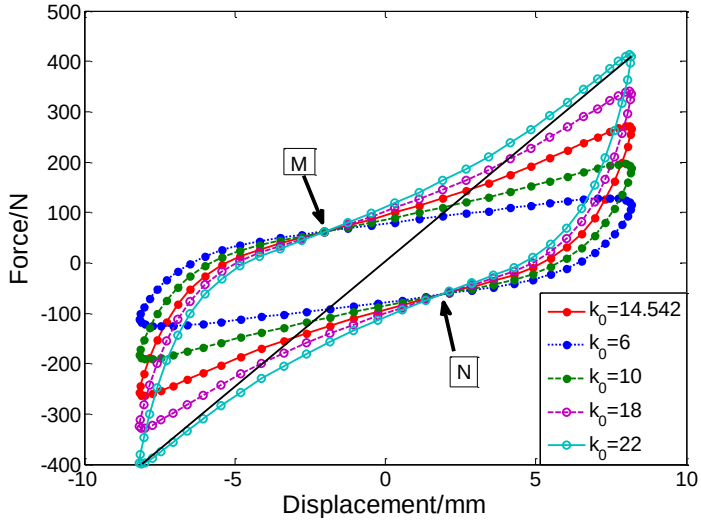

(a)

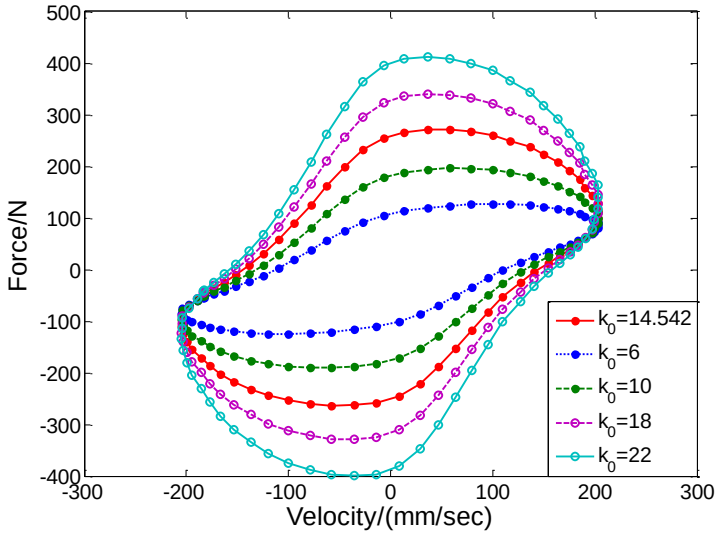

(b)

Figure 3.16 k_0 dependent responses of the proposed MRE isolator model: (a) Force vs. displacement; (b) Force vs. velocity

The effect of parameter A on the response shape is shown in Figure 3.17. It is noticed that the effect of adjusting A on hysteresis loops is very similar to that of changing k_0. Conclusions includes that the maximum force and effective stiffness vary linearly with A, and two critical points for strain stiffening exist as well, donated by P and Q. However, the strain stiffening range is [-4, 8] mm and [-8, 4] mm respectively which is larger than that of k_0, indicating that A is more sensitive than k_0 to this model.

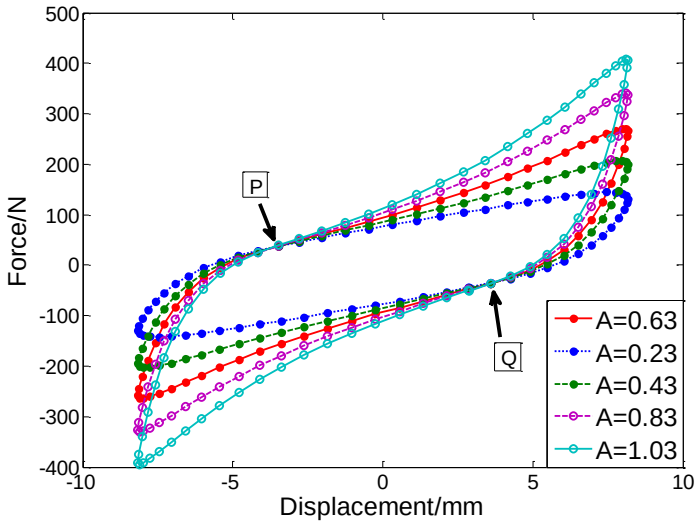

(a)

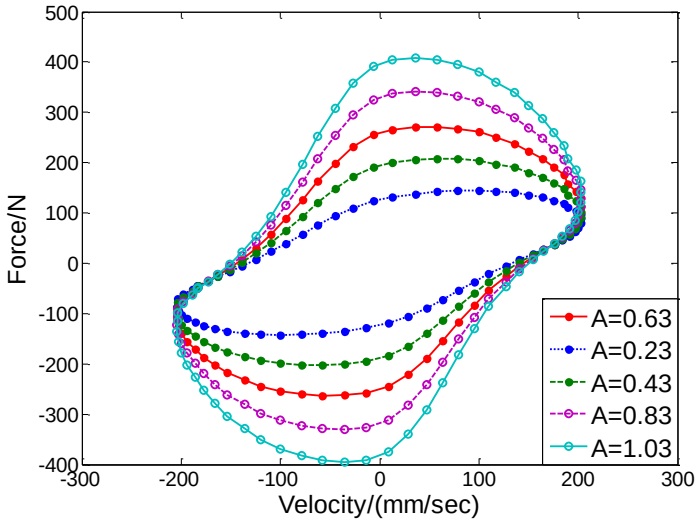

(b)

Figure 3.17 A dependent responses of the proposed MRE isolator model: (a) Force vs. displacement; (b) Force vs. velocity

β and γ have been recognized to shape the hysteresis loops. Figure 3.18 presents a series of hysteretic responses with respect to different β and γ. Figure 3.18(a) shows the effects of β on shaping hysteresis loops and Figure 3.18(b) shows that of γ. It is seen from Figure 3.18(a) that the nonlinearity tends to be more obvious as the value of β gets smaller. On the contrary, when β grows, the hysteretic shapes are inclined to be linear ellipses. One point needs to be emphasized is that when β is increased to a certain value, its influence on the shape is limited. As donated by an arrow in Figure 3.18(a), the hysteretic shapes remain an ellipse as the β increases from 1 to 2 with an increment of 0.2. Another important finding to add is that an effective β should be kept positive. In other words, β should fluctuate in an effective range for reproducing reasonable hysteretic shapes on condition that all the other referenced parameters are fixed. Speaking of the effect of γ, as noticed in Figure 3.18(b), it is very similar except minor differences to that of β. In the case when γ is negative, the nonlinearity level increases with the increasing absolute value of γ, otherwise, the hysteresis loops progress linearly. Also note that the responses remain linear when the value of γ is above zero.

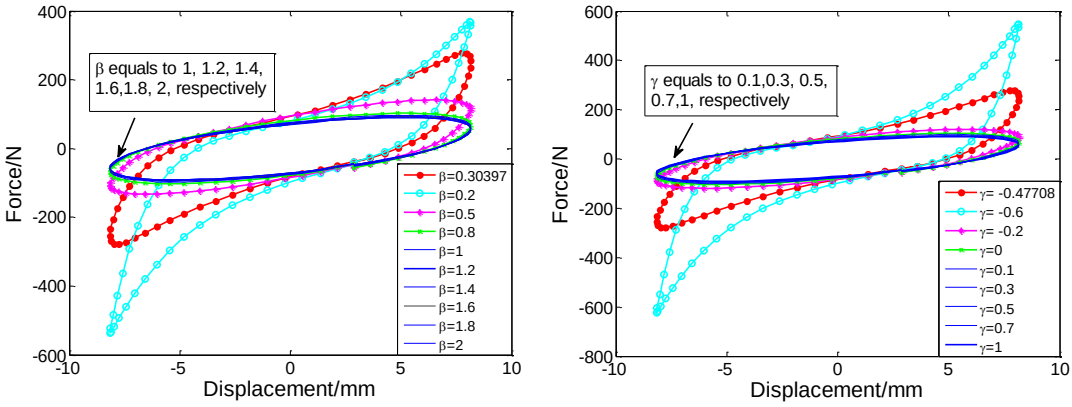

(a) (b)

Figure 3.18 β and γ dependent responses of the proposed MRE model: (a) β dependent response; (b) γ dependent response

Referring to the combinations of signs of $\beta+\gamma$ and $\gamma-\beta$, a leading study has been done in presenting five kinds of hysteretic shapes relating to five combinations of signs of $\beta+\gamma$ and $\gamma-\beta$. In this work, five cases will reappear for the purpose of validating the influence of β and γ on controlling the hysteresis loop shapes.

Table 3.4 Five combinations of β+γ and γ-β

Combinations			β	γ
Case 1	$\beta+\gamma>0$	$0<\gamma-\beta<\beta+\gamma$	0.1	0.3
Case2		$\gamma-\beta<0$	0.4	-0.3
Case3		$\gamma-\beta=0$	0.2	0.2
Case4	$\beta+\gamma=0$	$\gamma-\beta<0$	0.4	-0.4
Case5	$\beta+\gamma<0$	$\gamma-\beta<\beta+\gamma<0$	0.3	-0.6

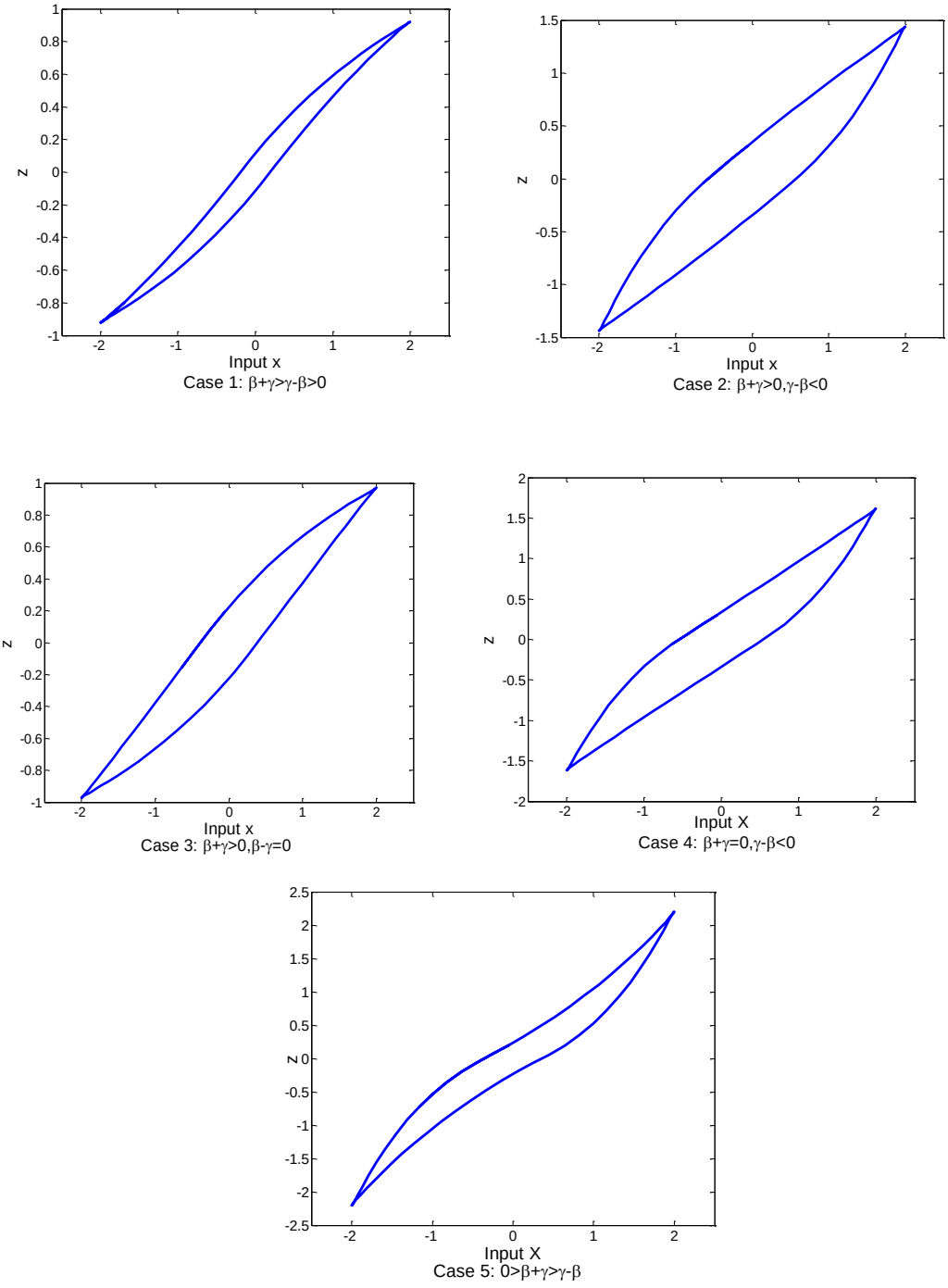

Figure 3.19 Different shapes for five kinds of combinations of β and γ.

For the reason that the hysteresis curves are produced by Eq. (2), it is natural the five cases will describe the relationship between the input displacement and the evolutionary variable z. Table 3.4 lists different values for β and γ to satisfy five combinations of $\beta + \gamma$ and $\gamma - \beta$ and the associated hysteretic shapes are plotted in Figure 3.19. As discussed above, β should be positive to be effective and γ has a wide variation range. Hence, the five cases are obtained by adjusting γ. It is clear that five different situations are presented as observed in reference [204]. And clearly the optimal values of $\beta + \gamma$ and $\gamma - \beta$ listed in Table 3.1 satisfies the combination of case one.

3.5 Conclusions

A highly adjustable MRE seismic isolator was designed, fabricated and tested. The performances reveal that the increase in loading amplitude leads to an increase in the damping capacity and maximum force but a light decrease in effective stiffness, that frequency poses minor influence on these three performance indicators, especially when it is above 0.1Hz, and that MRE exhibits field-dependent property that the effective stiffness and equivalent damping tend to increase with the progressively larger currents.

To take the maximum advantage of potential MRE material into control applications, a model for MRE isolator is developed. The resemblance between the predicted and measured response verify that the newly proposed model is competent to model the MRE isolator device. To make the proposed model more adaptive, the fluctuating magnetic field is taken into account. And the study on the dependence of the model to every parameter further improves the model to be more easily controlled and adjusted.

4 A NEW MRE ISOLATOR WITH SOFTENING STIFFNESS FOR VIBRATION REDUCTION

4.1 Introduction

MREs have attracted attentions of researchers in the development of smart isolators and absorbers due to their controllable stiffness and damping properties. For the purpose of mitigating unwanted structural and/or machinery vibrations, the traditional MRE based isolators have generally proven effective because the MR effect can increase the stiffness when the magnetic field is strengthened. This chapter presents a new MRE isolator with softening stiffness, i.e. its stiffness was reduced when the applied current was increased. This innovative work was accomplished by applying a hybrid magnet (electromagnet and permanent magnets) onto a multilayered MRE structure. To characterise this negative changing stiffness concept, a multilayered MRE isolator with a hybrid magnet was first designed, fabricated, and then tested to measure its properties. An obvious reduction of the effective stiffness and natural frequency of the proposed MRE isolator occurred when the current was continuously adjusted. On the other hand, this device could also work as a conventional MRE isolator as its effective stiffness and natural frequency also increased when a control current was applied. Further testing was carried out on a 1-degree-of-freedom system to assess how effectively this device isolated vibration. In this experiment, two cases were considered, and in each case vibration of the primary system was obviously attenuated under ON-OFF control logic, thus demonstrating the feasibility of this new design as an alternative adaptive vibration isolator.

4.2 Design and Fabrication

4.2.1 Fabrication of a multilayered MRE structure

The components used to fabricate an MRE include silicone sealant (Selleys Pty. Ltd), silicone oil (Sigma-Aldrich Pty. Ltd), and carbonyl iron particles (C3518, Sigma-Aldrich Pty Ltd). The weight ratio of these three materials was 1.5:1.5:7. The detailed fabrication procedure of MRE can refer to Section 2.2.3.

The multilayered MRE structure incorporates a traditional laminated rubber bearing 205, 206] that consists of multiple layers of thin MRE sheets and thin steel plates.

The inner steel plates give the required vertical load capacity and stiffness, while the MRE sheets offer horizontal flexibility which can be varied instantly under an applied magnetic field. This laminated bearing element consists of 10 layers of 1mm thick by 35mm diameter MRE sheets and 11 layers of 1mm thick by 35mm diameter steel sheets.

4.2.2 Design of hybrid magnet system

To use this multilayered MRE structure as an adaptive stiffness element, a controllable magnetic system that produces a uniform and powerful magnetic field to energise the low magnetic-conductive MRE materials must first be designed. One of the new designs that had to be developed for this study was an adjustable hybrid magnet system with permanent magnets and an electromagnetic coil. Although a similar idea can be found in [154] where a hybrid magnetic system was incorporated into an adaptive vibration absorber, the hybrid magnetic system designed and presented by this study differs significantly in its structure and operation compared to [154]. By including permanent magnets, a stable magnetic field could be applied to the laminated MRE and steel structure at all times without any power consumption. Then the electromagnetic coil is responsible for either strengthening or weakening the nominal magnetic field generated by the permanent magnets through adjusting the direction and magnitude of the applied current. The stiffness of the MRE materials was controlled by the superposition of these two magnetic fields. One clear advantage of this design is its ability to increase and decrease the magnitude of the hybrid magnetic field such that the stiffness of the MRE structure can be both increased and decreased such that the natural frequency of the system can be turned to be both above and below the passive natural frequency, which would be a desirable achievement for practical purpose.

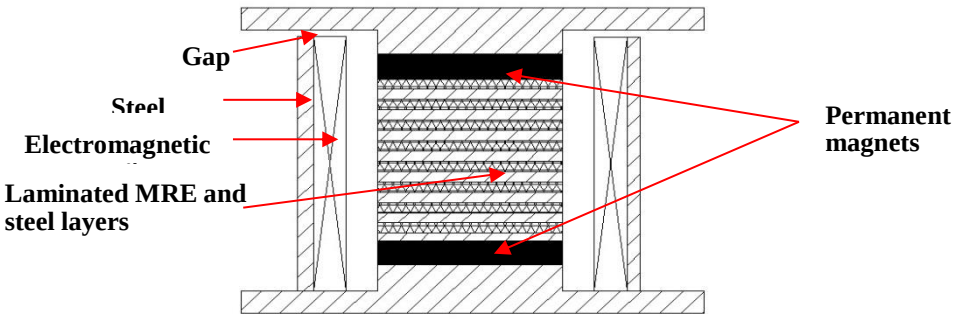

Figure 4.1 Schematic diagram of the hybrid magnetic system

Figure 4.1 shows the assembly of this hybrid magnetic system. To overcome the low magnetic permeability of MRE materials, two steel cylinders were placed at both ends of the laminated structure to increase magnetic conductivity [19] before the laminated structure was placed between the permanent magnets. The permanent magnets generate a vertical and stable magnetic field perpendicular to the laminated structure, so when this compact structure is placed inside the electromagnetic coil it becomes the magnetic core of the electromagnetic circuit, and because the electromagnetic field inside the solenoid is uniform and vertical, by adjusting the current, the hybrid magnetic system can work in different modes, as shown in Figure 4.2. The blue closed loop represents the magnetic circuit generated by the permanent magnets, while the yellow loop represents the adjustable magnetic circuit produced by the electromagnetic coil.

In this study, current passing through the coil can generate an electromagnetic field that is opposed to the permanent magnetic field and is defined as a positive current. In this case, as Figure 4.2 (a) shows, the overall magnitude of the hybrid magnetic field has been reduced. Otherwise, the current that increases the permanent magnetic field is defined as a control current, as shown in Figure 4.2 (b). When a positive current is applied the magnetic field generated by the permanent magnetic field would be reduced by the electromagnetic field, such that the higher the current the more of the magnetic field is reduced, but if the current keeps on increasing, the overall magnitude of the hybrid magnetic field would keep decreasing until it reached zero, after which the hybrid magnetic field would begin to increase in reverse. Correspondingly, the stiffness of the MRE based structure would decrease in the first stage and then increase as the current keeps growing, but when a negative current was applied, the permanent- and electro- magnetic fields would be in the same direction, which means that the superposition of the hybrid magnetic field would be enhanced, and the stiffness of the system would increase until it reached saturation where the control current keeps increasing.

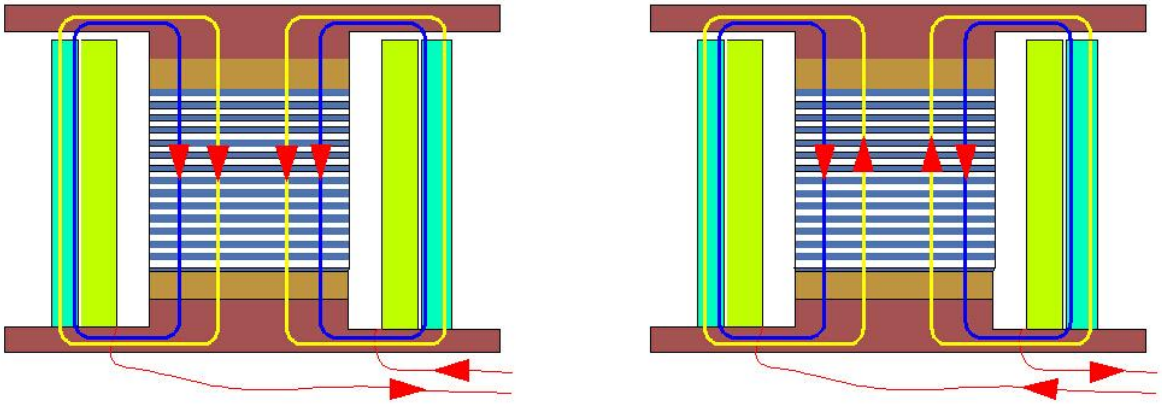

(a) (b)

Figure 4.2 Different working modes for hybrid magnetic system: (a) Hybrid magnetic field under positive current; (b) Hybrid magnetic field under negative current

4.2.3 Assembly of MRE based isolator

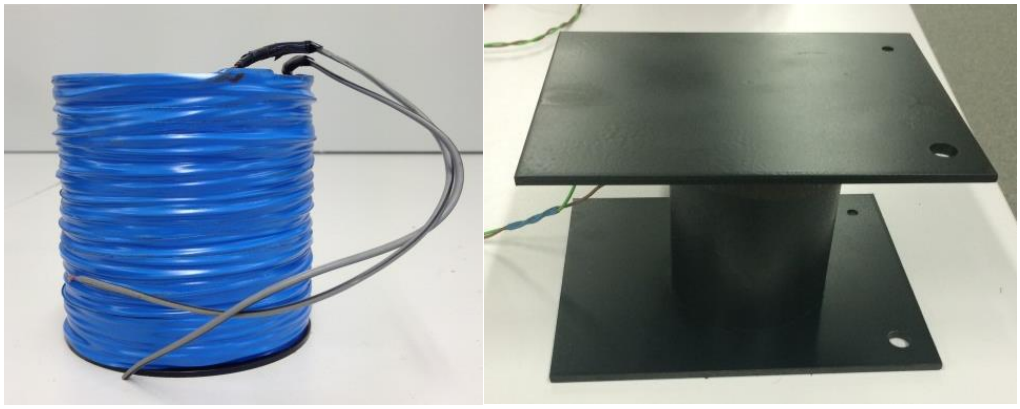

Figure 4.3 Photographs for electromagnetic coil and MRE isolator

Figure 4.3 shows the physical maps for the electromagnetic coil and the MRE based isolator. The rectangular bottom plate was appropriate for fixing the isolator to the base, through which the disturbance excitation is passed to the whole system. The top steel plate was used to support the weight. Such a new isolator has inherited the classical laminated structure and incorporated the hybrid magnetic system while being compact enough to be used safely and conveniently, and yet it is strong enough to maintain a high vertical stiffness while simultaneously providing lateral flexibility. Furthermore, this hybrid magnetic system makes the MRE isolator energy friendly and yet powerful enough to possess a high controllability over its characteristics.

4.3 Characterising the MRE isolator

4.3.1 Experimental setup

To evaluate and characterise the performance of the MRE base isolator prototype, a series of experimental tests were conducted under various loading conditions. A detailed experimental set up is shown in Figure 4.4 and a schematic diagram of the experimental set up is shown in Figure 4.5. The isolator was fixed to the bearing through an aluminum sheet. A base was fabricated to support the bearing in order to avoid any unwanted vibration in the measurement. The isolator was forced to vibrate horizontally by a shaker (VTS, .VC 100-8), which was driven by a signal source from a power amplifier (YE5871), and a laser sensor (MICRO-EPSILON Company) monitored the horizontal movement of the bottom plate. A force sensor (CA-YD-302) was mounted between the top plate of the isolator and the fixed rig to measure the lateral force produced by the isolator. During the test, the top plate and the force sensor remained motionless in order to eliminate any unwanted inertia force in the measurements. A DC power supply (THURLBY-THANDAR, INSTRUMENTS LTD) was used to provide DC current to energise the magnetic coil. The amount and direction of the output current could be adjusted to change the magnitude of the electromagnetic field. The interface connecting the computer and the device (amplifier and signal sensors) was supplied by the Data Acquisition (DAQ) board (LabVIEW PCI-6221, National Instruments Corporation. U.S.A). The LabVIEW program was designed to be the control unit and the display unit where harmonic excitation could be generated and the results displayed and recorded.

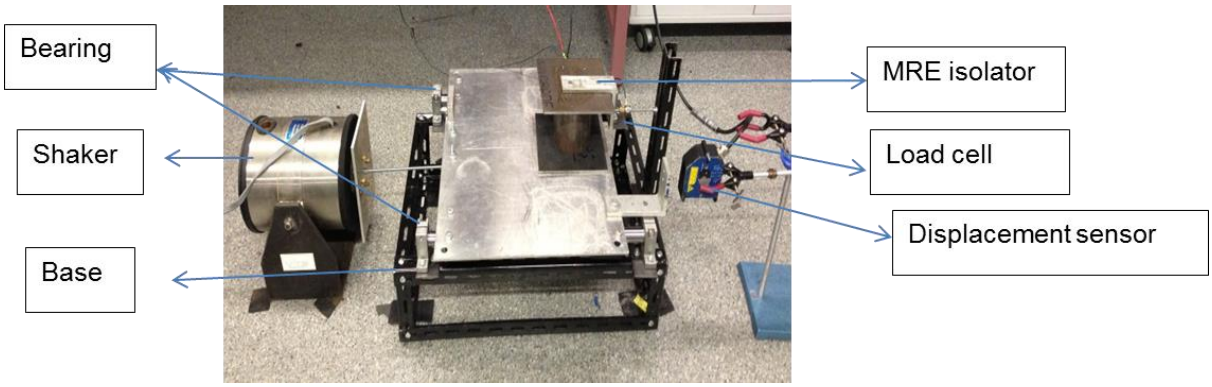

Figure 4.4 Experimental Setup for testing the MRE isolator

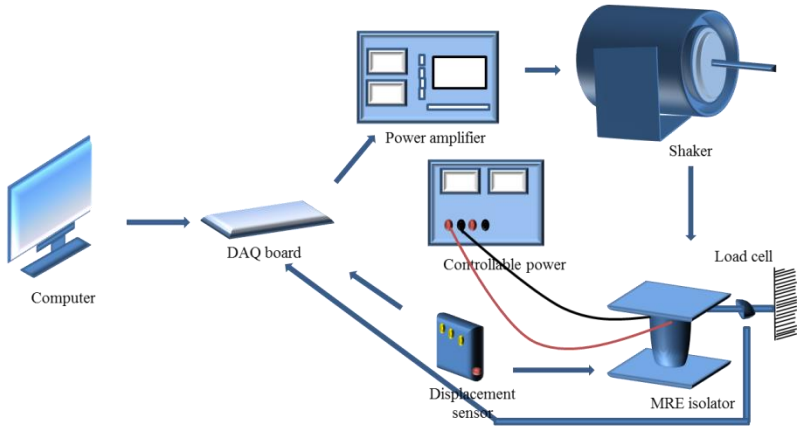

Figure 4.5 Schematic diagram for the experimental setup

In the first part of the test various harmonic inputs were used to assess the dynamic properties of the MRE based isolator. A wide range of frequencies, amplitudes, and currents were selected to demonstrate the ability of the isolator to become both 'softer' and 'harder', and both positive (1A, 2A, 3A, and 4A) and negative currents (-1A, -2A, -3A, and -4A) were considered. In each case, the sampling rate for the data acquisition was set to 1000Hz and at least 20 cycles were measured to stabilise the isolator. The transmissibility and phase of the isolator under different levels of current were also provided. To determine whether this design would offer an alternative solution for suppressing vibration, a vibration isolation experiment was conducted as the last part of these experiments.

4.3.2 Results of Dynamic testing

Figure 4.6 shows the force-displacement (Figure 4.6a) and force-velocity (Figure 4.6b) responses when the MRE isolator was run with a sinusoidal signal of five different amplitudes at a constant frequency (3 Hz) and current (4 A). This series of responses progressed from linear to nonlinear when the loading amplitudes were increased. This can be reasonably explained by the resistance from the rubber matrix and the magnetic force between iron particles that prevented the chain structure in the MRE materials from extending when a larger amplitude was applied. Another obvious finding was the measured force and equivalent damping which was indicated by the enclosed area of the force-displacement loop, and an evident increase in gain with ascending loading amplitudes. However, the lateral stiffness of the isolator, indicated by the slope of the force-displacement loop, decreased slightly as the amplitude increased.

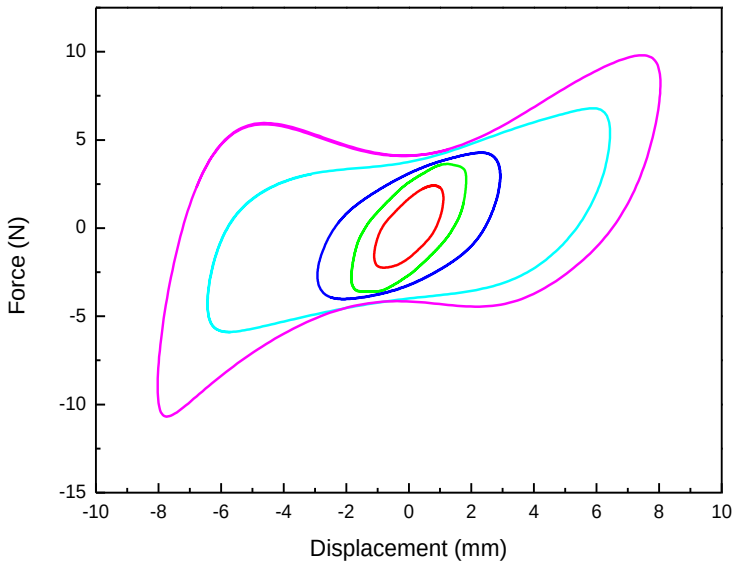

(a)

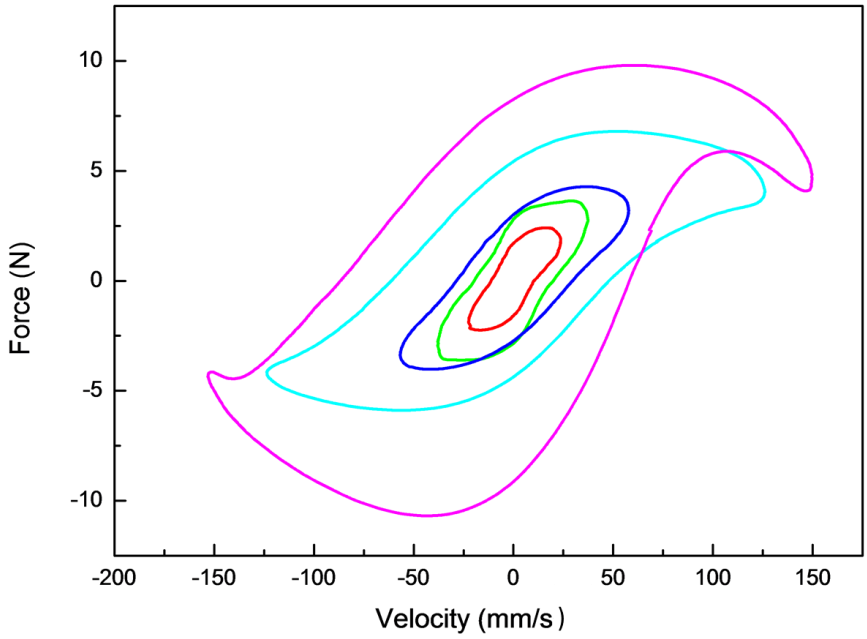

(b)

Figure 4.6 Experimental responses of the MRE isolator under sinusoidal inputs with different amplitudes: (a) Force vs. displacement; (b) Force vs. velocity

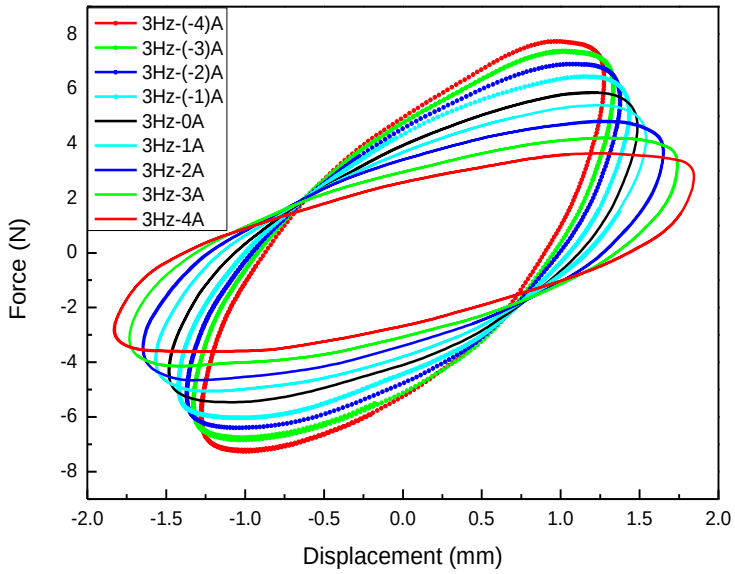

(a)

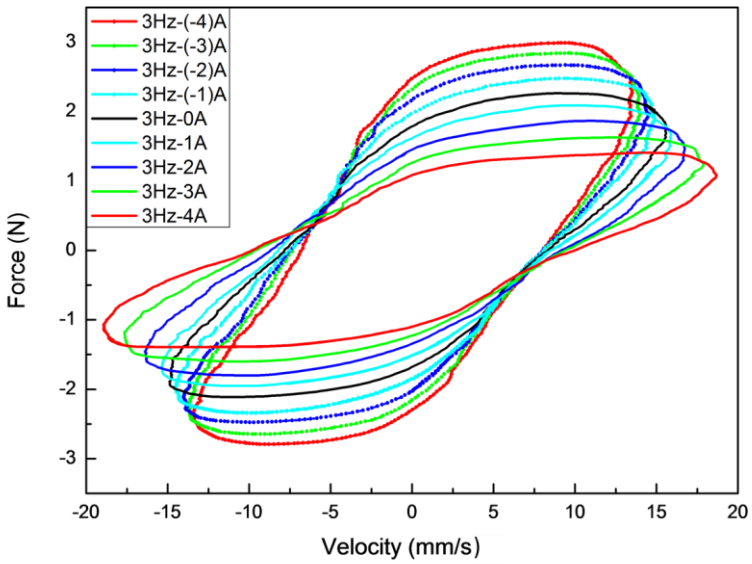

(b)

Figure 4.7 Experimental responses of the MRE isolator under sinusoidal inputs with different currents: (a) Force vs. displacement; (b) Force vs. velocity

One important highlight of this study was that the hybrid magnetic system enabled the MRE isolator to increase and decrease its lateral stiffness, i.e., the force-displacement and force-velocity performances under different levels of current (different magnetic density) but same frequency and amplitude are presented in Figure 4.7. As stated earlier, an electromagnetic field opposite to a permanent magnetic field was generated when a positive current was applied; thus the larger the current is, the smaller the superposition of the hybrid magnetic field will be. Contrarily, the hybrid magnetic field will be strengthened. To better describe the special properties the isolator can achieve, it was defined as a benchmark when no current was applied, as highlighted with a black font in Figure 4.7. But one point must be emphasized: the 'no current' was not equal to its usual passive status because there was a permanent magnetic field working on the system even when no current was applied. Indeed Figure 4.7 shows that the measured force and lateral stiffness tended to be smaller than the benchmark when a positive current was applied, while the equivalent damping (the enclosed area of the force-displacement loop) decreased as the overall magnitude of the hybrid magnetic system was reduced. In those cases where a negative current was applied, the measured force, and the lateral stiffness, as well as the equivalent damping, increased as the amount of current grew. The effective stiffness and equivalent damping of each loading case was calculated and is listed in Table 4.1. The details of the effective stiffness calculation can be found in [182].

Table 4.1 Effective stiffness of the MRE isolator under various applied currents

Current (A)	Effective Stiffness (kN/m)	Equivalent Damping (kN.s/m)
-4	5.31	0.2186
-3	5.08	0.2028
-2	4.62	0.1844
-1	4.13	0.1678
0	3.55	0.1500
1	3.15	0.1334
2	2.64	0.1185
3	2.28	0.09896
4	1.88	0.0800

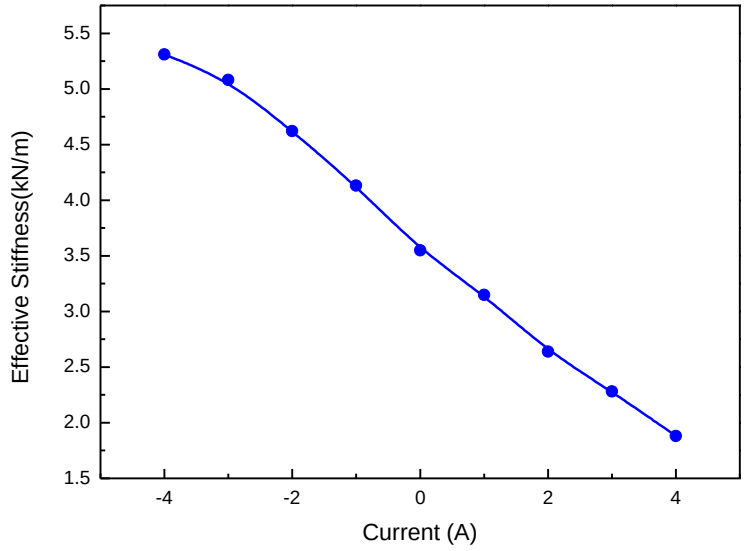

(a)

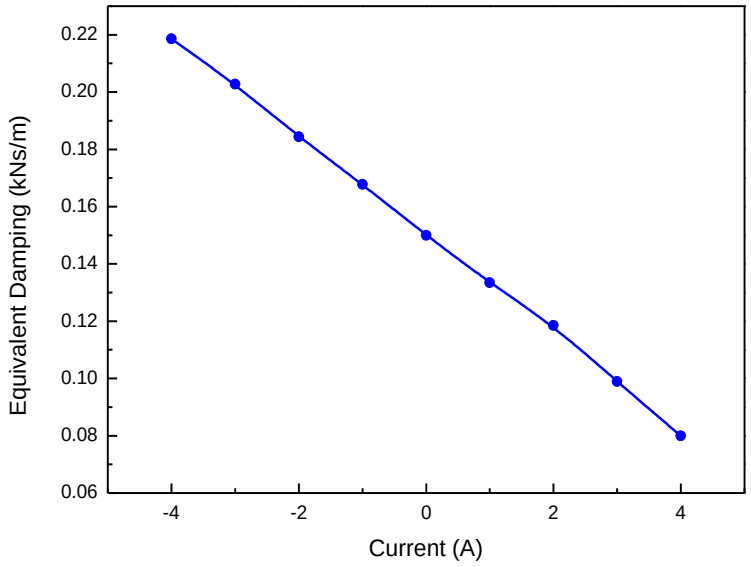

(b)

Figure 4.8 Effective stiffness and equivalent damping under various currents: (a) Effective stiffness vs. curren; (b) Equivalent damping vs. current

It can be summarised from the effective stiffness listed in Table 4.1 that minimum effective stiffness was achieved when the applied current was 4A and the relative change between the minimum and maximum values was 182.4%. Figure 4.8a shows the relationship between the effective stiffness and the current level, where the

effective stiffness was almost a linear function of the applied current in certain areas. Nevertheless, the effective stiffness was not evenly distributed when corresponding to the current, especially when the current was larger. A closer observation reveals that the relative increase of effective stiffness was smaller as the current diverged from zero negatively, which can reasonably be explained as follows. When the current changed to become negative from 0A, the hybrid magnetic field was strengthened as the current kept growing, so initially, the lateral stiffness of the isolator also kept on rising until it eventually reached its saturation point after it increased to a certain value. This explanation applies to Figure 4.8a where the current was negative and the curve gradually tended to become saturated. For those cases where the current was positive, the superposition of the hybrid magnetic field decreased at first and then increased inversely after it reached zero; therefore there must be a critical current that generates just enough of an electromagnetic field to totally eliminate the permanent magnetic field. Accordingly, the lateral stiffness of the isolator will decrease until it reaches its minimum and then begin to grow. Unfortunately, this critical point cannot be observed from Figure 4.8a due to the experimental limitation for a higher current level, but the effective stiffness still decreased linearly in terms of an ascending positive current. As with the effective stiffness, the equivalent damping presented by Figure 4.8b shows a linear relationship in terms of the current. The calculated equivalent damping can be increased or decreased along with the positive or negative current, which matches well with the observations from Figure 4.7.

4.3.3 Transmissibility and Phase responses

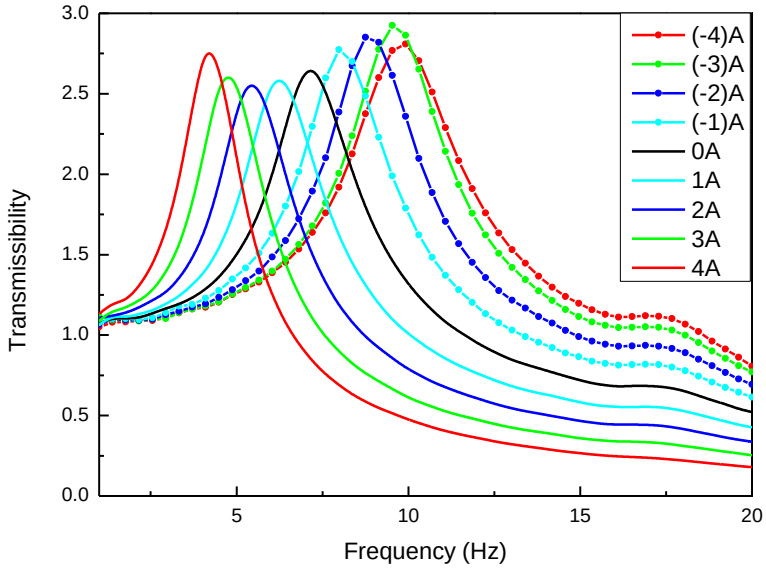

(a)

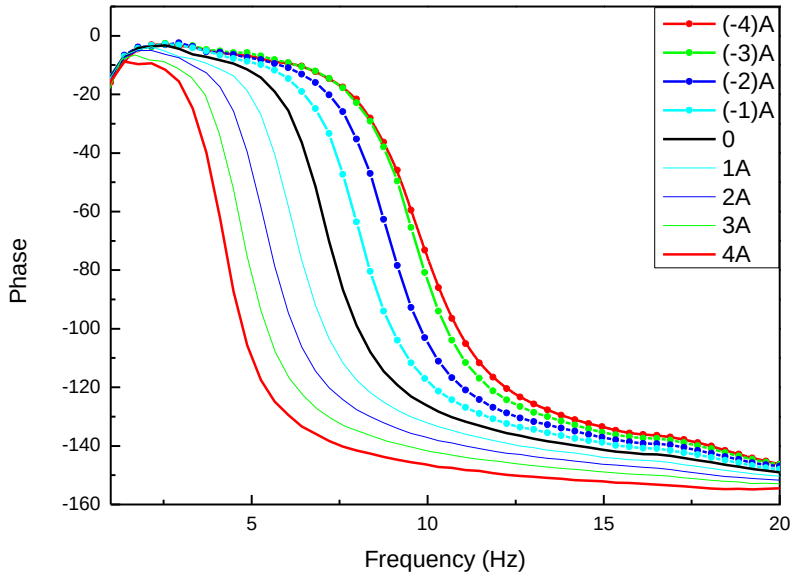

(b)

Figure 4.9 Transmissibility and phase of the MRE isolator under different magnetic field intensity: (a) Transmissibility vs. frequency; (b)Phase vs. frequeny

Table 4.2 Natural frequency of the MRE isolator under various applied currents

Current (A)	Natural Frequency (Hz)
-4	9.85
-3	9.60
-2	8.89
-1	8.04
0	7.14
1	6.23
2	5.43
3	4.75
4	4.20

In this test two accelerometers (CA-YD-106) were installed to measure the lateral acceleration of the top and bottom plates of the isolator respectively. In each case, a sinusoidal excitation with a frequency range sweeping from 1Hz to 20 Hz was used to drive the isolator under various current levels. Figure 4.9 presents the transmissibility and phase performances of the device under different loading conditions and Table 4.2 captures the natural frequency in each single case. Here the natural frequency shifted from 9.85Hz to 4.2Hz as the currents changed from -4A to 4A. The relative change in the natural frequency for these two edge cases was about 135%, demonstrating that the natural frequency of this isolation system can be increased and decreased from a nominal value. As the natural frequency of one system is expressed by:

$$f_0 = \frac{1}{2\pi}\sqrt{\frac{k_{eff}}{m}} \tag{4.1}$$

where f_0, k_{eff}, and m present the natural frequency, effective stiffness, and mass of the system, respectively. The relationship between the natural frequency and the current should show similarities between the effective stiffness and the current. As expected, Figure 4.10 shows that the trajectory of the natural frequency-current curve progress was identical to that shown in Figure 4.8. On one hand the natural frequency changed almost linearly in terms of applied current in some limited areas, but when the current increased or decreased to a larger level negatively or positively,

the natural frequency of the isolator kept climbing until it was saturated or it dropped to a minimum before it began to increase again.

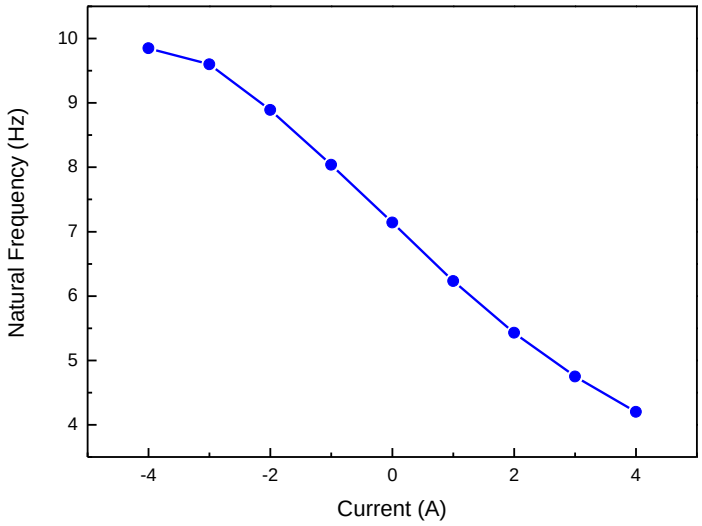

Figure 4.10 Natural frequency as a function of the current

4.4 Vibration isolation experiment

A vibration isolation experiment was conducted to assess the effectiveness of the MRE isolator as an isolation device. As Figure 4.11 shows, the mass attached to the top plate of the isolator served as the primary system. To determine the feasibility of the device as a vibration isolation system, two testing cases were included in this part. In the first case sinusoidal signals with a constant frequency were used as the means of excitation such that further testing subjected the system to a swept sinusoidal signal. In this testing system, the interface used was a Hilink (ZELTOM) board, as shown in Figure 4.11. The HILINK platform offers a seamless interface between physical plants and Matlab/Simulink to implement hardware-in-the-loop real-time control systems. It is fully integrated into Matlab/Simulink and has a broad range of inputs and outputs. Through the HILINK board, the displacement signal was input to the computer after being captured by the displacement sensor. After the captured signal was processed by the Simulink block, the block generated a current signal to the HILINK output channel, through which the output signal was sent to the amplifier.

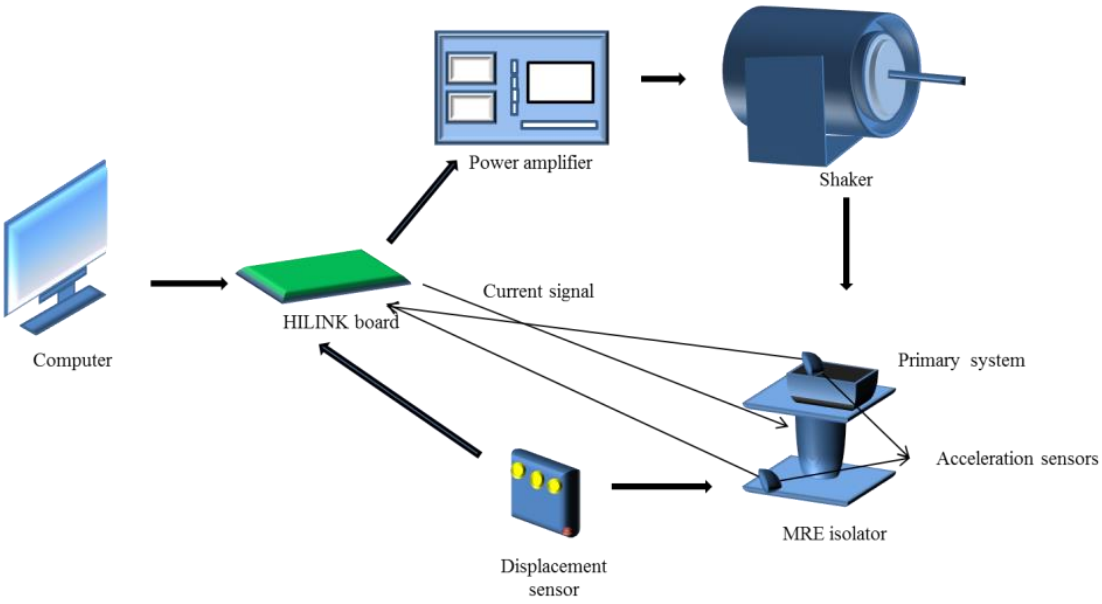

Figure 4.11 Schematic diagram of the vibration isolation experiment

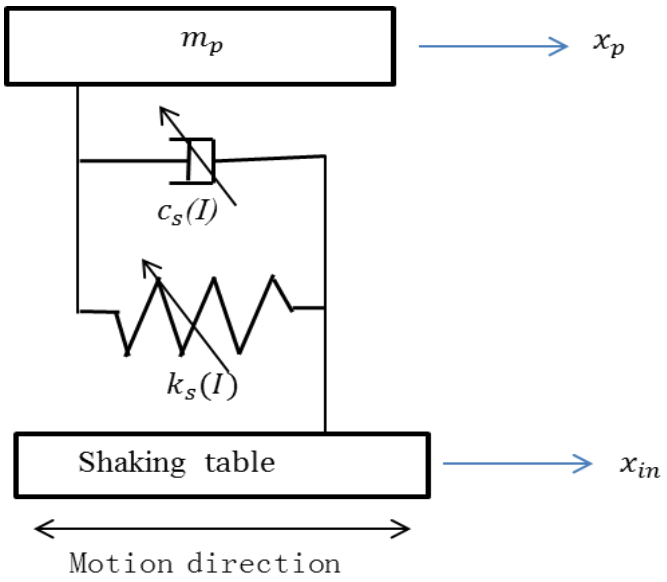

Figure 4.12 The single-degree-of-freedom system

The mathematic model of the vibration isolation system can be represented by a single-degree-of–freedom system, as shown in Figure 4.12. m_p is the mass of the primary system; $c_s(I)$ and $k_s(I)$ represent the controllable damping coefficient and lateral stiffness of the MRE isolator, respectively; x_p and x_{in} are the displacements of the primary system and the driving signal, respectively. The dynamic equation for the system is governed by:

$$m_p\ddot{x_p} + c_s(I)\left(\dot{x_p} - \dot{x_{in}}\right) + k_s(I)\left(x_p - x_{in}\right) = 0 \qquad (4.2)$$

The control algorithm chosen herein, i.e. ON-OFF control, aimed to shift the primary frequency as far away as possible from the frequency of the driving signal. The working logic of the ON-OFF control is such that the lateral stiffness and damping of the isolator will be decreased if the product of the relative displacement and relative velocity of the primary system with respect to the driving excitation is below zero. In other words, a positive current will be chosen if $x_p - x_{in}$ and $\dot{x_p} - \dot{x_{in}}$ are opposite to each other. Otherwise, if the relative displacement and relative velocity are in the same direction, lateral stiffness and damping should be increased. This control logic is concise and simple and yet efficient enough to obtain real time control. The ON-OFF control law is expressed as [31]:

$$I = \begin{cases} 0, & if\left(x_p - x_{in}\right)\left(\dot{x_p} - \dot{x_{in}}\right) > 0 \\ I_{MAX}, & if\left(x_p - x_{in}\right)\left(\dot{x_p} - \dot{x_{in}}\right) < 0 \end{cases} \qquad (4.3)$$

4.4.1 Sinusoidal Excitation

In order to obtain the natural frequency of the isolation system with the attached mass, where the input current was zero, the system was first excited by a swept sinusoidal, and the transmissibility is shown in Figure 4.13. The natural frequency captured was 5.55Hz. Since vibration around a natural frequency is the most severe, three sets of sinusoidal excitation with constant frequency of 5Hz, 5.55Hz, and 7Hz, respectively were used in the first test. To show how effective this vibration isolation was, each testing case was conducted as follows: no control law was applied to the system until the ON-OFF control was turned on; the control law lasted for some time and then it was turned off. This process was done by turning the amplifier, which was connected to the HILINK output channel, on or off.

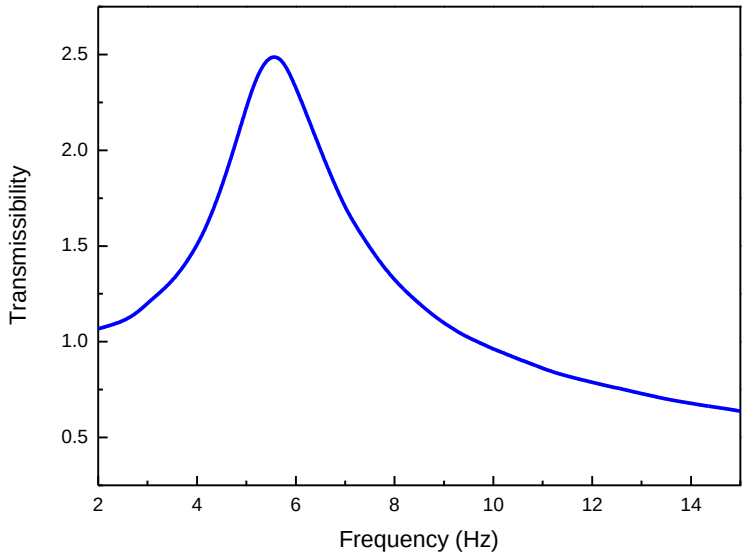

Figure 4.13 Frequency response of the isolation system

Figure 4.14 describes the acceleration measured under different sinusoidal excitations, and in each case, the acceleartion was clearly attenuated during the period when the ON-OFF control logic was working, as marked in Figure 4.14. The relative changes for each testing were 15%, 23.7%, and 28.6%, respectively, which clearly indicated that the MRE isolator was very effective on reducing vibration.

4.4.2 Swept Sinusoidal Excitation

To further evaluate the as-designed vibration isolation system, the response of the primary system under the swept sinusoidal excitation was measured. The working mode without control logic was defined as passive off and the one under ON-OFF control was defined as ON-OFF. A swept sinusoidal covers a frequency band from 2Hz to 15Hz. Figure 4.15 shows the results for the acceleration of the primary system between passive off and ON-OFF. It was noted that vibration in the primary system was significantly suppressed under the ON-OFF control algorithm, and therefore vibration isolation under the ON-OFF control, as shown by the experimental results, was very effecive.

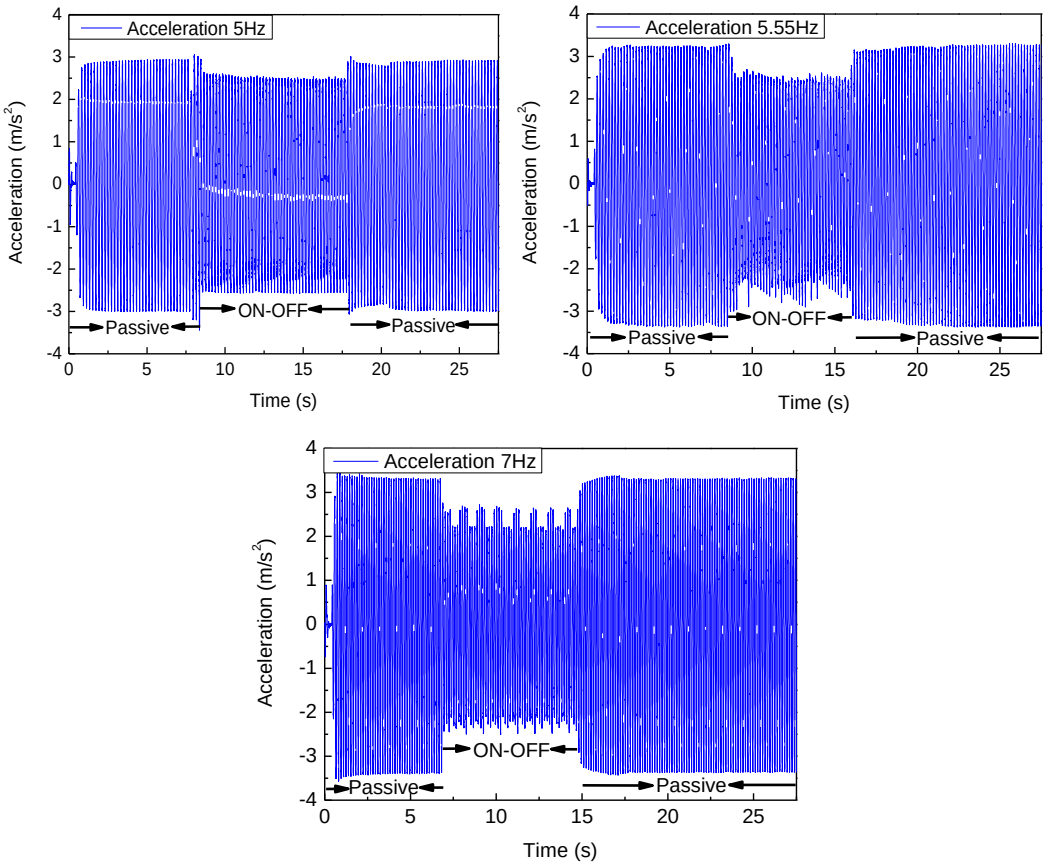

Figure 4.14 Acceleration responses under different sinusoidal excitations

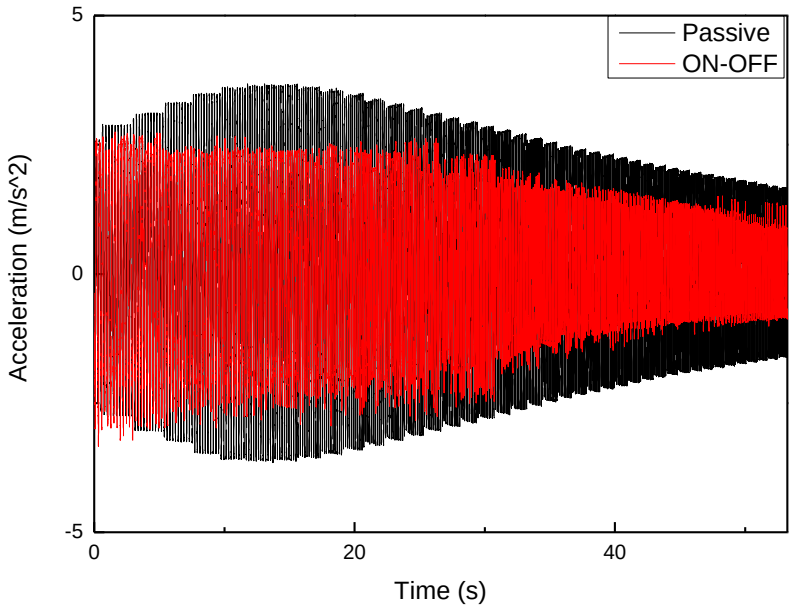

Figure 4.15 Responses under the swept sinusoidal excitation

4.5 Conclusions

A new MRE isolator that includes a hybrid magnetic system was designed and fabricated. This hybrid magnetic system generates a hybrid magnetic field which is the superposition of a permanent magnetic field and an electromagnetic field. The main contribution of this hybrid magnetic system is that it allows the overall magnitude of a magnetic field to be both increased and decreased, and accordingly, the lateral stiffness of the isolator can be both increased and decreased. To verify the specialty of this isolator, a series of dynamic tests were conducted and the results showed that the effective stiffness was reduced when a positive current was applied, and it grows under a negative current. The transmissibility and phase responses showed that the frequency range of the MRE isolator shifted when the applied current varied from -4A to 4A, thus demonstrating that the natural frequency of the isolation system can be increased and decreased. The isolator was also tested for its ability to avoid unwanted vibrations by subjecting the isolation system to sinusoidal signals with constant frequency and swept sinusoidal signals, respectively. Compared to the passive off case where no current was applied, the acceleration for both cases was obviously reduced under the ON-OFF control logic. The experimental results proved that the proposed MRE isolator is a qualified candidate for vibration isolation applications.

5 APPLICATION OF A MULTI-LAYER MRE ISOLATOR ON SUPPRESSING BUILDING VIBRATIONS UNDER SEISMIC EVENTS

5.1 Introduction

Protecting civil engineering structures from uncontrollable events such as earthquakes while maintaining their structural integrity and serviceability is very important. Following the research work introduced in Chapter 4, this chapter uses the stiffness softening MRE isolator in a scaled three story building. In order to construct a closed-loop system, a scaled three story building was designed and built according to the scaling laws, and then four MRE isolator prototypes were fabricated and utilised to isolate the building from the motion induced by a scaled El Centro earthquake. Fuzzy logic was used to output the current signals to the isolators, based on the real-time responses of the building floors, and then a simulation was used to evaluate the feasibility of this closed loop control system before carrying out an experimental test. The simulation and experimental results showed that the stiffness softening MRE isolator controlled by fuzzy logic proved to suppress any structural vibration.

5.2 Experimental setup

5.2.1 Dynamic performance of the stiffness softening MRE isolator.

This stiffness softening MRE isolator used a laminated structure of traditional isolators with 10 layers of MRE sheets bonded onto 11 layers of steel sheets. A permanent magnet was placed at each end of this laminated structure, which was placed along the central axis of the solenoid with an appropriate gap between them. The solenoid was enclosed in a steel cylinder with a top plate and bottom plate, in order to generate a closed loop magnetic field. There was also an appropriate gap between the top plate and steel cylinder for any possible relative movement. The overall magnetic field working on MRE was the superposition of the permanent magnetic field (PMF) and electrical magnetic field (EMF). The direction and the magnitude of the EMF were controlled by the direction and amount of applied direct current. To soften the lateral stiffness, an EMF that was opposed to the PMF was chosen so that the lateral stiffness of the isolator would decrease when the applied current increased, because part of the PMF was offset.

To demonstrate the stiffness softening capability of the MRE isolator, transmissibility under different levels of current were obtained by running the isolator with a sinusoidal swept frequency. As Figure 5.1 shows, two accelerometers measured the acceleration of the top and bottom plates, respectively. The transmissibility of the top and bottom accelerations versus the sweeping frequency is shown in Figure 5.2, and indicates that increasing the applied current decreases the natural frequency and the lateral stiffness of the isolator. The natural frequency decreased from 16.8Hz to 5Hz with a change percent of 70% when the current was changed from 0A to 3A.

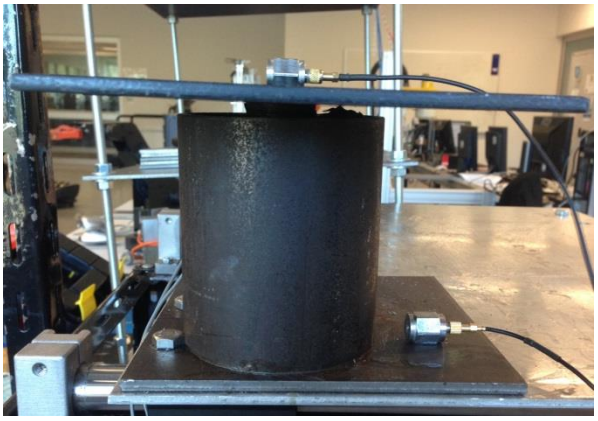

Figure 5.1 Prototype photograph of MRE isolator

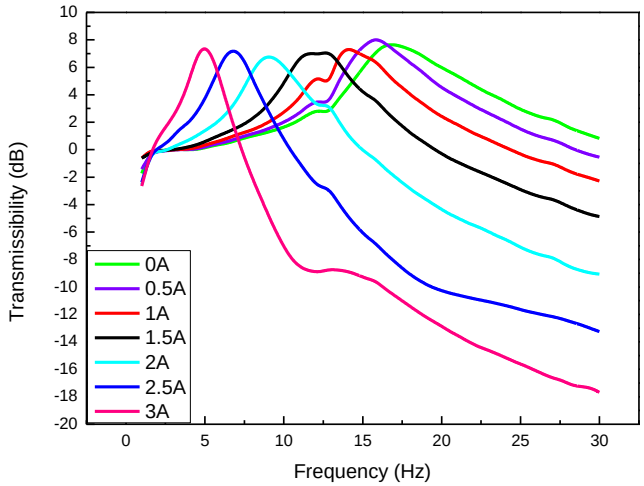

Figure 5.2 Transmissibility of the MRE isolator due to different current

5.2.2 Design of the scaled three story building.

A model three story building was designed and built with a length scale factor of 1:9. The height of the first two stories was 0.75m, which corresponds to a real three story building approximately 10m high. All the variables and dimensions were scaled down according to the scaling laws [207], with some examples shown in Table 5.1.

Table 5.1 Scaling factors of the variables

Variables	Length	Displacement	Acceleration	Time
Scaling factor	1:9	1:9	1	1:3

Figure 5.3 shows a schematic view of the scaled building model with four MRE isolators. The three story building with adjustable masses was fixed to the top plates of the four isolators, and the isolators were fixed to the shaking table via two linear shearings. The building with four isolators was forced to vibrate horizontally by a shaker (VTS, .VC 100-8) driven by a signal source from the computer through a power amplifier (YE5871). DC power was ready at hand to supply current signals to the isolators when needed.

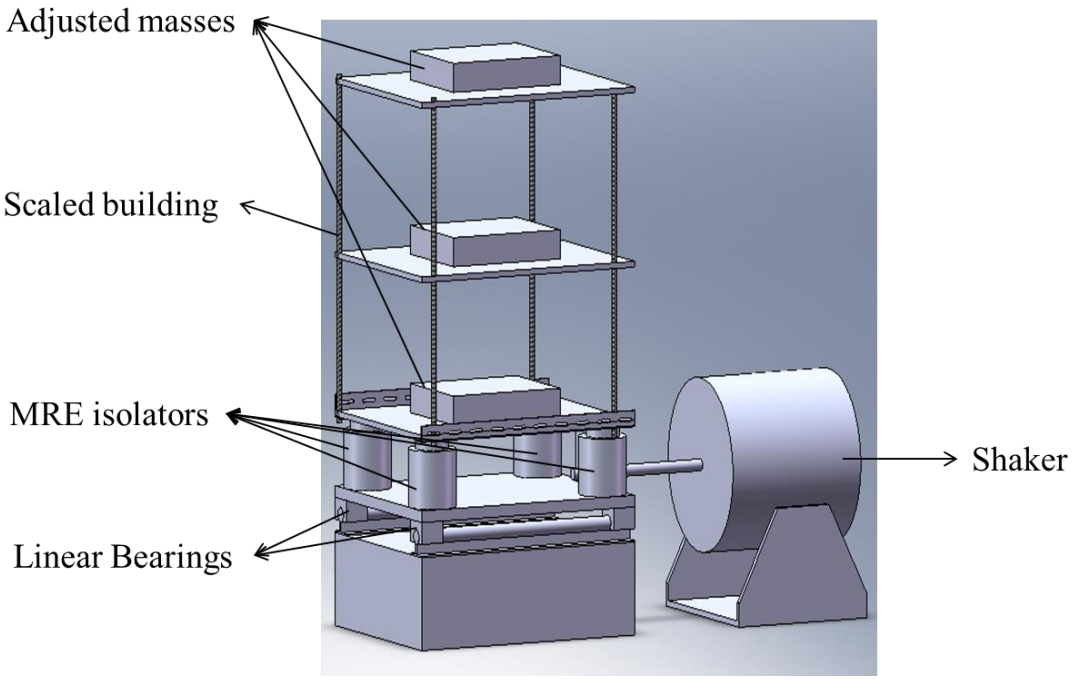

Figure 5.3 Schematic view of the scaled building model

5.2.3 Closed loop control system.

The interface used to link the software and hardware was a HILINK board (ZELTOM) that offers a seamless interface between physical plants and Matlab/Simulink to implement hardware-in-the-loop real-time control systems. It was fully integrated into Matlab/Simulink and has a broad range of inputs and outputs. Figure 5.4 shows a schematic diagram of the closed control system. The real-time responses of the building were transmitted to the computer through the HILINK input channels, after being processed and calculated by the controller in the computer, a current signal was sent to the isolators through the HILINK output channel.

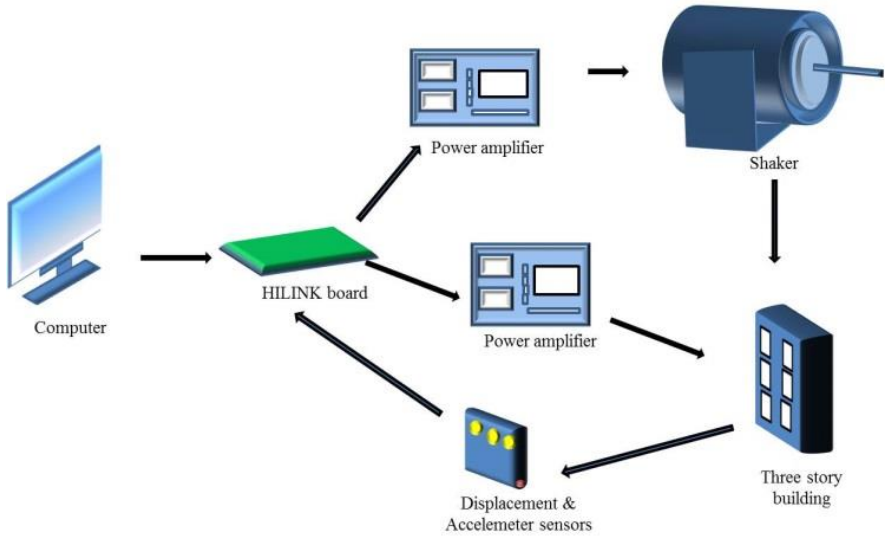

Figure 5.4 Schematic diagram of the closed-loop control system

Figure 5.5 shows the whole isolation system where the scaled El Centro seismic motion was used to excite the shake platform and the fuzzy logic controller designed in the Simulation (Section 3.2) was used to change the stiffness of the isolation system in real-time. Two laser displacement sensors (MICRO-EPSILON Company) were used to measure the relative displacements of the third floor to the first floor, and the first floor to the ground motions, respectively. Another laser sensor (DT20-X224Bx, SICK) recorded the displacement data of the 'ground motion', and three accelerometers recorded the accelerations of three floors, respectively. Three cases were considered in this experiment: 'fixed base' means the building was fixed to the shake table directly without isolators between them; 'passive' means no

control logic was applied to but isolators were included in this system; ‘controlled’ means the isolation system was controlled by fuzzy logic.

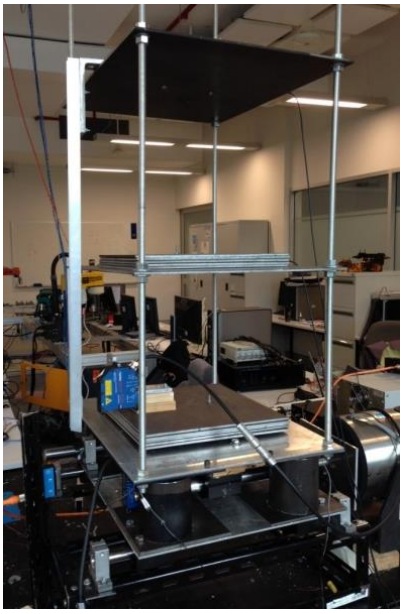

Figure 5.5 Photograph of the practical experimental setup

5.3 Simulation

5.3.1 Modelling the isolated building.

By considering a three degrees-of-freedom (DOF) linear building structure controlled by four isolators and subject to a horizontal earthquake excitation (1940 El Centro), as shown in Figure 5.6, the motion equations can be written as:

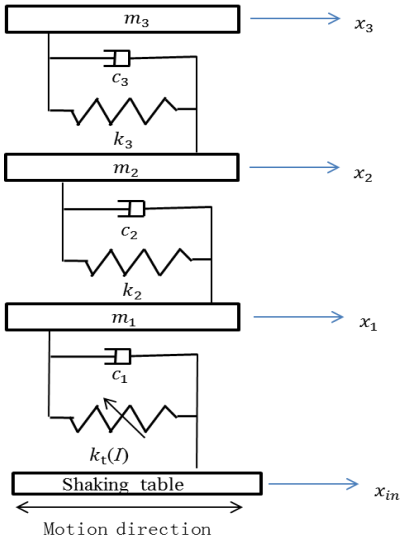

Figure 5.6 Mathematical model of the scaled building

$$m_1\ddot{x_1} + c_2(\dot{x_1} - \dot{x_2}) + k_2(x_1 - x_2) + c_1\dot{x_1} + k_t(I)x_1 = -m_1\ddot{x_g}$$

$$m_2\ddot{x_2} - c_2(\dot{x_1} - \dot{x_2}) - k_2(x_1 - x_2) + c_3(\dot{x_2} - \dot{x_3}) + k_3(x_2 - x_3) = -m_2\ddot{x_g}$$

(5.1)

$$m_3\ddot{x_3} - c_3(\dot{x_2} - \dot{x_3}) - k_3(x_2 - x_3) = -m_3\ddot{x_g}$$

$$M\ddot{X} + C\dot{X} + KX = -M\ddot{x_g}$$

where

$X = [x_1 \quad x_2 \quad x_3]^T$, $M = \begin{bmatrix} m_1 & 0 & 0 \\ 0 & m_2 & 0 \\ 0 & 0 & m_3 \end{bmatrix}$, $C = \begin{bmatrix} c_2 & -c_2 & 0 \\ -c_2 & c_2 + c_3 & -c_3 \\ 0 & -c_3 & c_3 \end{bmatrix}$

,$K = \begin{bmatrix} k_2 & -k_2 & 0 \\ -k_2 & k_2 + k_3 & -k_3 \\ 0 & -k_3 & k_3 \end{bmatrix}$,m_i (i=1, 2, 3) is the mass of the *i*th floor; x_i (*i*=1, 2, 3) is the relative displacement of the *i*th floor with respect to the ground; c_i (*i*=2, 3) and k_i (*i*=2, 3) is the damping and stiffness coefficients of inter floors, respectively; $c_t(I)$ and $k_t(I)$ are the current-dependent damping and stiffness coefficients of the isolators, respectively. The masses of the building model are identical for each story unit and given as m_i=25Kg, for *i*=1, 2, 3.

5.3.2 Fuzzy logic controller

Fuzzy logic control can offer a simple and robust framework for specifying nonlinear control laws that can accommodate uncertainty and imprecision [208, 209]. Alternatively, a fuzzy controller does not rely on the analysis and synthesis of the mathematical model of the process, so the uncertainties of input data from external loads and structural response sensors were treated in a much easier way by the fuzzy controller than with classical control theory. Fuzzy logic uses IF-THEN rules as an interface to connect the inputs and outputs, which means that continuous inputs are transformed into linguistic variables which are then converted into numerical values through defuzzication. In semiactive control, the numerical values provide control commands that vary the mechanical properties of a semiactive control device. In this study the relative displacement between the first and third floors, the first floor displacement, and the scaled earthquake velocity data were used as inputs to obtain the lateral stiffness of the MRE isolators controlled by the controller output.

The designing process of a fuzzy controller begins with choosing inputs and output, and defining the membership functions (MFs). As mentioned before, the inputs chosen were x_3-x_1, x_1, $\dot{x_g}$, where x_3-x_1 is the control target which is supposed to be

small as much as possible; x_1, is the relative displacement to the ground of the first floor, together with $\dot{x_g}$ which predicts the direction the earthquake will move and also determines the relative position of the isolators to the ground. Each input has two member functions which were abbreviated to: P-Positive, N-Negative. The output is the current signal and the membership functions were defined as: L-Large, S-Small. Table 5.2 gives the inference rule based on the three inputs. It should be noted that the softening lateral stiffness of the isolator corresponds to the largest value of the current.

Table 5.2 The inference rule of the fuzzy logic

Variable	MF							
x_3-x_1	N	N	N	N	P	P	P	P
x_1	N	P	N	P	N	P	N	P
$\dot{x_g}$	P	P	N	N	P	P	N	N
Isolator stiffness	Soft	Hard	Soft	Hard	Hard	Soft	Hard	Soft
Current	L	S	L	S	S	L	S	L

5.3.3 Simulation results

The 1940 El Centro record was chosen as the input to the simulation and experiment since it covers a wide frequency range. A Simulink model that incorporated the isolated building and fuzzy logic algorithm was built. The responses of the inter-story displacement and relative acceleration were good demonstrations for the effectiveness of the control logic. Figure 5.7 shows the maximum inter-story displacements of x_3-x_1 and x_2-x_1. Here the performances of the controlled case and passive case were much better than the fixed case. The maximum value under fuzzy logic was 28.6% and 36.4%, which was smaller than under the passive operation for x_3-x_1 and x_2-x_1, respectively. Figure 5.8 shows the simulation results in terms of relative acceleration under three cases. From an overall aspect, the controlled situation performed best and the fixed situation performed the worst. A closer analysis of the simulated data reveals that the peak accelerations $\ddot{x_3}$, $\ddot{x_2}$, and $\ddot{x_1}$, were reduced by 16.7%, 26.8%, and 15%, respectively, under fuzzy logic control, rather than under a passive operation. The simulation results verified that the isolated building performed better under fuzzy logic.

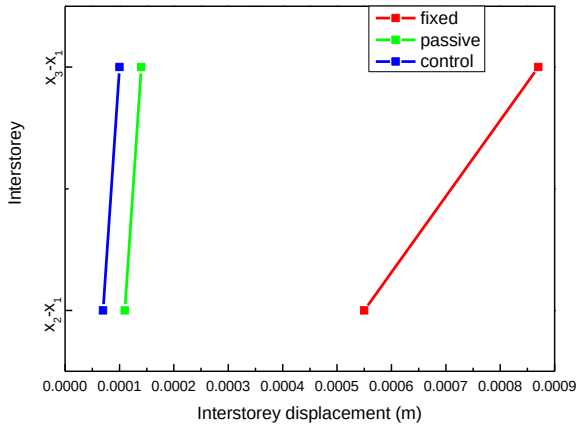

Figure 5.7 Maximum values of the inter-story displacement

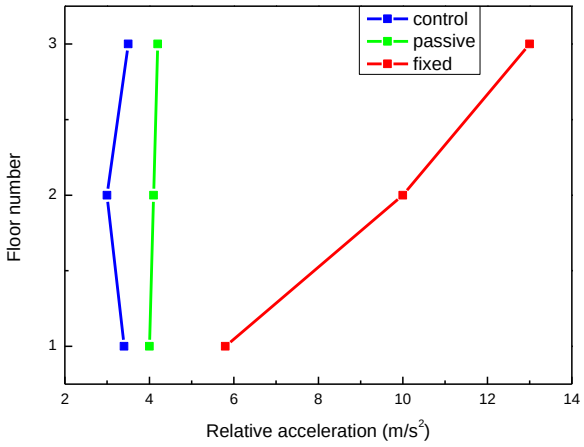

Figure 5.8 Maximum values of the relative accelerations for three floors

5.4 Experimental results and discussion

The transmissibility of the earthquake motion to the building was measured first by subjecting the isolation system to a sinusoidal sweeping signal, as shown in Figure 5.9. Obviously, the transmissibility decreased dramatically for the semi-active case, unlike the passive case, which was up to 38.7%. Figure 5.10 shows the first floor displacement to the 'ground motion' such that the magnitude under control was larger than in a passive operation. This was reasonable because the softened isolators under fuzzy logic gave the building more freedom to move, relative to the 'ground'. This did not alter the effectiveness of isolation because the objective was to minimise the inter-story displacement to protect the building from fracture or collapse. Figure

5.11 clearly shows the relative displacement between the first floor and the third floor in three cases, where obviously, the 'fixed base' had the worst performance and the controlled case had the minimum magnitude over the whole period. This minimisation of inter drift would really help the building survive seismic events. Now look at the accelerations of the second floor and the third floor individually, as shown in Figure 5.12 and Figure 5.13, respectively. The isolated building definitely performed better than the fixed one, as the difference between the passive case and fixed case show, but it is also clear that the maximum magnitude in the passive case decreased dramatically in the controlled case. Moreover, the reduction in vibration continued until the scaled earthquake ended.

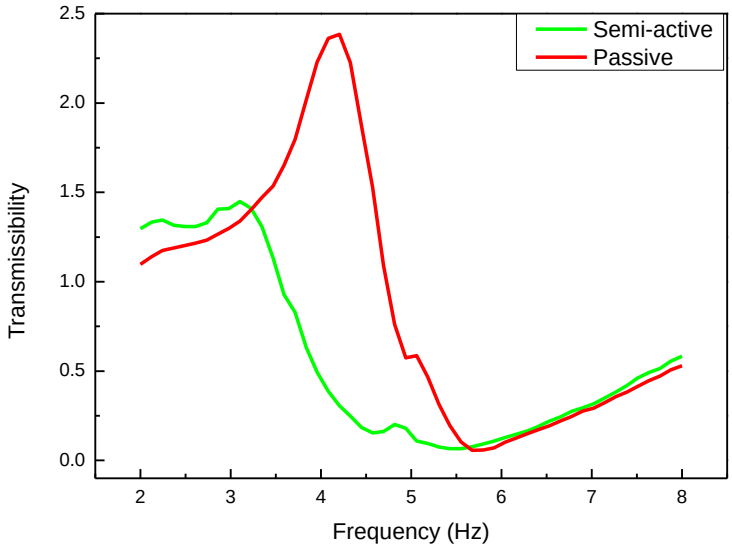

Figure 5.9 The transmissibility of earthquake motion to the building for passive and semi-active cases

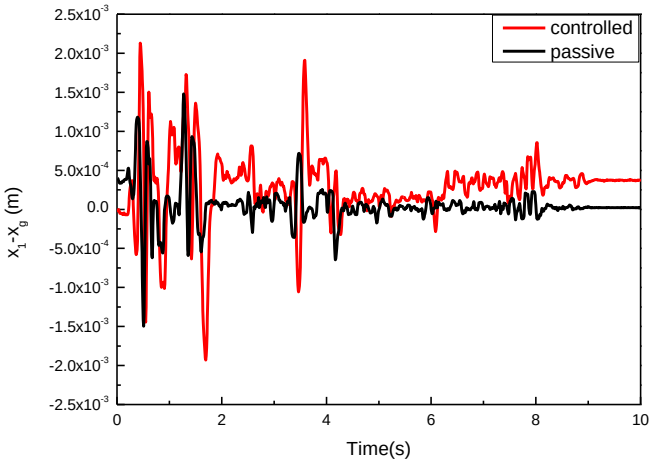

Figure 5.10 The relative displacement of the first floor to the ground

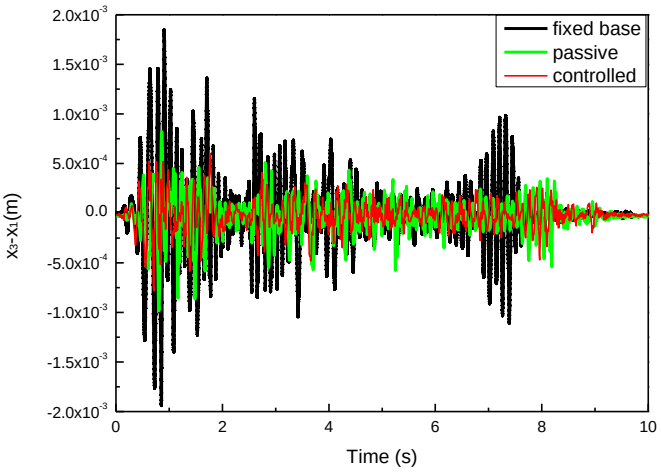

Figure 5.11 The relative displacement of the third floor to the first floor

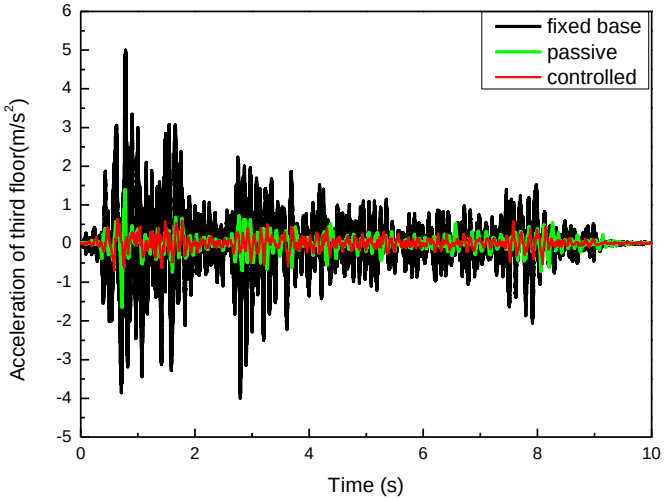

Figure 5.12 The acceleration response of the third floor

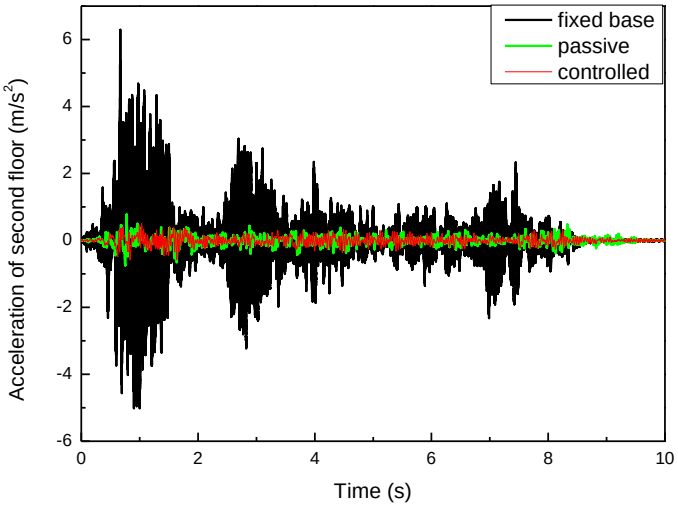

Figure 5.13 The acceleration of the second floor

Table 5.3 Peak responses of structures due to the El Centro earthquake

Control strategy	x_1-x_g (m)	x_3-x_1(m)	$\ddot{x}_3(m/s^2)$	$\ddot{x}_2(m/s^2)$
Fixed base	None	1.92×10^{-3}	5.02	Passive6.33
Passive	1.49×10^{-3}	9.91×10^{-4}	1.65	0.78
Controlled	2.14×10^{-3}	7.75×10^{-4}	0.67	0.58
Percent reduction ((controlled-passive)%/passive)	NA	21.80%	59.39%	25.64%
RMS(Controlled)	5.08E-04	1.38E-04	1.37E-01	1.03E-01
RMS (Passive)	2.42E-04	1.80E-04	1.83E-01	1.14E-01
RMS (Fixed)	0	4.14E-04	7.03E-01	8.30E-01
(RMS(Passive)-RMS(Control))%/ RMS(Passive)	NA	23.3%	25.1%	9.6%

The peak responses of the structures for each control strategy are provided in Table 5.3; obviously the fixed base did not perform as well as the passive case and controlled case. Moreover the data indicates that fuzzy logic control effectively reduced the peak responses due to the El Centro earthquake, particularly the inter-story drift and the accelerations. The maximum inter-story displacement (x_3-x_1) of 21.8% decreased more under fuzzy logic control than in a passive operation. It was remarkable that the peak third floor acceleration ($\ddot{x}_3$) was 59.4% smaller with fuzzy logic than with the passive control, while peak acceleration of the second floor ($\ddot{x}_2$) decreased by up to 25.6%. The superiority of the controlled case is also evidenced by the RMS values. It is seen that the RMS values for each parameter is much smaller under the fuzzy logic than under passive operation. These results are quite persuasive and indicate that fuzzy logic was a better choice than semi-active control.

5.5 Conclusions

A model three story building with a scaling factor of 1:9 was designed and built for experimental tests. Four MRE isolators that can remain stiff under normal operating conditions without any power consumption and soften its lateral stiffness to isolate the building from seismic hazards were mounted between the shake table and the model. A scaled El Centro earthquake motion was used as input to excite the isolation system, and fuzzy logic was used to output the current signal sent to change the mechanical property of the isolators in real-time. Both of these simulations and

the experimental results showed that fuzzy logic reduced the inter-story drift and acceleration over the full time range. The reductions in acceleration of the third floor and second floor were by approximately sixty per cent and one quarter, respectively, and relative displacement between the third floor and first floor decreased by more than 20 per cent. These results verified that the stiffness softening MRE isolators isolated vibrations and also proved that fuzzy logic was a better choice for semi-active control.

6 A SEMI-ACTIVE MRE TUNED MASS DAMPER FOR BUILDING PROTECTION BASED ON MAGNETORHEOLOGICAL ELASTOMERS

6.1 Introduction

Apart from the base isolator as one of the effective way for building protection from seismic events, tuned mass damper (TMD) is also an attractive method. This chapter investigates and evaluates a semi-active tuned mass damper which incorporates four multi-layered MRE structures. The four MRE structures formed a square and provided the tuned mass damper variable stiffness used to track the excitation frequencies. This design not only increases the stability of the tuned mass damper but more importantly eliminates the magnetic circuit gap in a design which we used in the past because all four of the magnetic circuits used to control the MRE isolators are closed circuits. In order to verify the capability of the MRE-based tuned mass damper to protect a building from an earthquake, extensive simulation and experimental testing were conducted. The swept sinusoidal signal and the scaled 1940 El Centro earthquake record were used to excite a scaled three story building. Both simulation and experiment have verified that the MRE-based tuned mass damper outperformed all other passive tuned mass dampers under either swept sinusoidal or seismic conditions.

6.2 Design and prototype of the proposed MRE TMD

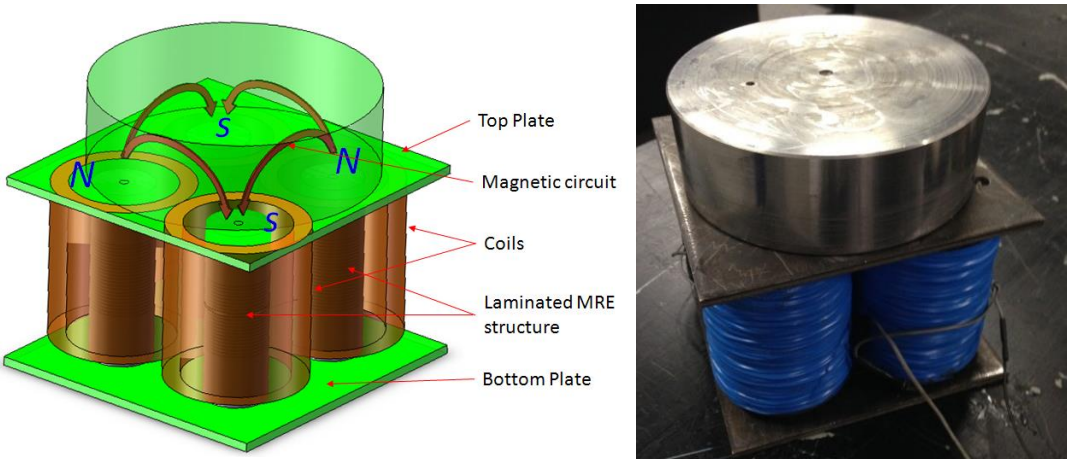

Figure 6.1 Structure and photograph of the MRETMD

One of the innovations in this design is the adoption of the multi-layered MRE and steel structure. This multi-layered structure has been popular and used for MRE

isolators [20, 21, 197] and absorbers [210] for the advantages that it not only improves the overall conductivity of MRE but enables large lateral displacement as well. However, one big challenge is the inevitable magnetic flux leakage (MFL) [211]. The most challenging target in designing the magnetic circuit of the MRE-based device is to form an enclosed magnetic path with minimum leakage. Only in this way can the magnetic flux leakage can be minimized and the magnetic flux density maximized in the MRE. To avoid any magnetic flux leakage, this study proposes a new design which assembles four multi-layered MRE structures together, as shown in Figure 6.1. It is seen that the four multi-layered structures form a square layout which is a more stable structure and retains sufficient lateral flexibility. These four structures are in series connection when current is applied. The most noteworthy point of this design is that one totally closed magnetic circuit forms between any two adjacent multi-layered structures and thus there are a total of four closed magnetic circuit. Any two adjacent structures have opposed winding directions of solenoid, so that they will generate opposed magnetic fields when the current is applied. It is shown in Figure 6.1 that the magnetic induction lines come out of the N-pole one solenoid and go inside the S-pole of one adjacent solenoid, or vice versa. The clear advantage of this design is that it guarantees most of the magnetic flux pass through the MRE structures with minimum magnetic flux leakage. The prototype of the proposed MRETMD is also shown in Figure 6.1. A mass of 8 Kg is attached on the top of the MRE structures to improve the energy absorption efficiency of the TMD. The detailed size of the MRE TMD is shown in Table 6.1.

Table 6.1 PARAMETERS OF MRE TMD

Parameters	Values		Parameters	Values
h_1	40 mm		L_1	50 mm
h_2	1 mm		L_2	5 mm
d_1	35 mm		L_3	100 mm
d_2	55 mm		L_4	5 mm
d_3	80 mm		L_5	5 mm
Excitation coil	1000 turns			

After prototype was constructed, the magnetic flux density passing through the MRE was calculated using the following equations.

The magnetic resistance of the MRE layers and steel layers can be calculated by:

$$R_1 = \frac{20h_2}{\pi(d_1/2)^2\mu_1\mu_0} + \frac{20h_2}{\pi(d_1/2)^2\mu_2\mu_0} \quad (6.1)$$

The magnetic resistance of the four steel pillars is:

$$R_2 = \frac{4h_1}{\pi(d_1/2)^2\mu_2\mu_0} \quad (6.2)$$

The magneticresistances of the top and bottom plates are:

$$R_3 = \frac{2d_3}{2d_3L_5\mu_2\mu_0} \quad (6.3)$$

where μ_0 is the vacuum permeability; μ_1 is the relative permeability of the MRE and μ_2 is the relative permeability of the low carbon steel.

The overall magnetic resistance is given by:

$$R_m = R_1 + R_2 + R_3 \quad (6.4)$$

Thus the following equation can be obtained following Ohm's law:

$$2NI = B_g S_g R_m \quad (6.5)$$

where S_g is the area of the MRE layers and B_g is the magnetic flux density of the MRE layers. NI is the magnetomotive force of one coil. The calculation results of the two structures are shown in Table 6.2. Based on these results, it can be seen that the new structure can generate stronger magnetic flux density under the same current.

Table. 6.2 The magnetic flux density of the two structures

Currents	0A	0.5A	1A	1.5A	2A	2.5A
B_g (Prior design) T	0	0.08	0.17	0.25	0.34	0.42
B_g (New design) T	0	0.12	0.24	0.36	0.49	0.60

6.3 Frequency shift test of the MRETMD

6.3.1 Experimental setup

The frequency-shift property is a key criterion to evaluate the effectiveness and controllability of a semi-active MRETMD. In this experiment, a series of tests using swept sinusoidal signals were conducted to measure the frequency-shift performance. Figure 6.2 illustrates the detailed experimental setup, which mainly consists of the shaker and the horizontal vibration platform. The MRETMD was fixed onto the platform with two accelerometers (CA-YD-106) installed onto the top and bottom plates, respectively, measuring their lateral accelerations. This vibration platform was forced to vibrate horizontally by a shaker (VTS, VC 100-8) driven by a harmonic signal generated by a computer and amplified by a power amplifier (YE5871). A DC power supply (THURLBY-THANDAR, INSTRUMENTS LTD) was used to provide current signals to the solenoids. A data acquisition (DAQ) board was used as the interface between the hardware and the software and transferred the measured accelerations to the computer. The signal collection, recording, and processing were developed using the LabVIEW program. With this system, the transmissibility of the laminated MRETMD with different currents was recorded and displayed directly onto the computer.

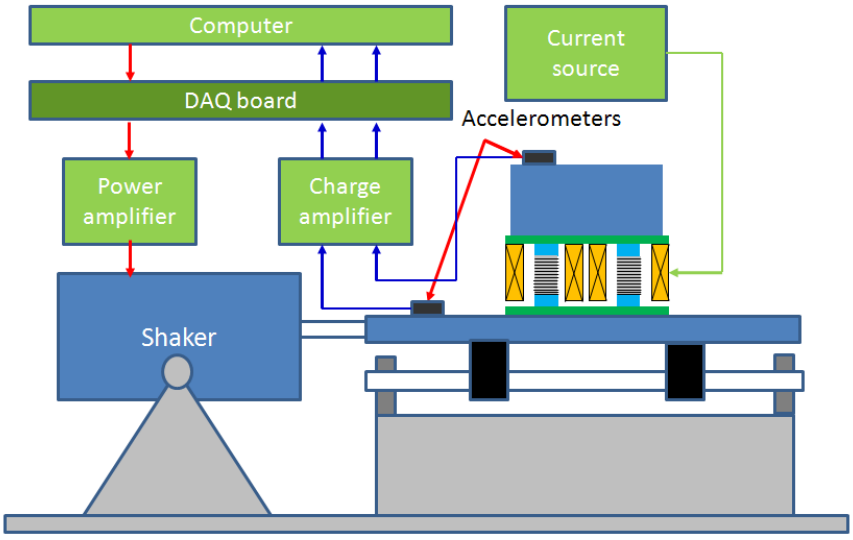

Figure 6.2 Experimental set up for testing the frequency shift property of MRETMD

6.3.2 Testing results

In this test, the DC current was varied from 0A to 2.5A with a step of 0.5A. A total of 6 testing cases were conducted. Figure 6.3 records the frequency-shift performances (transmissibility and phase) under various current conditions. It is seen that the natural frequency increased from 3.1Hz to 7.1Hz when the current was changed from 0A to 2.5A. The relative change of the natural frequency was about 229%, demonstrating that this MRETMD has a wide effective frequency bandwidth.

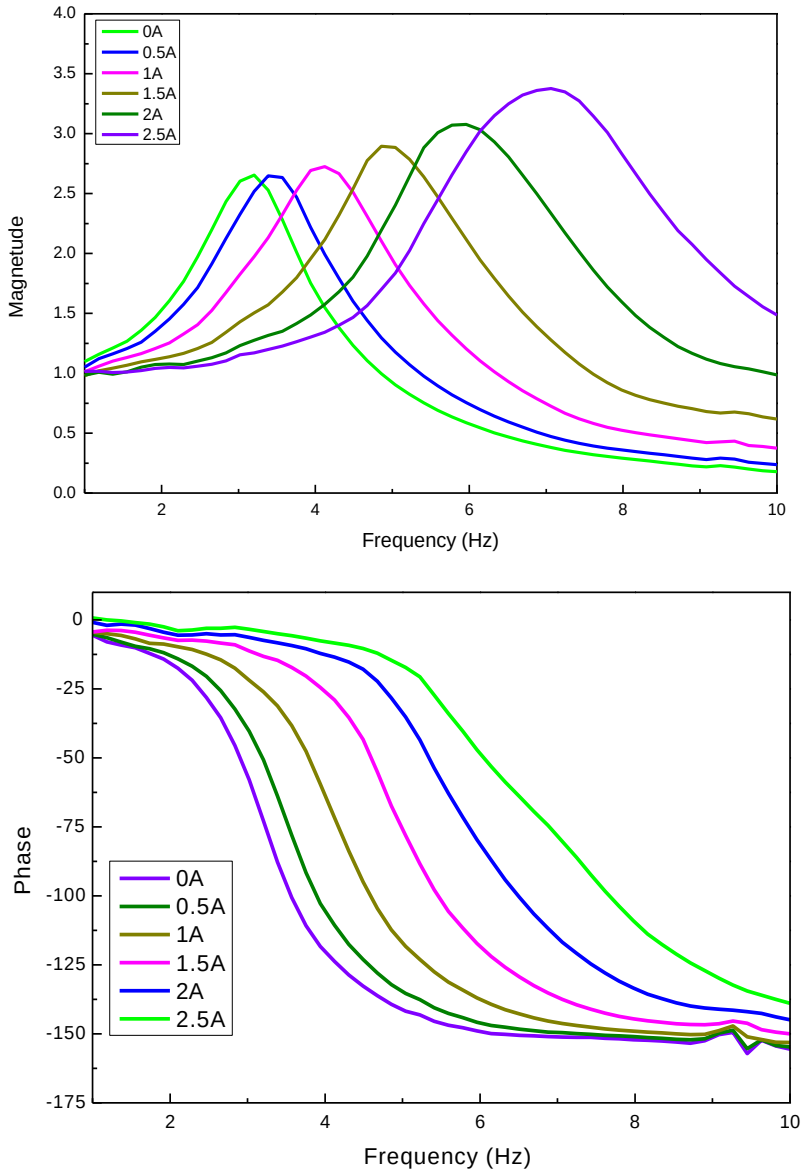

Figure 6.3 Transmissibility of the MRETMD under different currents

6.4 Simulation of the scaled building with MRETMD

6.4.1 Modelling the isolated building

A three story building model was designed and built first. All the variables and dimensions were scaled down according to the scaling laws in [207]. Detailed scaled rules can be referenced to Table 5.1. The height of the building is 0.75m, which corresponds to a real three story building of approximately 6.75m high. By considering a three degrees-of-freedom (DOF) linear building structure with a MRETMD on the top subject to ground motion, as shown in Figure 6.4, the motion equations can be written as:

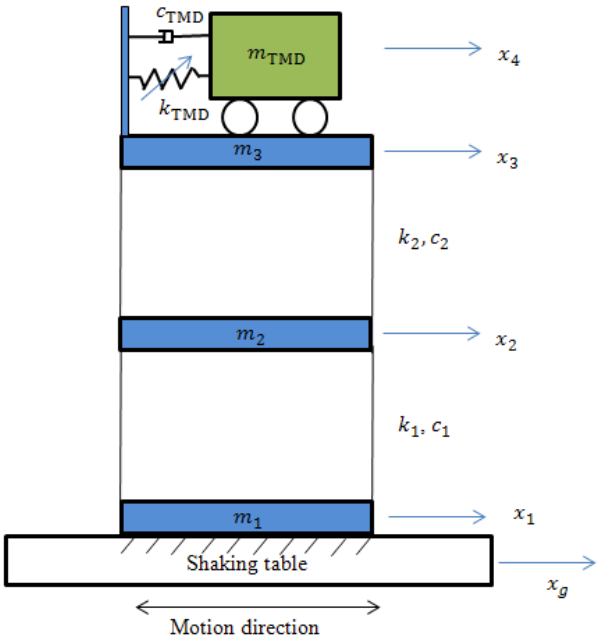

Figure 6.4 Mathematical model of the scaled building

$$m_2\ddot{x}_2 + c_2(\dot{x}_2 - \dot{x}_3) + k_2(x_2 - x_3) + c_1\dot{x}_2 + k_1x_2 = m_2\ddot{x}_g \quad (6.6)$$

$$m_3\ddot{x}_3 - c_2(\dot{x}_2 - \dot{x}_3) - k_2(x_2 - x_3) + c_{TMD}(\dot{x}_3 - \dot{x}_4) + k_{TMD}(x_3 - x_4) = m_3\ddot{x}_g \quad (6.7)$$

$$m_{TMD}\ddot{x}_4 - c_{TMD}(\dot{x}_3 - \dot{x}_4) - k_{TMD}(x_3 - x_4) = m_{TMD} \quad (6.8)$$

where $X = [x_1 \quad x_2 \quad x_3]^T$, $M = \begin{bmatrix} m_1 & 0 & 0 \\ 0 & m_2 & 0 \\ 0 & 0 & m_3 \end{bmatrix}$, $C = \begin{bmatrix} c_2 & -c_2 & 0 \\ -c_2 & c_2 + c_3 & -c_3 \\ 0 & -c_3 & c_3 \end{bmatrix}$,$K = \begin{bmatrix} k_2 & -k_2 & 0 \\ -k_2 & k_2 + k_3 & -k_3 \\ 0 & -k_3 & k_3 \end{bmatrix}$, m_i (i=1, 2, 3) is the mass of the *i*th floor; x_i (*i*=1, 2, 3) is the relative displacement of the *i*th floor with respect to the ground; c_i (*i*=1, 2) and k_i (*i*=1, 2) is the damping and stiffness coefficients of inter floors, respectively; c_{TMD} and k_{TMD} are the current-dependent damping and stiffness coefficients of the MRETMD, respectively. The masses of the building model are identical for each story unit and given as m_i=25Kg, for *i*=1, 2, 3.

6.4.2 Fuzzy logic controller

Fuzzy logic control can offer a simple and robust framework for specifying nonlinear control laws that can accommodate uncertainty and imprecision [208, 209].

Alternatively, a fuzzy controller does not rely on the analysis and synthesis of the mathematical model of the process, so the uncertainties of input data from external loads and structural response sensors were treated in a much easier way by the fuzzy controller than with classical control theory. Fuzzy logic uses IF-THEN rules as an interface to connect the inputs and outputs, which means that continuous inputs are transformed into linguistic variables which are then converted into numerical values through defuzzication. In semiactive control, the numerical values provide control commands that vary the mechanical properties of a semiactive control device. In this study, the relative displacement and velocity between the top plate and bottom plate of the MRETMD were used as inputs to control the lateral stiffness of the MRETMD controlled by the controller output.

The designing process of a fuzzy controller begins with choosing inputs and output, and defining the membership functions (MFs). As mentioned before, the inputs chosen were $x_4 - x_3$ and $\dot{x_4} - \dot{x_3}$. Each input has two member functions which were abbreviated to: P-Positive, N-Negative. The output is the current signal and the membership functions were defined as: L-Large, S-Small. Table 6.3 gives the inference rule based on the two inputs.

Table 6.3 The inference rules of the fuzzy logic

Variables	MF			
$x_4 - x_3$	N	N	P	P
$\dot{x_4} - \dot{x_3}$	N	P	P	N
MRETMD stiffness	Hard	Soft	Hard	Soft
Current	L	S	L	S

6.4.3 Simulation results.

A Simulink model that incorporated the three story building model was built. The swept sinusoidal signal and the scaled 1940 El Centro record were then chosen as the input to the simulation program. The simulation results include the transmissibility responses under the swept sinusoidal signal, and the peak values for the accelerations and relative displacement under El Centro motions, of the third floor and the second

floor. Figure 6.5 and Figure 6.6 show the transmissibility responses of the third floor and the second floor to ground motion, respectively. Each of the two figures includes nine cases which are the building without TMD, seven different 'passive' cases, and a semi-active TMD. Here the 'passive' means that a certain current level was applied to the MRETMD, such as 0A, 0.5A, etc., so that these passive MRETMDs are different from each other but with fixed parameters (stiffness and damping), while the semi-active case means that the parameters of the MRETMD can be continuously adjusted in real time. From Figure 6.5 and Figure 6.6, it is seen that the testing result of the case without TMD has only one peak while the other seven passive cases all have two peaks; and that the two peaks of each curve shifted to the right when the applied current increased. The lowest point between the two peaks of any passive curve indicates the most effective point where the MRETMD absorbed the largest amount of energy. From Figure 6.5 and Figure 6.6, it can be seen that the effective points of each passive MRETMD are near their natural frequencies and shifted to right with the increase of currents. In terms of the semi-active MRETMD, it can vary its natural frequency to trace the excitation frequency based on STFT control algorithm [31]. Thus, the semi-active MRETMD can reach all the most effective points and is shown as the red line in Figure 6.5 and Figure 6.6. The semi-active MRETMD can reach the lowest transmissibility and outperforms all other passive TMDs. In order to further verify the effectiveness of MRETMD, the performance of the MRETMD controlled by fuzzy logic control algorithm was evaluated under earthquake excitation. The simulation results are shown in Figure 6.7 and Figure 6.8. It is seen that the peak values of acceleration and relative displacement change as the currents changes, but the responses of semi-active remain the best among all cases, especially for the relative displacement. These two figures effectively demonstrated the efficiency of the semi-active MRETMD outperforms than other passive TMD on reducing the accelerations and relative displacements.

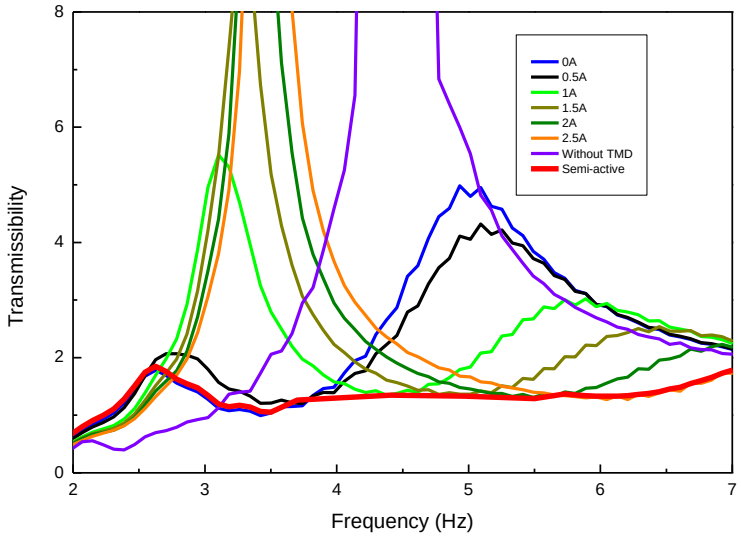

Figure 6.5 Transmissibility from ground to the third floor under the swept sinusoidal signal

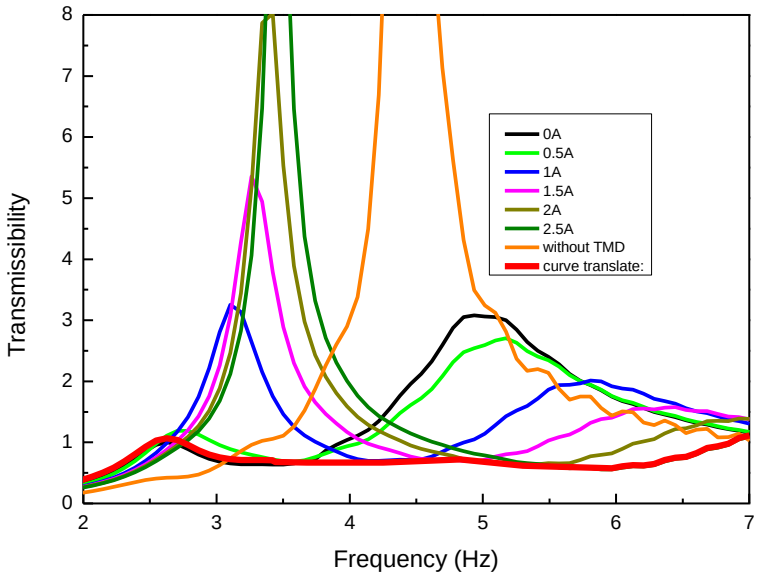

Figure 6.6 Transmissibility from ground to the second floor under the swept sinusoidal signal

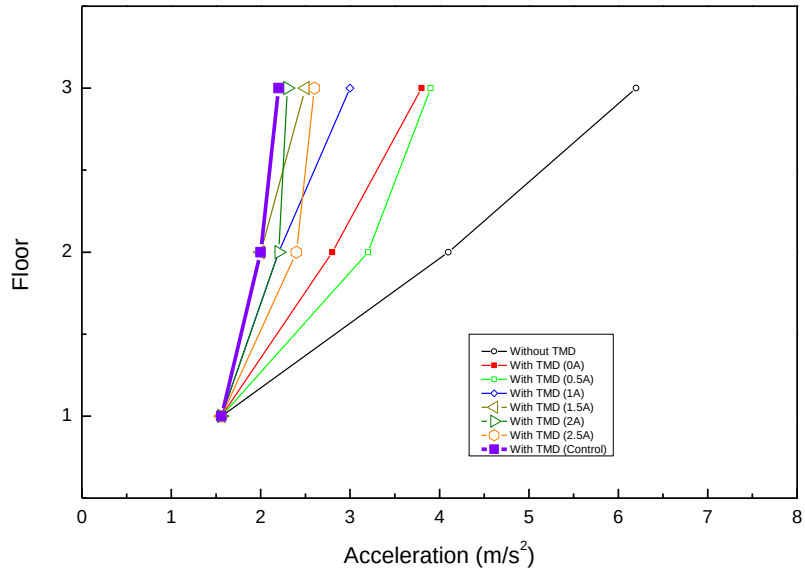

Figure 6.7 Peak values of acceleration of three floors with respect to the ground under El Centro motions

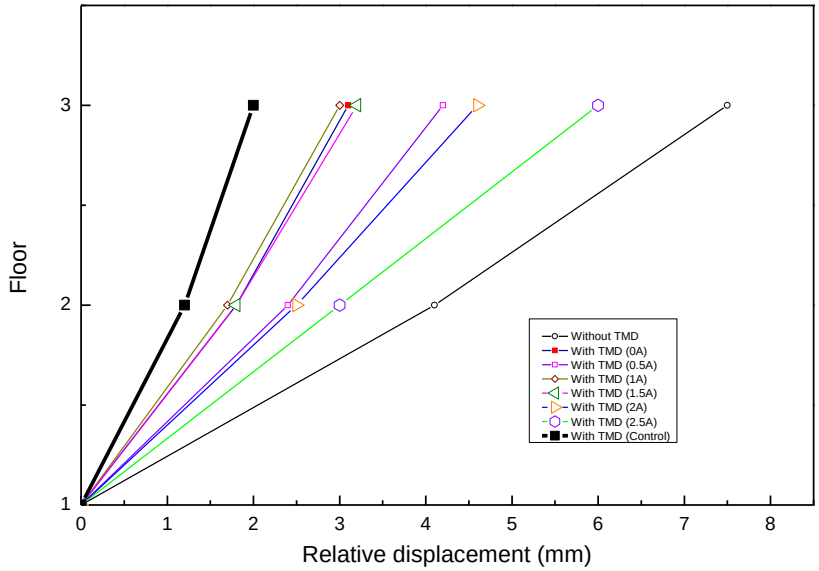

Figure 6.8 Peak values of relative displacement of three floors with respect to the ground under El Centro motions

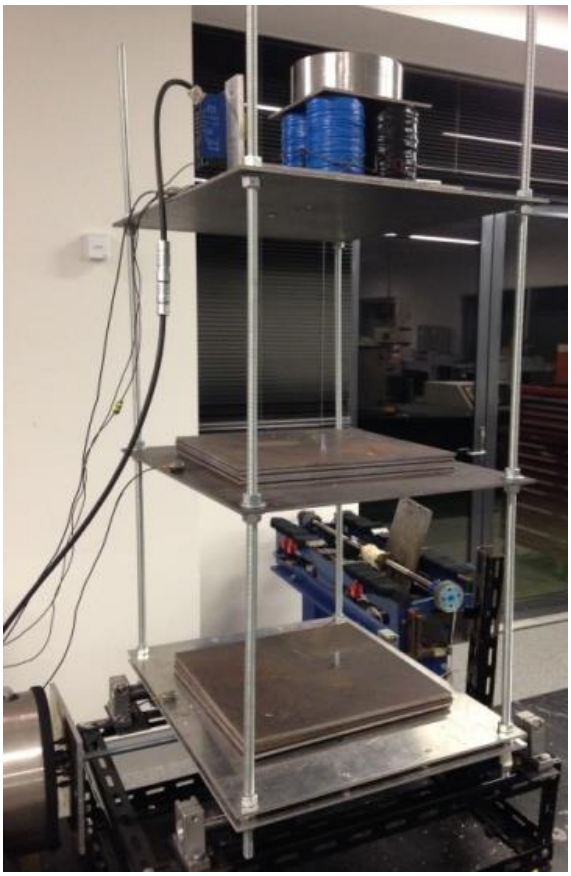

Figure 6.9 Photograph of the practical experimental set up

6.5 Experimental verification

6.5.1 Experiment setup

Figure 6.9 shows the whole experimental set up where the three story building model was fixed onto the platform with the MRETMD mounted on the top. The first floor stays relatively static with the vibration platform since they are screwed together. Three accelerometers (CA-YD-106) were used to measure the accelerations and displacements of the three floors, respectively. A laser displacement sensor (MICRO-EPSILON Company) was mounted on the top floor to monitor the relative motion between the top plate and the bottom one of the MRETMD. The first part of the experiment was conducted by running the whole system under the swept sinusoidal excitations, which consisted of a total of 8 cases for study and comparison. The second part used the scaled 1940 El Centro data as the excitation to simulate a real seismic scenario. The following subsections have given the detailed illustrations and analyses.

6.5.2 Experimental result under swept excitation

Figure 6.10 and Figure 6.11 show the transmissibility from the ground to the third and the second floors, respectively, under the swept sinusoidal excitations. The testing conditions are the same as used in the simulation results shown by Figure 6.5 and Figure 6.6. A total of six passive TMD with different currents and the building without TMD were tested. The observations in the experimentally obtained results match well with that in the simulation results (Figure 6.5 and Figure 6.6). There is only one peak for the case without TMD and two peaks for the six passive cases. The testing results indicate that the most effective vibration absorption points of each passive TMD shifted to right with the increase of current. The semi-active MRETMD controlled by STFT algorithm can trace the excitation frequency and reach the most effective vibration absorption points under each excitation frequency and its transmissibility, which outperforms than all of the passive TMDs, is shown as red lines in Figure 6.10 and Figure 6.11.

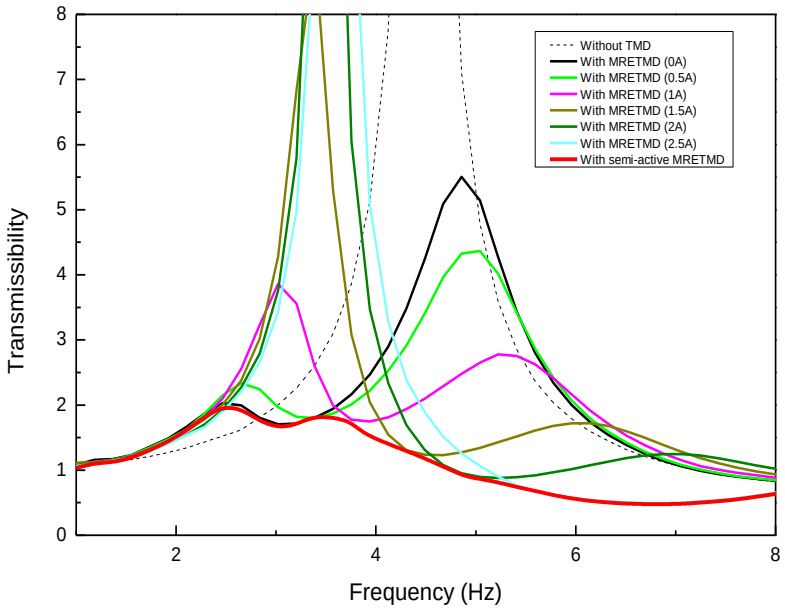

Figure 6.10 Experimentally obtained transmissibility from ground excitation to the third floor

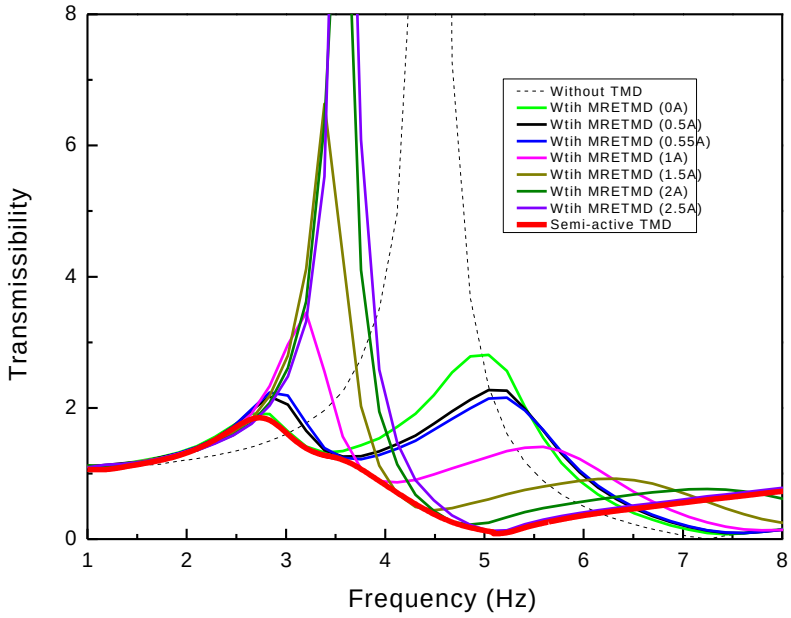

Figure 6.11 Experimentally obtained transmissibility from ground excitation to the second floor

6.5.3 Experiment results under earthquake excitation

Three testing cases were included in this part, which are the three story building without the MRETMD, with passive MRETMDs, and with semi-active MRETMD under fuzzy logic. Figure 6.12 shows the relative displacement between the ground and the third floor. It is obvious that the building without a TMD has the largest peak response and performs worst during the entire time history; the passive case (no current applied to the MRETMD) has better performance than the first testing case, though, are much less than the semi-active case where fuzzy logic was used. Similarly, the same observations can be found from Figure 6.13 which shows the relative displacement between the ground and the second floor. The responses of the case without MRETMD remain the worst and responses of semi-active case perform best among these three cases.

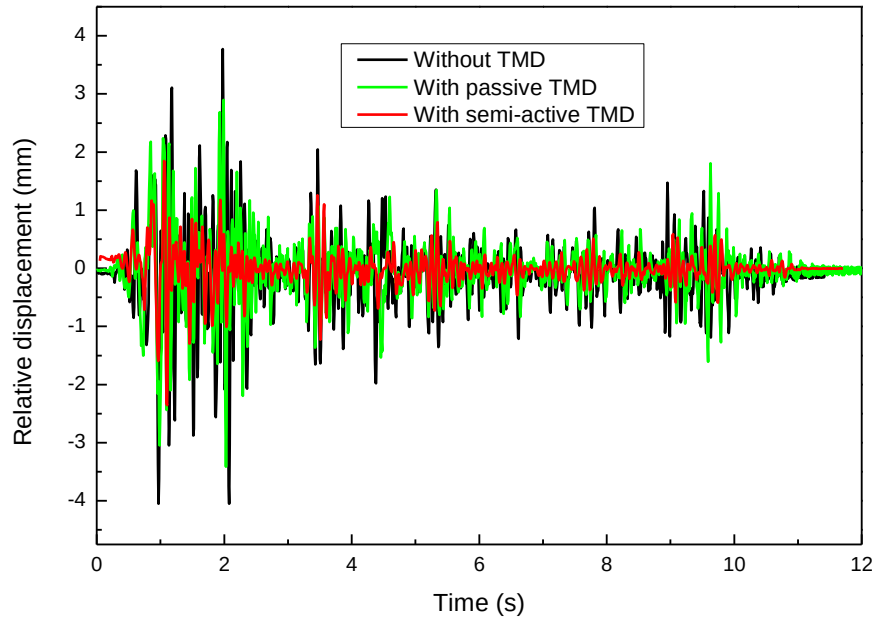

Figure 6.12 Relative displacement between ground and the third floor

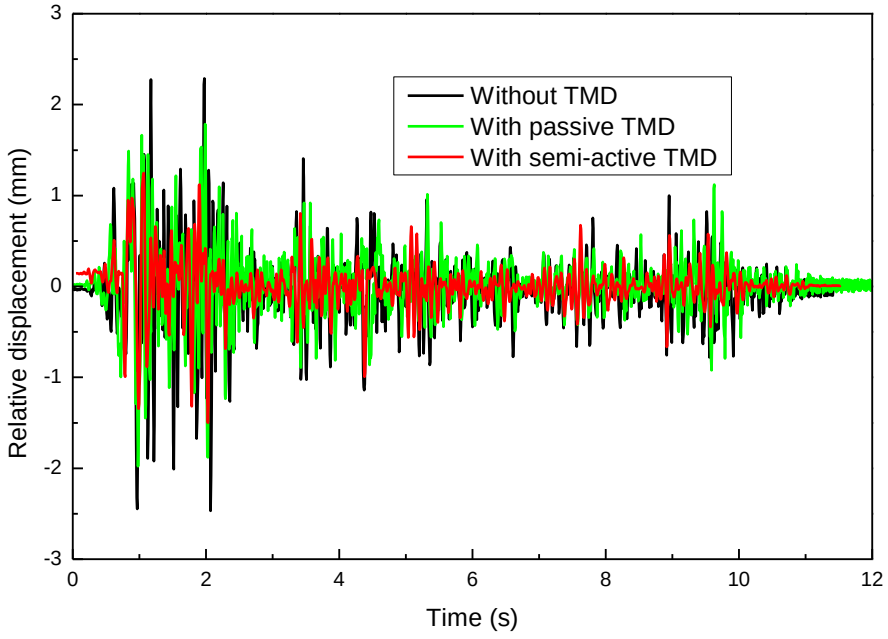

Figure 6.13 Relative displacement between ground and second floor

Figure 6.14 and Figure 6.15 show the accelerations of the third floor and the second floor under three cases, respectively. It is seen that the acceleration responses of the first case are comparable to those of the passive case during some periods; however, the semi-active case still performs best during the whole time history. Table 6.4 shows the RMS of the inter-story drift and floor accelerations. Figure 6.16 and Figure 6.17, which correspond to the simulation results shown by Figure 6.7 and

Figure 6.8, present the relative acceleration and relative displacement of each floor with respect to the ground, respectively. Similarly, each of the two figures includes eight testings which are the building without TMD, six different 'passive' cases, and a semi-active case. Each of the seven passive cases has fixed parameters but is different from each other due to different current levels, while the semi-active used the fuzzy logic control so that the parameters of the MRETMD can be continuously adjusted in real time. The experimental results are consistent with the simulation results shown by Figure 6.7 and Figure 6.8. The peak values of the accelerations and relative displacements under semi-active control remains the smallest among all the cases, especially for the relative displacement. All of the observations and analyses from the experimental results have verified sufficiently that this semi-active MRETMD under fuzzy logic guarantees the best vibration reduction performance among all the tested cases.

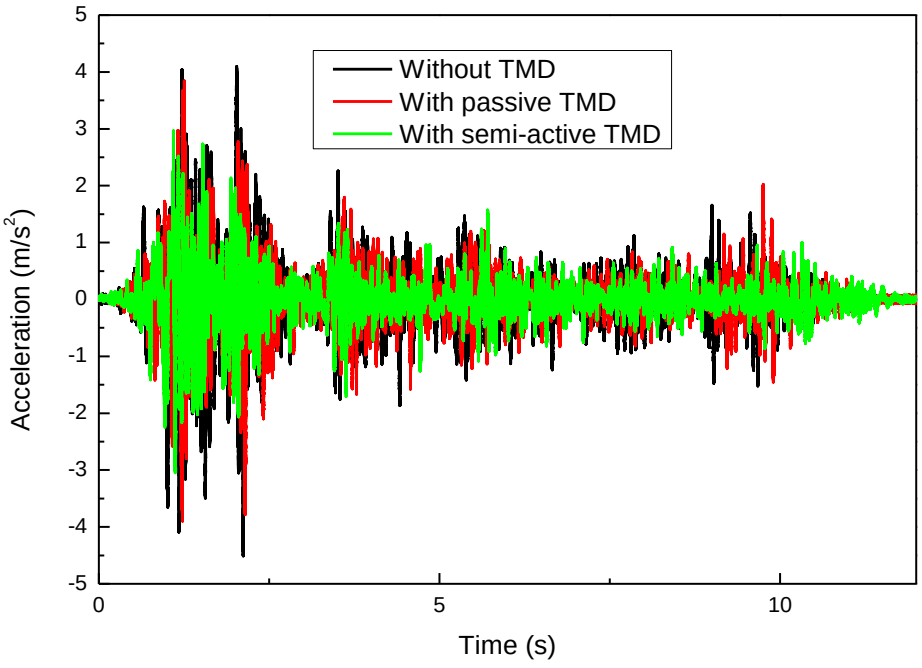

Figure 6.14 Acceleration of the third floor

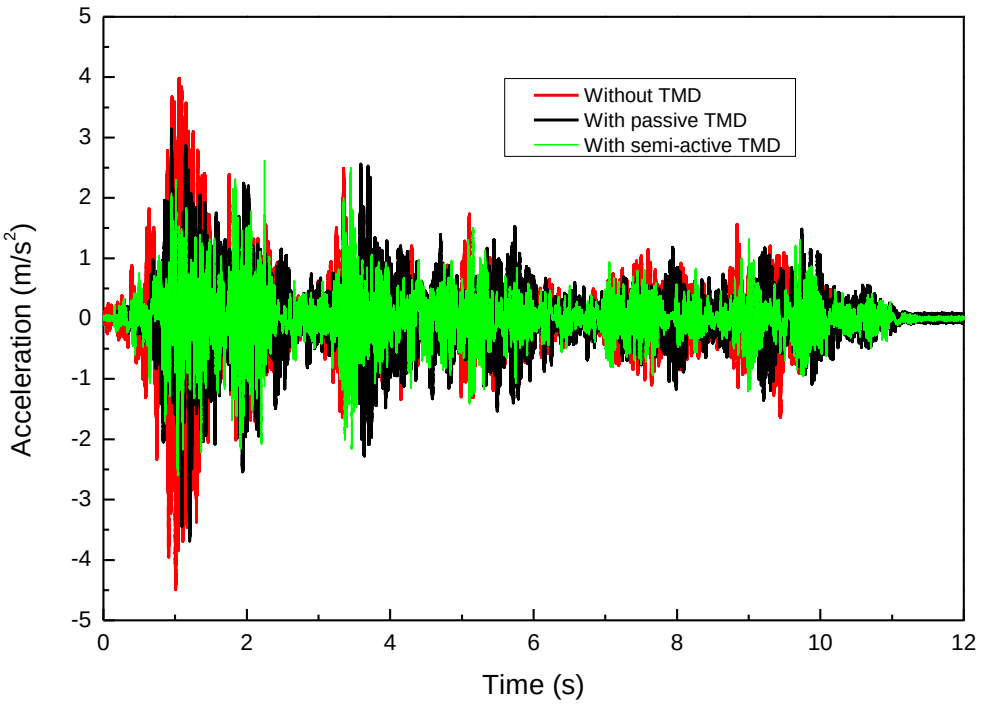

Figure 6.15 Acceleration of the second floor

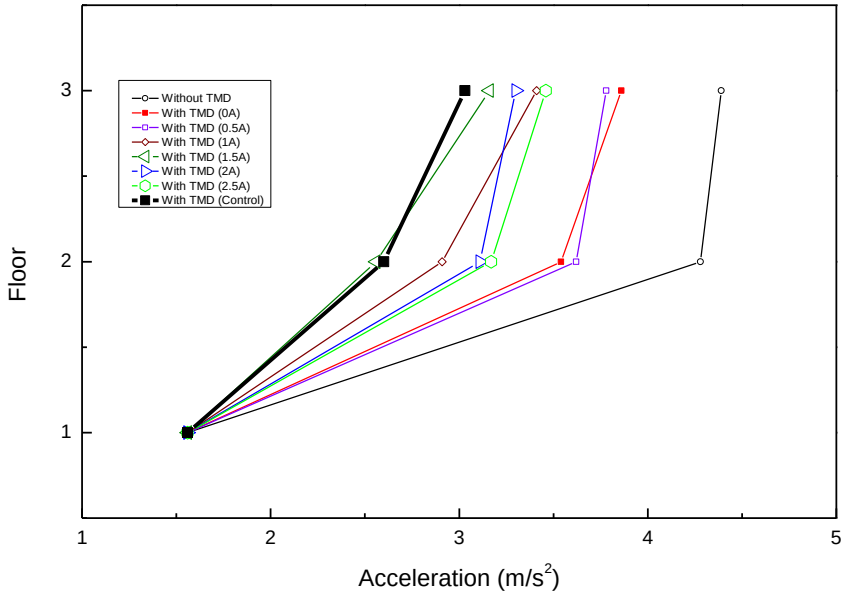

Figure 6.16 Peak accelerations of the building floors with different TMDs

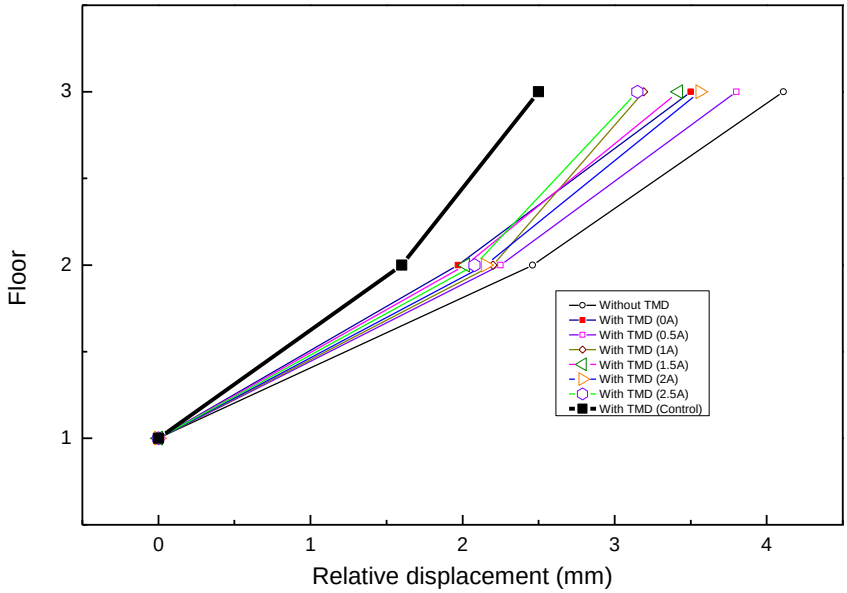

Figure 6.17 Peak relative displacements of the building floors with different TMDs

Table 6.4 RMS of the inter-story drift and accelerations

Control strategy	x_3-x_g (m)	x_2-x_g(m)	$\ddot{x}_3(m/s^2)$	$\ddot{x}_2(m/s^2)$
RMS(Semi-active)	0. 31	0. 26	0. 43	0. 44
RMS (Passive)	0. 54	0. 34	0. 52	0. 54
RMS (Without TMD)	0. 67	0. 42	0. 68	0. 64
(RMS(Passive)-RMS(Semi-active)%/ RMS(Passive)	43. 3%	24. 9%	16. 8%	19. 6%

6.6 Conclusions

This chapter introduced an innovative MRETMD which included four multi-layered MRE structures. This new design not only maintains the advantage of big lateral flexibility but also improves the efficiency of the magnetic field by generating four closed magnetic circuits. The frequency shifted from 3.1Hz to 7.1Hz when the current was changed from 0A to 2.5A has indicated the effectiveness and controllability of the MRETMD as a method to reduce vibrations. The simulation and experimental results fully verified its potential to protect the building from ground motions. The transmissibility responses, the relative displacement, and the relative acceleration as well as the peak displacement and the acceleration have

clearly showed the superiority of the semi-active MRETMD over the passive TMDs or the case without TMD.

7 A NEW MRE TMD WITH DOUBLE NATURAL FREQUENCIES FOR WIDE FREQUENCY BANDWIDTH VIBRATION REDUCTION

7.1 Introduction

As an extension of the work in Chapter 6, the design of an adaptive tuned vibration TMD is refined to have two natural frequencies in this chapter for vibration reduction. The innovation of the new MRETMD is the adoption of the eccentric mass on the top of the multilayered MRE structure and thus the proposed TMD has two vibration modes: one in the torsional direction and the other in translational direction. This property enables the TMD to expand its effective bandwidth and to be more capable of reducing the vibrations especially dealing with those vibrations with multi-frequencies. The MRETMD was designed and tested on a horizontal vibration table. The test results illustrate that the MRETMD realized double natural frequencies, both of which are controllable. Inertia's influence on the dynamic behavior of the TMD is also investigated in order to guide the design of the MRE TMD. Additionally, the experimentally obtained natural frequencies coincide with the theoretical data, which sufficiently verifies the feasibility of this new design. The last part in terms of the vibration absorption ability also proves that both of these two natural frequencies play a great role in absorbing vibration energy.

7.2 Design and analysis of the MRETMD

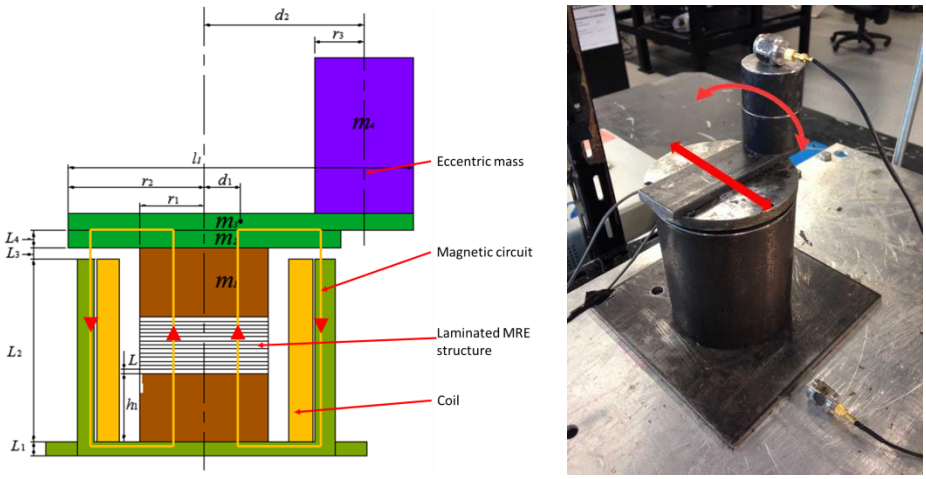

(a) (b)

Figure 7.1 The schematic sketch and the prototype of the proposed TMD: (a) Schematic sketch; (b) Prototype

7.2.1 The structure of the MRE TMD

Figure 7.1 presents the schematic sketch and the photograph of the proposed TMD. The first important component of the proposed TMD is a cylindrical structure which encompasses a multilayered MRE pillar (m_1), a solenoid, a steel cylinder, top plate (m_2), and bottom plate. This structural combination has been widely approved and used recently for its advantages that provide the translational flexibility and improve the conductivity of the MRE as well as protect the MRE from bulging.

The weight ratio of carbonyl iron particles (C3518, Sigma-Aldrich Pty Ltd), silicon rubber (Selleys Pty. Ltd), and silicon oil (Sigma-Aldrich Pty. Ltd) used for the MRE fabrication is 7:1.5:1.5. The MRE sample was tested under a sinusoidal rotary excitation with swept strain amplitude and frequency of 5 Hz. The MRE modulus under magnetic field strength of 0mT, 110mT, 220mT, 330mT, 440mT, and 1100mT was obtained, respectively. The magnetic field strength was adjusted through tuning the current. The storage modulus and loss modulus of the prepared MRE with respect to different magnetic flux densities are shown in Figure 7.2.

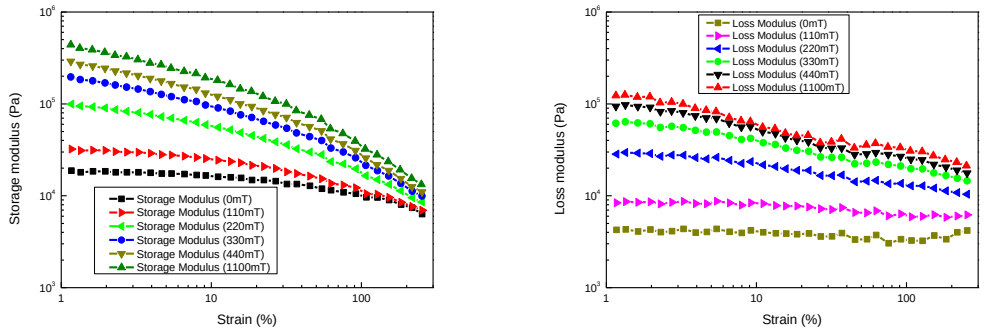

(a) (b)

Figure 7.2 The storage modulus and loss modulus of MRE under different magnetic flux densities: (a) Storage modulus; (b) Loss modulus

After the fabrication and test of the MRE, the multilayered MRE structure which consists of 7 layers of MRE sheets and 7 layers of steel sheets can be built. The main reason to design 7 layers of MRE sheets is to balance the resonance frequency in torsional direction and the travel stroke of the oscillator. The thickness and the diameter of the MRE sheets and the steel sheets are 1 mm and 35 mm, respectively. This configuration has been widely approved and used recently for its advantages that provide the translational flexibility and improve the conductivity of the MRE as

well as protect the MRE from bulging. The lateral flexibility of the laminated structure also increases the oscillator stroke. This means that a laminated MRE TMD can absorb more energy, especially for vibrations with larger amplitude. This compact MRE structure is fixed to two iron pillars with each end, respectively. A solenoid is then used to house the MRE structure. The strength and direction of the generated electromagnetic field can be controlled by changing the magnitude and direction of the applied current. A 5 mm thick cylindrical steel cover was finally installed outside the solenoid to close the magnetic circuit, shown as the yellow lines in Figure 7.1.

The most important part of the TMD is the eccentric mass (m_4). It is connected to the main cylindrical structure through a steel beam (m_3) which is fixed to the top of the top plate (m_2). The top plate and the eccentric mass together make it possible for the TMD to have two vibration modes; one is from the torsional motion and the other from the translational motion, as indicated in the TMD photograph.

7.2.2 Analysis of the MRE TMD

To explain how these two vibration modes are produced, theoretical derivation and analysis are provided below.

With reference to [212], the increased shear modulus of MRE with different magnetic fields can be calculated by:

$$\Delta G = 36\phi\mu_o\mu_l\beta^2\vec{H}_o^{\,2}\left(\frac{a}{d}\right)^3\zeta \tag{7.1}$$

where $\beta = (\mu_p - \mu_l)(\mu_p + 2\mu_l) \approx 1$, μ_o is the vacuum permeability, $\mu_p \approx 1000$ and $\mu_l \approx 1$ are the relative permeability of the particles and silicon rubber, respectively. ϕ is the volume fraction, a is the average particle radius, d is the particle distance before deflection, $\vec{H}_o$ is the intensity of the applied magnetic field, and $\zeta = \sum_{j=1}^{n}\frac{1}{j^3} \approx 1.202$.

The torsional stiffness of the ith MRE sheet can be written as:

$$K_{ri} = \frac{GI_p}{L} = \frac{(G_o+\Delta G)I_p}{L} = \frac{(G_o+36\phi\mu_o\mu_l\beta^2\vec{H}_o^{\,2}\left(\frac{a}{d}\right)^3\zeta)I_p}{L} \tag{7.2}$$

where G is the overall shear modulus, G_o is the initial shear modulus of MRE, L is the thickness of the MRE sheet. I_p is the polar moment of inertia of the MRE layer and can be calculated by:

$$I_p = \pi r_1^{\,4}/512 \tag{7.3}$$

where r_1 is the radius of the MRE layer.

The torsional stiffness of the whole laminated MRE pillar can be calculated by the following equation:

$$\frac{1}{k_{rw}} = \sum_{i=1}^{7} \frac{1}{k_{ri}} + \sum_{j=1}^{7} \frac{1}{k_{rj}} \tag{7.4}$$

where k_{rw} is the overall torsional stiffness of the laminated MRE pillar, k_{rj} is the torsional stiffness of steel sheet. It is known that $k_{ri} \ll k_{rj}$, therefore k_{rw} can be simplified as:

$$k_{rw} = \frac{k_{ri}}{7}$$

(7.5)

The natural frequency of the laminated MRE TMD in torsional direction can be written as:

$$f_r = \frac{1}{2\pi}\sqrt{\frac{k_{rw}}{J}} = \frac{1}{2\pi}\sqrt{\frac{k_{ri}}{7J}} \tag{7.6}$$

where J is the moment of inertia of the oscillator.

The moment of inertia can be calculated by the following equations:

$$J = \frac{m_1 {r_1}^2}{2} + \frac{m_2 {r_2}^2}{2} + \frac{m_3 {l_1}^2}{12} + m_3 {d_1}^2 + \frac{m_4 {r_3}^2}{2} + m_4 {d_2}^2 \tag{7.7}$$

The main sizes of the designed MRE TMD are shown in Table 7.1. By substituting equations (7.2), (7.3) and (7.7) into (7.6), the torsional natural frequency of the laminated MRE TMD can be expressed as:

$$f_r = \frac{1}{2\pi}\sqrt{\frac{(G_o + 36\phi\mu_o\mu_l\beta^2 {\vec{H}_o}^2 \left(\frac{a}{d}\right)^3 \zeta)\pi {r_1}^4}{3584L\left(\frac{m_1 {r_1}^2}{2} + \frac{m_2 {r_2}^2}{2} + \frac{m_3 {l_1}^2}{12} + m_3 {d_1}^2 + \frac{m_4 {r_3}^2}{2} + m_4 {d_2}^2\right)}} \tag{7.8}$$

The natural frequency of the MRE TMD in translational direction can be calculated by [212]:

$$f_t = \frac{1}{2\pi}\sqrt{\frac{(G_o + 36\phi\mu_o\mu_l\beta^2 {\vec{H}_o}^2 \left(\frac{a}{d}\right)^3 \zeta)A}{7(m_1 + m_2 + m_3 + m_4)L}} \tag{7.9}$$

where A is the area of the MRE layer, the magnetic field $\vec{H}_o$ can be calculated by the calculation method in [212]:

$$NI = B_{MRE} S_{MRE} R_m \tag{7.10}$$

$$B_{MRE} = \mu_{MRE} \vec{H}_o \tag{7.11}$$

$$R_m = R_1 + R_2 + R_3 + R_4 + R_5 \tag{7.12}$$

where NI is the magnetomotive force of coil, B_{MRE} is the magnetic flux density passing through MRE and S_{MRE} is the flux area of MRE. R_1, R_2, R_3, R_4, and R_5 are the magnetic resistances of seven MRE layers, two steel pillars, air gap, steel yoke, top and bottom plates, respectively.

Thus the frequency shift property of the as-designed MRE TMD in torsional and translational direction can be calculated.

Table 7.1 Parameters of self-sensing MRE TMD

Parameters	Values		Parameters	Values
h_1	45 mm		L_1	5 mm
L	1 mm		L_2	100 mm
l_1	110mm		L_3	5 mm
r_1	18mm		L_4	7 mm
r_2	45mm		m_1	0.2kg
r_3	18mm		m_2	0.37kg
Excitation coil	1000 turns		m_3	0.13kg
			m_4	0.4kg

7.3 Experimental test of the MRE TMD

7.3.1 Experiment setup

In this part, the experimental tests were mainly focused on studying the dynamic properties and the influence of the inertia of the oscillator on the behaviors of the proposed TMD. Figure 7.3 shows the photograph of the experimental set up. The TMD was fixed onto the vibration platform driven by a shaker (VTS, VC 100-8). Two accelerometers (CA-YD-106) were used to measure the accelerations of the excitation and the eccentric mass, respectively. A DC power supply (THURLBY-THANDAR, INSTRUMENTS LTD) was used to provide current to the TMD solenoid. A data acquisition (DAQ) board was used as the interface between the hardware and the software and transferred the measured accelerations to the computer. The signal collection, recording, and processing systems were developed using the LabVIEW program.

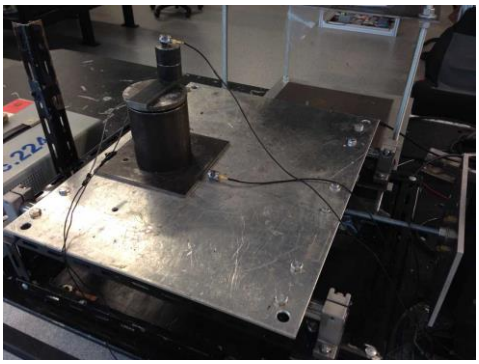

Figure 7.3 Experimental setup for characterizing the TMD

7.3.2 The frequency shift property testing

The frequency shift property is a key criterion to evaluate the effectiveness and controllability of a semi-active TMD for the reason it reflects the effective frequency bandwidth and the natural frequency of the TMD. The wider the frequency bandwidth is, the more capable the TMD is. In this experiment, a total of six tests using swept sinusoidal signals were conducted to measure the frequency-shift performance. The DC current signal was changed from 0A to 2.5A with a step of 0.5A. Figure 7.4(a) shows the transmissibility of the TMD. The highest point in the transmissibility is the resonance point. From Figure 7.4(a), it is obvious that each case has two resonance points, for example, when the current was 2A, the resonances occur at 5.39Hz and 22.4Hz, respectively. Table 7.2 gives the actual values of the natural frequencies with respect to the currents. Based on this result, it can be seen that the TMD with two resonances has wider effective frequency range (from 2.6 Hz to 5.88 Hz and from 11.15 Hz to 26 Hz) compared with its counterpart torsional TMD (from 2.6 Hz to 5.88 Hz) and translational TMD (from 11.15 Hz to 26 Hz). In addition, compared with the TMD with single natural frequency, it has two effective frequency ranges, which means it can better handle multi-frequency vibration disturbance.

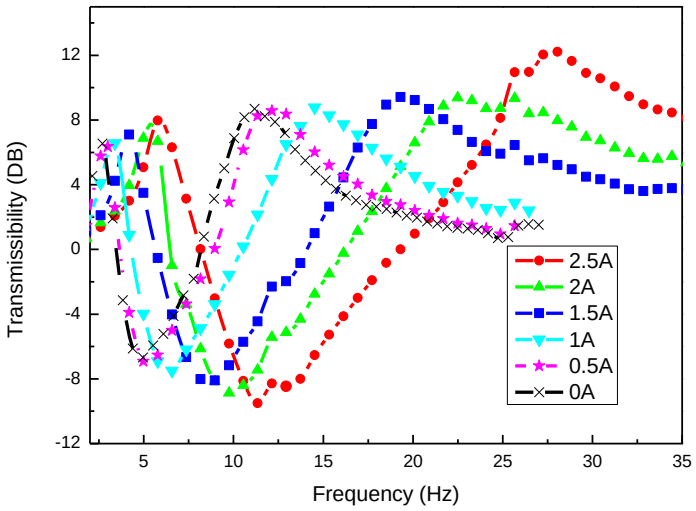

(a)

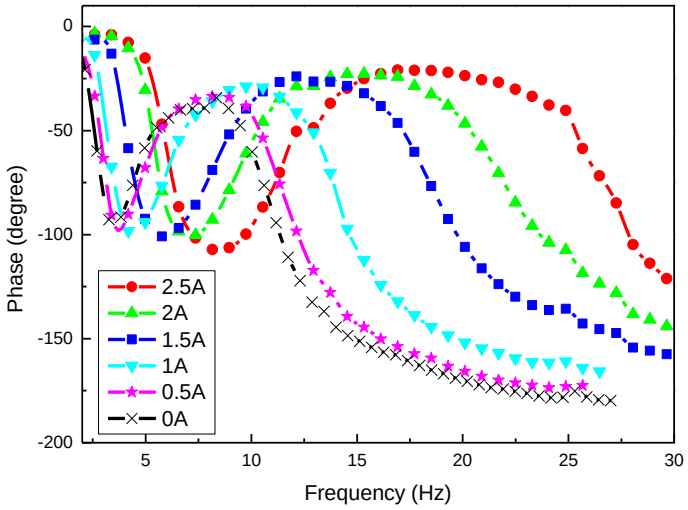

(b)

Figure 7.4 The transmissibility of the TMD under different currents: (a). Amplitude; (b). Phase

.

Table 7.2 The torsional natural frequency and the translational natural frequency via current

Current	0A	0.5A	1A	1.5A	2A	2.5A	Relative change
Torsional natural frequency (Hz)	2.6	2.83	3.26	4.14	5.39	5.88	126%
Translational natural frequency (Hz)	11.15	12.1	14.6	19.34	22.4	26	133%

It is noteworthy that the natural frequencies of these two modes do not overlap. It is to say the maximum natural frequency of the first mode comes before the minimum natural frequency of the second mode. Corresponding to the transmissibility shown by Figure 7.4(a), Figure 7.4(b) is the phase difference between the eccentric response and the excitation. From Figure 7.4 (b), the phase difference reaches negative ninety degrees twice for each condition of current. This means this TMD has reached resonance twice.

7.3.3 Investigation of the influence of the inertia on the two resonances

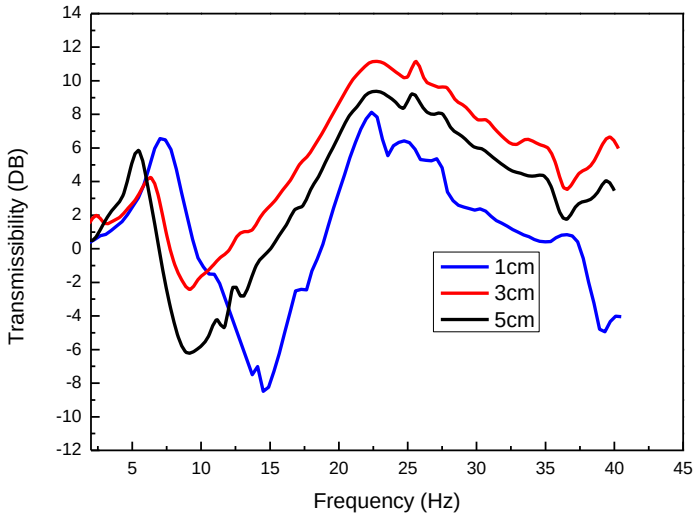

Figure 7.5 The effect of changing the distance d_2 on the two resonances

As mentioned above, the position (d_2) and the weight (m_4) of the eccentric mass will significantly affect the frequency shift property of the proposed TMD. The change of either the position (the moment arm) or the eccentric mass will cause the change of

the moment of inertia of the eccentric mass. The following parts investigated how the inertia of the eccentric mass influenced the two resonances. Figure 7.5 show the influence of the moment arm of the eccentric mass on the resonances. As can be seen the moment arm was set as 1cm, 3cm, and 5cm, respectively. It is observed that the first mode natural frequency decreases as the moment arm increases. This can be explained using Equation (7.7) and (7.8): the increase of moment arm causes an increment on the inertia, which cause a decrease in the natural frequency. It is also seen from Equation (7.9) that the moment arm d_2 has no function relationship with the translational natural frequency, which matches well with the observations in Figure 7.5 that the second mode natural frequency almost remains unchanged. Therefore, it can be concluded that the first mode natural frequency can be changed, independent of the second mode frequency, through the adjustment of the moment arm d_2.

Figure 7.6 shows the influence of different masses on the two resonances. Three cases were considered in this testing and each case has a different eccentric mass. The whole curve shifted to the left when the mass was increased, which means that the increased eccentric mass reduced the two natural frequencies. This observation stays consistent with the theoretical analysis derived by Equation (7.8) and (7.9). From the above experimental results and discussion, changing either the moment arm, d_2, or the eccentric mass, m_4, will produce different transmissibility responses (i.e. frequency bandwidth), which will provide this TMD more choices to meet different requirements.

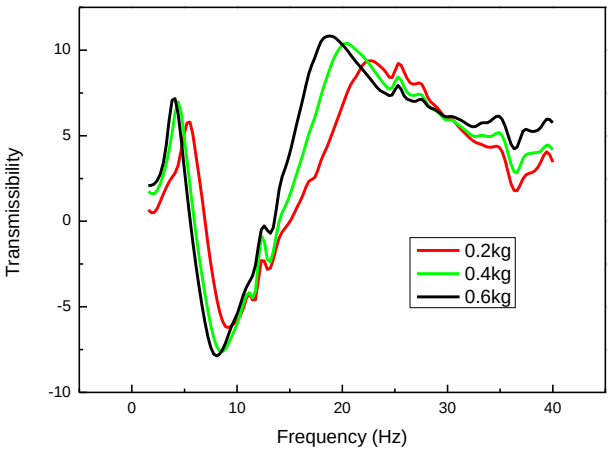

Figure 7.6 The effect of changing the eccentric mass on the two resonances

The simulation results based on the theoretical analysis in section 2 (equations (7.8) and (7.9)) are given. The simulation results include the torsional and the translational natural frequencies under different applied current, different d_2, and different m_4. Figures 7.7-7.9 show the comparison results between the experimentally obtained natural frequencies and the theoretical data. It is seen from Figures 7.7 and 7.8, for both the translational and the torsional natural frequency, the experimental results agree well with the theoretical results when the applied current and d_2 were changed. In Figure 7.9, even though the experimental data deviate slightly from the theoretical prediction when it comes to the translational motion, it still reflects the right change tendency of the translational natural frequency.

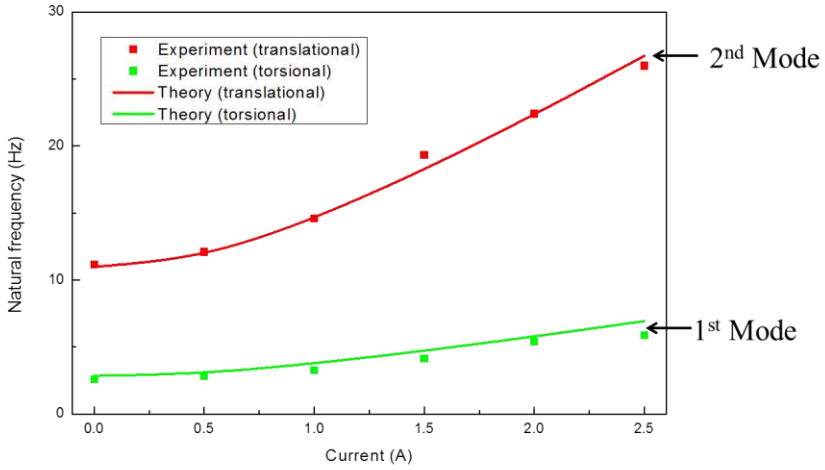

Figure 7.7 The comparison between the theory and experiment under different current

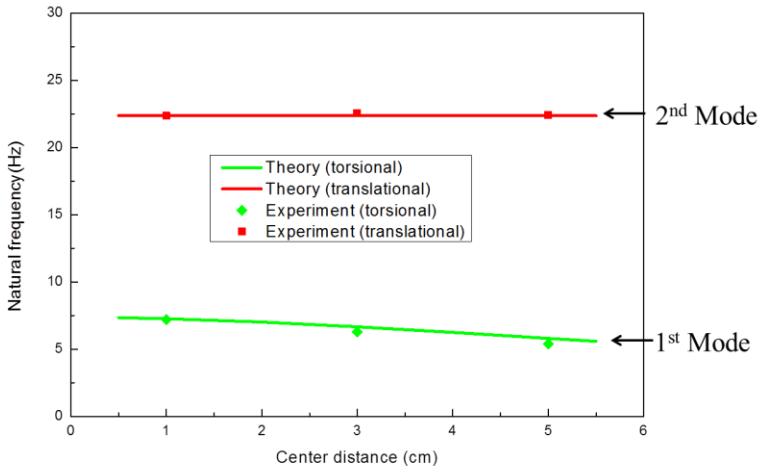

Figure 7.8 The comparison between the theory and experiment under different moment arm

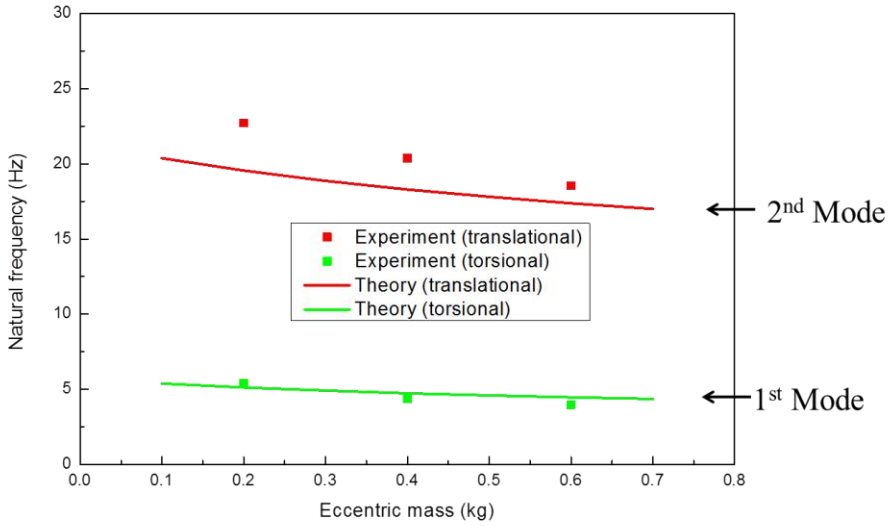

Figure 7.9 The comparison between the theory and experiment under different eccentric mass

7.4 Vibration absorption evaluation

Upon the successful development and characterization of the proposed TMD, it is also evaluated in terms of its vibration absorption effectiveness. Figure 7.10 shows the photograph of the experimental set up. The adaptive tuned vibration TMD was attached on the top of a mass which works as the primary system. Two accelerometers acquired the accelerations of the primary system and the excitation, respectively, and transmitted them to the computer. The vibration absorption capability of the TMD is also indicated by the transmissibility. However, the transmissibility here is defined as the ratio of the acceleration of the object to the excitation. Therefore, the transmissibility will decrease when the excitation frequency is close to the TMD's natural frequency. Please be noted that although the TMD uses torsional and translational direction vibration modes, the two resonance TMD is designed to control one direction vibration of the primary system: the translational direction. The translational vibration of the primary system can not only induce the translational vibration of the oscillator of the TMD but also its torsional vibration because of the existence of the eccentric mass. As a result, both of the two mode resonances are effective to absorb the translational vibration of the primary system. In this case, the new MRE TMD can occupy both resonance ranges to further expand its effective frequency bandwidth compared with TMD with one natural frequency.

A total of six cases corresponding to coil currents of 0A, 0.5A, 1A, 1.5A, 2A, 2.5A were tested. Comparatively, the semi-active case, which means that the stiffness of the MRE TMD can be controlled according to different excitation frequencies, is also evaluated. In terms of the semi-active controlled MRE TMD, a short time Fourier transform (STFT) control algorithm was used to control its stiffness to trace the excitation frequency. The working principle of the STFT is explained by equations (7.13)-(7.18).

For the first step, the time segment can be calculated by multiplying the signal x(t) by a window function h(t):

$$x_\tau(t) = x(t)h(t-\tau) \tag{7.13}$$

where τ is the fixed time, and t is the running time. The hamming window is used as the window function. After that, the Fourier transform for the modified signal is calculated as:

$$X_\tau(\omega) = \frac{1}{\sqrt{2\pi}} \int x(t)h(t-\tau)e^{-j\omega t}dt \tag{7.14}$$

The energy density of the windowed signal at the fixed time τ can be calculated by

$$P(\tau,\omega) = |X_\tau(\omega)|^2 = \left|\frac{1}{\sqrt{2\pi}} \int x(t)h(t-\tau)e^{-j\omega t}dt\right|^2 \tag{7.15}$$

which can provide the time–frequency distribution. Then the instantaneous frequency at time τ is given by

$$\langle\omega\rangle_\tau = \frac{1}{|x(\tau)|^2} \int \omega\,|X_\tau(\omega)|^2 d\omega \tag{7.16}$$

After determining the excitation frequency, the natural frequency of the MRE TMD should be tuned to trace the excitation frequency so that the object's vibration can be attenuated. In other words, the desired natural frequency of the MRE TMD f_r and f_t can be known. Based on the relationship between current I and the natural frequency of the TMD given in equation (7.8)-(7.10), the desired current can be calculated by the following two equations.

When the excitation frequency is within the torsional resonance range, the current can be calculated by:

$$I = \frac{\mu_{MRE}\vec{H}_o S_{MRE} R_m}{N} = \frac{\mu_{MRE} S_{MRE} R_m}{N} \sqrt{\frac{3584L(2\pi f_r)^2\left(\frac{m_1 {r_1}^2}{2} + \frac{m_2 {r_2}^2}{2} + \frac{m_3 {l_1}^2}{12} + m_3 {d_1}^2 + \frac{m_4 {r_3}^2}{2} + m_4 {d_2}^2\right) - \pi {r_1}^4 G_o}{36\pi {r_1}^4 \phi \mu_o \mu_l \beta^2 \left(\frac{a}{d}\right)^3 \zeta}}$$

(7.17)

Similarly, when the excitation frequency is in the translational resonance range, the current can be calculated by:

$$I = \frac{\mu_{MRE}\vec{H}_o S_{MRE} R_m}{N}$$

$$= \frac{\mu_{MRE} S_{MRE} R_m}{N} \sqrt{\frac{7(2\pi f_t)^2 (m_1+m_2+m_3+m_4)L - AG_o}{36\phi\mu_o\mu_l\beta^2\left(\frac{a}{d}\right)^3 \zeta A}} \quad (7.18)$$

Figure 7.11 shows the testing procedure. The acquired acceleration signals were processed by the STFT algorithm to analyze the excitation frequency fe. After the excitation frequency is obtained, the controller will calculate the desired current for MRE TMD based on equation (7.17) and (7.18) so as to tune the natural frequency of the MRE TMD to trace the excitation frequency. Upon receiving the current signal, the power amplifier will power the current signal to adjust the stiffness of the MRE to track the excitation frequency. The vibration absorption performances of different passive MRE TMDs (with different constant currents) and semi-active controlled MRE TMD are shown in Figure 7.12. The vibration absorption points of each passive MRE TMDs have been displayed with different alphabets. For the passive MRE TMD, all of them have two vibration absorption points induced by the two vibration modes, respectively. For example, when the current is 1.5A, the absorption points are D (torsional resonance effective point) and J (translational resonance effective point). The red line in Figure 7.12 is the tested result of the semi-active MRE TMD under the frequency trace control. It is noteworthy that this semi-active transmissibility almost connects all the lower points. This means the controlled semi-active TMD remains in a most effective status all the time when the STFT control algorithm applied.

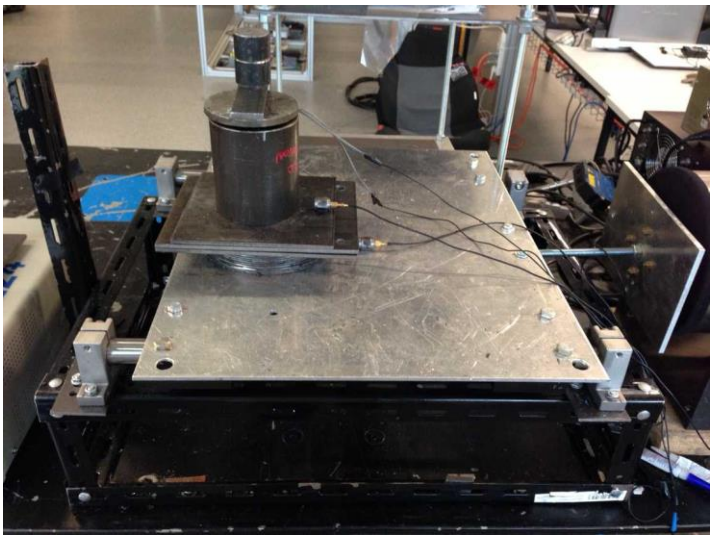

Figure 7.10 Experiment set up for vibration absorption

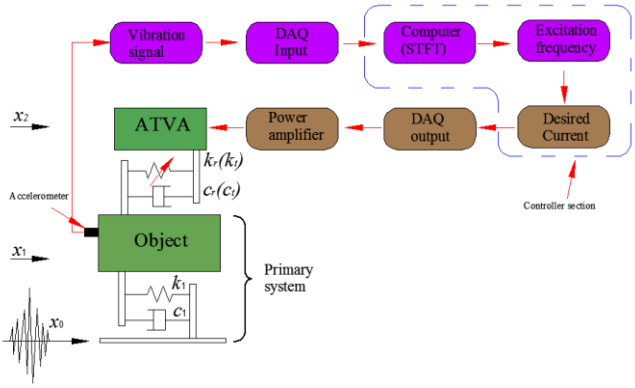

Figure 7.11 The flow chart for the semi-active control

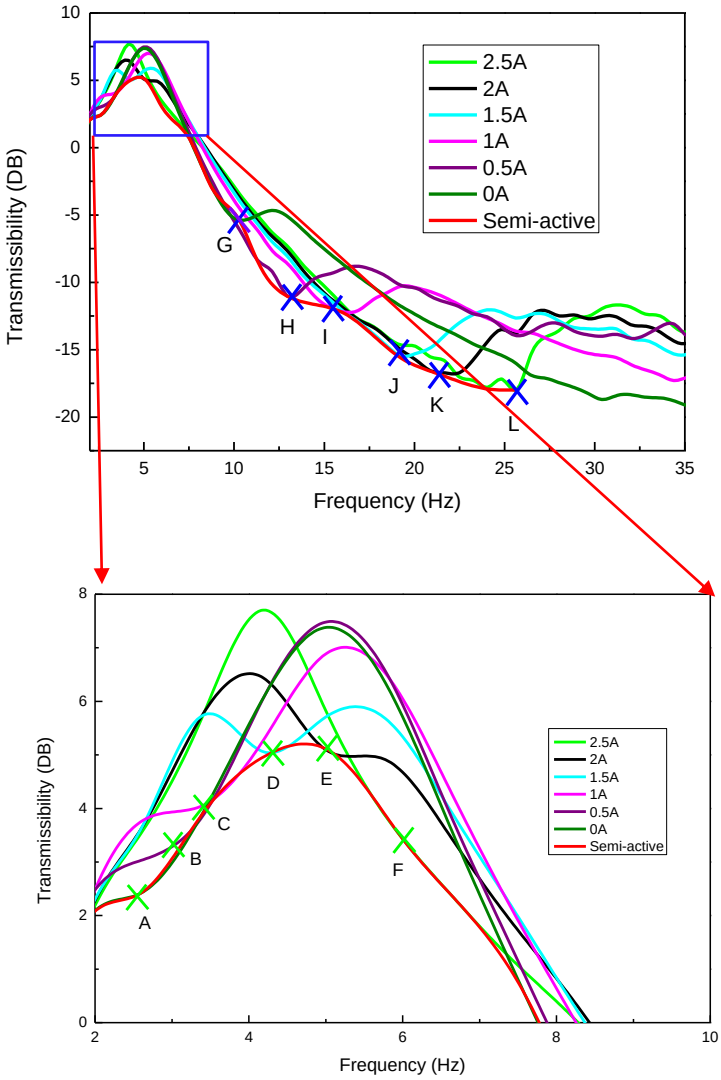

Figure 7.12 Transmissibility response indicating the vibration absorption effectiveness

7.5 Conclusions

A MRE based vibration TMD involving an eccentric mass was designed, implemented, and tested in this study. The eccentric mass enables the TMD to have a torsional vibration mode as well as the translational vibration mode. The transmissibility and the phase difference show that these two natural frequencies of different vibration modes increase as the applied current increases, and the torsional natural frequency changes from 2.6Hz to 5.88Hz with a relative change of 126% while the translational natural frequency varies from 11.15 Hz to 26 Hz. In addition, the frequency bandwidth can be adjusted according to different working conditions by adjusting the moment of inertia. The theoretical analysis and its consistence with

the experimental results provide evidence that this new design is effective and feasible. Additionally, the vibration absorption experiment demonstrates that both of resonances of the proposed TMD effectively absorbs vibration energy, implying that the new TMD can further expand its effective frequency range compared with an MRE TMD having only a single resonance.

8 CONCLUSIONS AND FUTURE WORK

8.1 Conclusions

The main objectives of this dissertation are to investigate the up-to-date aseismic technology for buildings, with special emphasis on the research and development of MRE based devices and applications. This research develops and progresses focusing on the following aspects: material choosing and study, device design and development, device modelling, theoretical and experimental evaluation, etc. The contents of this dissertation have met the predetermined goals. The main original contributions of this research include a comprehensive review on MRE and its application, modelling a stiffness hardening MRE isolator, a new device design, i.e. stiffness softening MRE isolator, comprehensive experimental evaluation and verification, and development of an MRE based tuned mass damper with newly proposed structure and magnetic circuit.

8.1.1 Modelling the multi-layered MRE isolator

Successful device development and design is exciting, though, it is not the ultimate goal. Instead, successful practical application of the designed devices is the ultimate pursuit. To achieve this, a series of extra work including modelling and control logic development has to be done. Finding an appropriate model that can accurately describe the unique characteristics of devices is a necessary step before advanced control logic can be accessed. In chapter 3, a phenomenological model is proposed to simulate the mechanical property of MRE isolators. Special attention is paid to the properties of Mullins effect, strain stiffening, and nonlinear loops of the MRE isolator. It is worth mentioning that the parameter-dependence investigation of the model performance is significantly helpful with accurate parameter adjustment if certain performance metric must be met. The precise modelling of the MRE isolator has enabled the exploitation of advanced control algorithms.

8.1.2 Stiffness softening MRE isolator

It has to be admitted that MRE based base isolator has attracted considerable research attention in recent years. This kind of technology has evolved from single layer to multiple layers isolators, from stiffness hardening to stiffness softening.

Considering the actual situation that a really effective base isolator should decouple the protected structure from the ground motion by becoming soft, a stiffness softening MRE isolator is designed and presented in chapter 4. This MRE isolator can operate in a passive mode with relatively high stiffness under normal operating conditions by using a pair of permanent magnets, and it becomes relatively soft when earthquakes occur by triggering the electromagnetic coil the magnetic circuit to cancel the field of the permanent magnets. This design provides a higher level of cost reduction, power efficiency, and sustainability. Its aseismic capability on a scaled three building is evaluated and verified in chapter 5. The inter-story drift and accelerations of the three-story building model are obviously reduced by using this stiffness softening MRE isolator. This successful proof-of-concept has made this stiffness softening MRE isolator a potential candidate for practical aseismic application.

The requirements of the MRE isolator include two aspects: the first one is to provide enough vertical support capability; the second one is to maintain larger stroke range. In order to achieve these two goals, passive laminated rubber-based isolator has been widely used and its feasibility has been verified. Our design only replaced the natural rubber with MRE material, which means the MRE isolator possesses the above two advantage and it is feasible to be utilized for the structure of real dimension.

8.1.3 MRE based tuned mass damper

Apart from base isolation technology, tuned mass dampers are also a widely accepted means for protecting building from earthquakes. However, a tuned mass damper using an MRE as a stiffness element is seldom reported in the literature. The advantage brought by using MREs is that the device can have multiple natural frequencies by adjusting the stiffness of MRE so that it can more effectively deal with the variability and unpredictability of earthquakes. To improve this MRE based tuned mass damper, a little more thought is paid to the structure and magnetic circuit of this MRE tuned mass damper. The square layout of four multi-layered MRE structures increases the stability and lateral flexibility of this device and meanwhile, reduces the magnetic leakage because four closed magnetic circuit are formed. Besides the creative design, the vibration reduction capability is always the most important evaluation standard for a new device. A scaled three story building acts as

the protected subject and the scaled El Centro earthquake motion data is chosen as the seismic event to evaluate the vibration reduction effectiveness of the MRE tuned mass damper. Both the simulation results and experimental results verify that this MRE tuned mass damper is of protecting buildings from earthquakes. As a means to increase the number of natural frequencies of MRETMD, an eccentric mass was attached to a multi-layered MRE structure so that the MRETMD has two natural frequencies. In this way, the controllable MRETMD can handle with vibrations with multiply frequencies.

8.2 Future Work

(1) For material itself, the mechanical properties of MREs should be further explored. For example, their properties can be adjusted by considering changing the compositions, component ratios, and fabrication conditions. Expectations of the potential applications of MREs should cover more adaptive devices rather than just limit to vibration isolation and absorption. One possible solution for this is to find a new operation mode for MRE. Extra attention should be paid to those MREs with longer life span, stronger intensity, higher stability, and better permeability because such materials are in high demand. For example, natural rubber based MRE has higher stability and longer life span than the silicon rubber based MRE.

(2) Optimized design of parameters of MRE devices need to be carried out according to actual requirement in order to get the best performance.

(3) Advanced controllers, such as robust control and sliding mode control, that can enhance the response time, adaptability, and controllability of MRE devices need to be designed, evaluated, and optimized.

(4) Design of magnetic circuit still needs improvement and optimization for the purpose of energizing thick MREs with large size. To meet the required performance, large sized MREs are needed to be placed in the devices and thus a strong magnetic flux is required to fully energize these materials. A possible solution for this problem may be found by the optimal design of the magnetic circuit, such as coil placement.

(5) As mentioned above, practical application and even commercialization is always the ultimate destination of theoretical investigation. In this regard, it is not enough to limit research to the lab scale. Large scale that matches practical equipment or devices is what the future research must focus on.

REFERENCES

[1] S. Nagarajaiah and S. Xiaohong, "Response of base-isolated USC hospital building in Northridge earthquake," *Journal of structural engineering*, vol. 126, pp. 1177-1186, 2000.

[2] N. Makris, "Rigidity-plasticity-viscosity: can electrorheological dampers protect base-isolated structures from near-source ground motions?," *Earthquake Engineering and Structural Dynamics*, vol. 26, pp. 571-592, 1997.

[3] T. Soong and B. Spencer Jr Reviewer, "Active structural control: theory and practice," *Journal of Engineering Mechanics*, vol. 118, pp. 1282-1285, 1992.

[4] T. Soong and A. Reinhorn, "An overview of active and hybrid structural control research in the US," *The structural design of tall buildings*, vol. 2, pp. 193-209, 1993.

[5] B. Spencer and M. K. Sain, "Controlling buildings: a new frontier in feedback," *IEEE Control Systems*, vol. 17, pp. 19-35, 1997.

[6] G. Housner, L. A. Bergman, T. K. Caughey, A. G. Chassiakos, R. O. Claus, S. F. Masri, *et al.*, "Structural control: past, present, and future," *Journal of engineering mechanics*, vol. 123, pp. 897-971, 1997.

[7] T. Kobori, "Past, present and future in seismic response control in civil engineering structures," in *3rd world Conference on Structural Control*, 2002, pp. 9-14.

[8] T. Soong and B. Spencer, "Supplemental energy dissipation: state-of-the-art and state-of-the-practice," *Engineering Structures*, vol. 24, pp. 243-259, 2002.

[9] B. SpencerJr, "Civil engineering applications of smart damping technology," 2002.

[10] O. Padalka, H. Song, N. Wereley, J. Filer, and R. Bell, "Stiffness and damping in Fe, Co, and Ni nanowire-based magnetorheological elastomeric composites," *Magnetics, IEEE Transactions on*, vol. 46, pp. 2275-2277, 2010.

[11] Y. Han, W. Hong, and L. E. Faidley, "Field-stiffening effect of magneto-rheological elastomers," *International Journal of Solids and Structures*, vol. 50, pp. 2281-2288, 2013.

[12] F. Naeim and J. M. Kelly, *Design of seismic isolated structures: from theory to practice*: John Wiley & Sons, 1999.

[13] P. Komodromos and S. Stiemer, "Seismic isolation for earthquake resistant structures," *Applied Mechanics Reviews*, vol. 54, p. 112, 2001.

[14] P. Pan, D. Zamfirescu, M. Nakashima, N. Nakayasu, and H. Kashiwa, "Base-isolation design practice in Japan: introduction to the post-Kobe approach," *Journal of Earthquake Engineering*, vol. 9, pp. 147-171, 2005.

[15] H. Yoshioka, J. Ramallo, and B. Spencer Jr, "“Smart” base isolation strategies employing magnetorheological dampers," *Journal of engineering mechanics*, vol. 128, pp. 540-551, 2002.

[16] M. Behrooz, X. Wang, and F. Gordaninejad, "Performance of a new magnetorheological elastomer isolation system," *Smart Materials and Structures*, vol. 23, p. 045014, 2014.

[17] M. Behrooz, X. Wang, and F. Gordaninejad, "Modeling of a new semi-active/passive magnetorheological elastomer isolator," *Smart Materials and Structures*, vol. 23, p. 045013, 2014.

[18] Y. Li, J. Li, W. Li, and B. Samali, "Development and characterization of a magnetorheological elastomer based adaptive seismic isolator," *Smart Materials and Structures*, vol. 22, p. 035005, 2013.

[19] Y. Li, J. Li, T. Tian, and W. Li, "A highly adjustable magnetorheological elastomer base isolator for applications of real-time adaptive control," *Smart Materials and Structures*, vol. 22, p. 095020, 2013.

[20] J. Yang, S. Sun, H. Du, W. Li, G. Alici, and H. Deng, "A novel magnetorheological elastomer isolator with negative changing stiffness for vibration reduction," *Smart Materials and Structures*, vol. 23, p. 105023, 2014.

[21] J. Yang, H. Du, W. Li, Y. Li, J. Li, S. Sun, *et al.*, "Experimental study and modeling of a novel magnetorheological elastomer isolator," *Smart Materials and Structures*, vol. 22, p. 117001, 2013.

[22] J. Yang, S. Sun, T. Tian, W. Li, H. Du, G. Alici, *et al.*, "Development of a novel multi-layer MRE isolator for suppression of building vibrations under

seismic events," *Mechanical Systems and Signal Processing*, vol. 70, pp. 811-820, 2016.

[23] P. Walsh and J. Lamancusa, "A variable stiffness vibration absorber for minimization of transient vibrations," *Journal of sound and vibration*, vol. 158, pp. 195-211, 1992.

[24] N. Fisco and H. Adeli, "Smart structures: part I—active and semi-active control," *Scientia Iranica*, vol. 18, pp. 275-284, 2011.

[25] N. Fisco and H. Adeli, "Smart structures: part II—hybrid control systems and control strategies," *Scientia Iranica*, vol. 18, pp. 285-295, 2011.

[26] J. C. Chang and T. T. Soong, "Structural control using active tuned mass dampers," *Journal of the Engineering Mechanics Division*, vol. 106, pp. 1091-1098, 1980.

[27] B. Spencer Jr and S. Nagarajaiah, "State of the art of structural control," *Journal of structural engineering*, vol. 129, pp. 845-856, 2003.

[28] M. Abdel-Rohman, H. H. Leipholz, and V. H. Quintana, "Optimal control of civil engineering structures," *Journal of the Engineering Mechanics Division*, vol. 106, pp. 57-73, 1980.

[29] J. Juang, S. Sae-Ung, and J. Yang, "Active control of large building structures," *Structural control*, pp. 663-676, 1980.

[30] R. Miller, S. Masri, T. Dehghanyar, and T. Caughey, "Active vibration control of large civil structures," *Journal of Engineering Mechanics*, vol. 114, pp. 1542-1570, 1988.

[31] B. Samali, J. Yang, and S. Liu, "Active control of seismic-excited buildings," *Journal of Structural Engineering*, vol. 111, pp. 2165-2180, 1985.

[32] B. Samali, J. Yang, and C. Yeh, "Control of lateral-torsional motion of wind-excited buildings," *Journal of engineering mechanics*, vol. 111, pp. 777-796, 1985.

[33] M. Shinozuka, E. Samaras, and C. Paliou, "Active Control of Floating Structures," in *Structural Control*, ed: Springer, 1987, pp. 651-668.

[34] T. Soong, A. Reinhorn, and J. Yang, "A standardized model for structural control experiments and some experimental results," in *Structural control*, ed: Springer, 1987, pp. 669-693.

[35] T. Soong and G. Skinner, "Experimental study of active structural control," *Journal of the Engineering Mechanics Division,* vol. 107, pp. 1057-1067, 1981.

[36] T. Soong, R. Lin, L. Chung, and A. Reinhorn, "Experimental evaluation of optimal control algorithms for seismic applications," in *Proc. of ASCE Engineering Mechanics Division 6th Specialty Conference, at SUNY, Buffalo, New York,* 1987, pp. 20-22.

[37] F. E. Udwadia and S. Tabaie, "Pulse control of structural and mechanical systems," *Journal of the Engineering Mechanics Division,* vol. 107, pp. 1011-1028, 1981.

[38] J.-N. Yang, "Application of optimal control theory to civil engineering structures," *Journal of the engineering Mechanics Division,* vol. 101, pp. 819-838, 1975.

[39] J. N. Yang, A. Akbarpour, and P. Ghaemmaghami, "Optimal control algorithms for earthquake-excited building structures," in *Structural control,* ed: Springer, 1987, pp. 748-761.

[40] J. Yang, A. Akbarpour, and P. Ghaemmaghami, "Instantaneous optimal control algorithms for structures under seismic excitations," *National Center for Earthquake Engineering Research, Technical Report NCEER-TR-87-0007,* 1987.

[41] J. N. Yang, "Control of tall building under earthquake excitation," *Journal of the Engineering Mechanics Division,* vol. 108, pp. 833-849, 1982.

[42] J. Yao and T. Soong, "Importance of experimental studies in structural control," *Preprint,* pp. 84-010, 1984.

[43] J. Yao, "Concept of structural control," *Journal of the Structural Division,* vol. 98, 1972.

[44] T. T. Soong and M. C. Costantinou, *Passive and active structural vibration control in civil engineering* vol. 345: Springer, 2014.

[45] T. T. Soong and G. F. Dargush, *Passive energy dissipation systems in structural engineering*: Wiley, 1997.

[46] D. M. Bergman and S. C. Goel, *Evaluation of cyclic testing of steel-plate devices for added damping and stiffness*: Department of Civil Engineering, University of Michigan, 1987.

[47] A. S. Whittaker, V. V. Bertero, C. L. Thompson, and L. J. Alonso, "Seismic testing of steel plate energy dissipation devices," *Earthquake Spectra*, vol. 7, pp. 563-604, 1991.

[48] C. Tsai and H. Lee, "Applications of viscoelastic dampers to high-rise buildings," *Journal of structural engineering*, vol. 119, pp. 1222-1233, 1993.

[49] R. Skinner, J. Kelly, and A. Heine, "Hysteretic dampers for earthquake - resistant structures," *Earthquake Engineering & Structural Dynamics*, vol. 3, pp. 287-296, 1974.

[50] A. S. Pall and C. Marsh, "Response of friction damped braced frames," *Journal of Structural Engineering*, vol. 108, pp. 1313-1323, 1982.

[51] I. D. Aiken and J. M. Kelly, "Earthquake simulator testing and analytical studies of two energy-absorbing systems for multistory structures," University of California, Berkeley, 1990.

[52] D. K. Nims, P. J. Richter, and R. E. Bachman, "The use of the energy dissipating restraint for seismic hazard mitigation," *Earthquake Spectra*, vol. 9, pp. 467-489, 1993.

[53] T. Fitzgerald, T. Anagnos, M. Goodson, and T. Zsutty, "Slotted bolted connections in aseismic design for concentrically braced connections," *Earthquake Spectra*, vol. 5, pp. 383-391, 1989.

[54] C. E. Grigorian, T.-S. Yang, and E. P. Popov, "Slotted bolted connection energy dissipators," *Earthquake Spectra*, vol. 9, pp. 491-504, 1993.

[55] T. Fujita, "Seismic isolation and response control for nuclear and non-nuclear structures," in *Spec. Issue for the Exhibition of the 11th Intl. Conf. on SMiRT*, 1991.

[56] K. Kasai, J. A. Munshi, M. Lai, and B. Maison, "Viscoelastic damper hysteretic model: theory, experiment and application," in *Proc., ATC*, 1993, pp. 17-1.

[57] S. S. Rao and F. F. Yap, *Mechanical vibrations* vol. 4: Addison-Wesley New York, 1995.

[58] R. Villaverde, "Seismic control of structures with damped resonant appendages," in *Proceedings of the First World Conference on Structural Control*, 1994, pp. 113-122.

[59] K. Xu and T. Igusa, "Dynamic characteristics of multiple substructures with closely spaced frequencies," *Earthquake engineering & structural dynamics*, vol. 21, pp. 1059-1070, 1992.

[60] H. Yamaguchi and N. Harnpornchai, "Fundamental characteristics of multiple tuned mass dampers for suppressing harmonically forced oscillations," *Earthquake engineering & structural dynamics*, vol. 22, pp. 51-62, 1993.

[61] M. Setareh, "Use of the doubly-tuned mass dampers for passive vibration control," in *Proceedings of the First World Conference on Structural Control*, 1994.

[62] G. Li, Z. Shen, and B. Choo, "A ring-like pendulum for reducing seismic response of tall chimneys," in *Proc., First World Conf. on Struct. Control*, 1994.

[63] A. Kareem, "The next generation of tuned liquid dampers," in *Proc., First World Conf. on Struct. Control, FPS*, 1994, pp. 19-28.

[64] S. Limin, "Semi-analytical modelling of tuned liquid damper (TLD) with emphasis on damping of liquid sloshing," University of Tokyo, 1991.

[65] H. Yeh, D. Reed, J. Yu, and S. Gardarsson, "Performance of tuned liquid dampers under large amplitude excitation," in *Proc., Second International Workshop on Structural Control*, 1996, pp. 432-443.

[66] V. Gattulli, R. Lin, and T. Soong, "Nonlinear control laws for enhancement of structural control effectiveness," in *5th US National Conference for Earthquake Engineering*, 1994, pp. 971-980.

[67] T. Kobori, N. Koshika, K. Yamada, and Y. Ikeda, "Seismic‐response‐controlled structure with active mass driver system. Part 1: Design," *Earthquake Engineering & Structural Dynamics*, vol. 20, pp. 133-149, 1991.

[68] S. Dyke, B. Spencer Jr, M. Sain, and J. Carlson, "Seismic response reduction using magnetorheological dampers," in *Proceedings of the IFAC World Congress*, 1996, pp. 145-150.

[69] S. Dyke, B. Spencer Jr, M. Sain, and J. Carlson, "Experimental verification of semi-active structural control strategies using acceleration feedback," in *Proc. of the 3rd Intl. Conf. on Motion and Vibr. Control*, 1996, pp. 291-296.

[70] S. Dyke, B. Spencer Jr, M. Sain, and J. Carlson, "Modeling and control of magnetorheological dampers for seismic response reduction," *Smart materials and structures,* vol. 5, p. 565, 1996.

[71] K. M. Popp, M. Kröger, W. hua Li, X. Z. Zhang, and P. B. Kosasih, "MRE properties under shear and squeeze modes and applications," *Journal of Intelligent Material Systems and Structures,* vol. 21, pp. 1471-1477, 2010.

[72] R. Bonnecaze and J. Brady, "Dynamic simulation of an electrorheological fluid," *The Journal of chemical physics,* vol. 96, pp. 2183-2202, 1992.

[73] N. M. Wereley, J. Lindler, N. Rosenfeld, and Y.-T. Choi, "Biviscous damping behavior in electrorheological shock absorbers," *Smart Materials and Structures,* vol. 13, p. 743, 2004.

[74] B. Liu, W. Li, P. B. Kosasih, and X. Zhang, "Development of an MR-brake-based haptic device," *Smart materials and structures,* vol. 15, p. 1960, 2006.

[75] R. Jacob, "Magnetic fluid torque and force transmitting device," ed: Google Patents, 1951.

[76] J. Rabinow, "The magnetic fluid clutch," *Transactions of the American Institute of Electrical Engineers,* vol. 67, pp. 1308-1315, 1948.

[77] Z. Rigbi and L. Jilken, "The response of an elastomer filled with soft ferrite to mechanical and magnetic influences," *Journal of magnetism and magnetic materials,* vol. 37, pp. 267-276, 1983.

[78] M. R. Jolly, J. D. Carlson, B. C. Muñoz, and T. A. Bullions, "The magnetoviscoelastic response of elastomer composites consisting of ferrous particles embedded in a polymer matrix," *Journal of Intelligent Material Systems and Structures,* vol. 7, pp. 613-622, 1996.

[79] M. R. Jolly, J. D. Carlson, and B. C. Munoz, "A model of the behaviour of magnetorheological materials," *Smart Materials and Structures,* vol. 5, p. 607, 1996.

[80] L. Davis, "Model of magnetorheological elastomers," *Journal of Applied Physics,* vol. 85, pp. 3348-3351, 1999.

[81] M. Kallio, *The elastic and damping properties of magnetorheological elastomers*: VTT Technical Research Centre of Finland, 2005.

[82] M. Lokander and B. Stenberg, "Performance of isotropic magnetorheological rubber materials," *Polymer Testing,* vol. 22, pp. 245-251, 2003.

[83] M. V. Gandhi and B. Thompson, *Smart materials and structures*: Springer Science & Business Media, 1992.

[84] J. M. Ginder, M. E. Nichols, L. D. Elie, and S. M. Clark, "Controllable-stiffness components based on magnetorheological elastomers," in *SPIE's 7th Annual International Symposium on Smart Structures and Materials*, 2000, pp. 418-425.

[85] A.-M. A. Lerner and K. A. Cunefare, "Adaptable vibration absorber employing a magnetorheological elastomer with variable gap length and methods and systems therefor," ed: Google Patents, 2006.

[86] G. Bossis, C. Abbo, S. Cutillas, S. Lacis, and C. Métayer, "Electroactive and electrostructured elastomers," *International Journal of Modern Physics B*, vol. 15, pp. 564-573, 2001.

[87] J. M. Ginder, W. F. Schlotter, and M. E. Nichols, "Magnetorheological elastomers in tunable vibration absorbers," in *SPIE's 8th Annual International Symposium on Smart Structures and Materials*, 2001, pp. 103-110.

[88] J. R. Watson, "Method and apparatus for varying the stiffness of a suspension bushing," ed: Google Patents, 1997.

[89] A.-M. A. Lerner, "The design and implementation of a magnetorheological silicone composite state-switched absorber," 2005.

[90] S. Bednarek, "The giant magnetostriction in ferromagnetic composites within an elastomer matrix," *Applied Physics A: Materials Science & Processing*, vol. 68, pp. 63-67, 1999.

[91] M. J. Wilson, A. Fuchs, and F. Gordaninejad, "Development and characterization of magnetorheological polymer gels," *Journal of applied polymer science*, vol. 84, pp. 2733-2742, 2002.

[92] A.-M. Albanese and K. A. Cunefare, "Properties of a magnetorheological semi-active vibration absorber," in *Smart structures and materials*, 2003, pp. 36-43.

[93] J. L. Leblanc, "Rubber–filler interactions and rheological properties in filled compounds," *Progress in polymer science*, vol. 27, pp. 627-687, 2002.

[94] I. Bica, "Influence of the magnetic field on the electric conductivity of magnetorheological elastomers," *Journal of Industrial and Engineering Chemistry*, vol. 16, pp. 359-363, May 2010.

[95] L. Chen, X. Gong, and W. Li, "Effect of carbon black on the mechanical performances of magnetorheological elastomers," *Polymer Testing,* vol. 27, pp. 340-345, 2008.

[96] G. Stepanov, S. Abramchuk, D. Grishin, L. Nikitin, E. Y. Kramarenko, and A. Khokhlov, "Effect of a homogeneous magnetic field on the viscoelastic behavior of magnetic elastomers," *Polymer,* vol. 48, pp. 488-495, 2007.

[97] S. A. Demchuk and V. A. Kuz'min, "Viscoelastic properties of magnetorheological elastomers in the regime of dynamic deformation," *Journal of Engineering Physics and Thermophysics,* vol. 75, pp. 396-400, 2002.

[98] J. L. Leblanc, "Rubber-filler interactions and rheological properties in filled compounds," *Progress in Polymer Science,* vol. 27, pp. 627-687, May 2002.

[99] I. Bica, "Influence of the transverse magnetic field intensity upon the electric resistance of the magnetorheological elastomer containing graphite microparticles," *Materials Letters,* vol. 63, pp. 2230-2232, Oct 2009.

[100] X. L. Gong, X. Z. Zhang, and P. Q. Zhang, "Fabrication and characterization of isotropic magnetorheological elastomers," *POLYMER TESTING,* vol. 24, pp. 669-676, Aug 2005.

[101] W. H. Li, K. Kostidis, X. Z. Zhang, Y. Zhou, and Ieee, *Development of a Force Sensor Working with MR Elastomers*, 2009.

[102] Y. Shen, M. F. Golnaraghi, and G. R. Heppler, "Experimental research and modeling of magnetorheological elastomers," *Journal of Intelligent Material Systems and Structures,* vol. 15, pp. 27-35, Jan 2004.

[103] T. Tian, W. Li, G. Alici, H. Du, and Y. Deng, "Microstructure and magnetorheology of graphite-based MR elastomers," *Rheologica acta,* vol. 50, pp. 825-836, 2011.

[104] G. Liao, X. Gong, S. Xuan, C. Kang, and L. Zong, "Development of a real-time tunable stiffness and damping vibration isolator based on magnetorheological elastomer," *Journal of Intelligent Material Systems and Structures,* vol. 23, pp. 25-33, 2012.

[105] Y. Shen, M. F. Golnaraghi, and G. Heppler, "Experimental research and modeling of magnetorheological elastomers," *Journal of Intelligent Material Systems and Structures,* vol. 15, pp. 27-35, 2004.

[106] H.-x. Deng, X.-l. Gong, and L.-h. Wang, "Development of an adaptive tuned vibration absorber with magnetorheological elastomer," *Smart Materials and Structures,* vol. 15, p. N111, 2006.

[107] W. Li, X. Zhang, and H. Du, "Magnetorheological elastomers and their applications," in *Advances in Elastomers I*, ed: Springer, 2013, pp. 357-374.

[108] J. M. Ginder, M. E. Nichols, L. D. Elie, and J. L. Tardiff, "Magnetorheological elastomers: properties and applications," in *1999 Symposium on Smart Structures and Materials*, 1999, pp. 131-138.

[109] L. Chen, X. Gong, and W. Li, "Microstructures and viscoelastic properties of anisotropic magnetorheological elastomers," *Smart Materials and Structures,* vol. 16, p. 2645, 2007.

[110] L. Borcea and O. Bruno, "On the magneto-elastic properties of elastomer–ferromagnet composites," *Journal of the Mechanics and Physics of Solids,* vol. 49, pp. 2877-2919, 2001.

[111] M. Lokander and B. Stenberg, "Improving the magnetorheological effect in isotropic magnetorheological rubber materials," *Polymer Testing,* vol. 22, pp. 677-680, 2003.

[112] T. Shiga, A. Okada, and T. Kurauchi, "Magnetroviscoelastic behavior of composite gels," *Journal of Applied Polymer Science,* vol. 58, pp. 787-792, 1995.

[113] M. Yalcintas and H. Dai, "Vibration suppression capabilities of magnetorheological materials based adaptive structures," *Smart Materials and Structures,* vol. 13, p. 1, 2003.

[114] G. Zhou and Z. Jiang, "Deformation in magnetorheological elastomer and elastomer–ferromagnet composite driven by a magnetic field," *Smart Materials and Structures,* vol. 13, p. 309, 2004.

[115] G. Zhou, "Shear properties of a magnetorheological elastomer," *Smart materials and structures,* vol. 12, p. 139, 2003.

[116] G. Zhou and J. Li, "Dynamic behavior of a magnetorheological elastomer under uniaxial deformation: I. Experiment," *Smart Materials and Structures,* vol. 12, p. 859, 2003.

[117] L. Chen, X.-l. Gong, and W.-h. Li, "Damping of magnetorheological elastomers," *Chinese journal of chemical physics,* vol. 21, pp. 581-585, 2008.

[118] W. Li, Y. Zhou, and T. Tian, "Viscoelastic properties of MR elastomers under harmonic loading," *Rheologica acta,* vol. 49, pp. 733-740, 2010.

[119] H. Yin, L. Sun, and J. Chen, "Magneto-elastic modeling of composites containing chain-structured magnetostrictive particles," *Journal of the Mechanics and Physics of Solids,* vol. 54, pp. 975-1003, 2006.

[120] X. Zhang, W. Li, and X. Gong, "An effective permeability model to predict field-dependent modulus of magnetorheological elastomers," *Communications in Nonlinear Science and Numerical Simulation,* vol. 13, pp. 1910-1916, 2008.

[121] M. Yu, Y.-q. Xia, and X.-r. Yan, "Analysis and verification on the chain-like model with normal distribution of magnetorheological elastomer," *Chinese Journal of Chemical Physics,* vol. 22, pp. 545-550, 2009.

[122] X. Guan, X. Dong, and J. Ou, "Predicting performance of polymer-bonded Terfenol-D composites under different magnetic fields," *Journal of Magnetism and Magnetic Materials,* vol. 321, pp. 2742-2748, 2009.

[123] P. Melenev, Y. Raikher, G. Stepanov, V. Rusakov, and L. Polygalova, "Modeling of the field-induced plasticity of soft magnetic elastomers," *Journal of Intelligent Material Systems and Structures,* p. 1045389X11403819, 2011.

[124] K. Danas, S. Kankanala, and N. Triantafyllidis, "Experiments and modeling of iron-particle-filled magnetorheological elastomers," *Journal of the Mechanics and Physics of Solids,* vol. 60, pp. 120-138, 2012.

[125] E. Galipeau and P. P. Castañeda, "A finite-strain constitutive model for magnetorheological elastomers: magnetic torques and fiber rotations," *Journal of the Mechanics and Physics of Solids,* vol. 61, pp. 1065-1090, 2013.

[126] J. Wu, X. Gong, Y. Fan, and H. Xia, "Anisotropic polyurethane magnetorheological elastomer prepared through in situ polycondensation under a magnetic field," *Smart Materials and Structures,* vol. 19, p. 105007, 2010.

[127] O. Padalka, H. Song, N. Wereley, J. Filer II, and R. Bell, "Stiffness and damping in Fe, Co, and Ni nanowire-based magnetorheological elastomeric composites," *IEEE Transactions on Magnetics,* vol. 46, pp. 2275-2277, 2010.

[128] S. Demchuk and V. Kuz'min, "Viscoelastic properties of magnetorheological elastomers in the regime of dynamic deformation," *Journal of Engineering Physics and Thermophysics*, vol. 75, pp. 396-400, 2002.

[129] S. Abramchuk, D. Grishin, E. Y. Kramarenko, G. Stepanov, and A. Khokhlov, "Effect of a homogeneous magnetic field on the mechanical behavior of soft magnetic elastomers under compression," *Polymer Science Series A*, vol. 48, pp. 138-145, 2006.

[130] Y. Wang, Y. Hu, L. Chen, X. Gong, W. Jiang, P. Zhang, *et al.*, "Effects of rubber/magnetic particle interactions on the performance of magnetorheological elastomers," *Polymer Testing*, vol. 25, pp. 262-267, 2006.

[131] L. Meunier, G. Chagnon, D. Favier, L. Orgéas, and P. Vacher, "Mechanical experimental characterisation and numerical modelling of an unfilled silicone rubber," *Polymer Testing*, vol. 27, pp. 765-777, 2008.

[132] N. Kchit, P. Lancon, and G. Bossis, "Thermoresistance and giant magnetoresistance of magnetorheological elastomers," *Journal of Physics D: Applied Physics*, vol. 42, p. 105506, 2009.

[133] N. Kchit and G. Bossis, "Electrical resistivity mechanism in magnetorheological elastomer," *Journal of Physics D: Applied Physics*, vol. 42, p. 105505, 2009.

[134] J.-H. Koo, F. Khan, D.-D. Jang, and H.-J. Jung, "Dynamic characterization and modeling of magneto-rheological elastomers under compressive loadings," *Smart Materials and Structures*, vol. 19, p. 117002, 2010.

[135] W. Zhang, X.-l. Gong, T.-l. Sun, Y.-c. Fan, and W.-q. Jiang, "Effect of cyclic deformation on magnetorheological elastomers," *Chinese Journal of Chemical Physics*, vol. 23, pp. 226-230, 2010.

[136] W. Zhang, X. Gong, W. Jiang, and Y. Fan, "Investigation of the durability of anisotropic magnetorheological elastomers based on mixed rubber," *Smart Materials and Structures*, vol. 19, p. 085008, 2010.

[137] L. Chen and S. Jerrams, "A rheological model of the dynamic behavior of magnetorheological elastomers," *Journal of Applied Physics*, vol. 110, p. 013513, 2011.

[138] X. Gong, G. Liao, and S. Xuan, "Full-field deformation of magnetorheological elastomer under uniform magnetic field," *Applied Physics Letters*, vol. 100, p. 211909, 2012.

[139] F. Gordaninejad, X. Wang, and P. Mysore, "Behavior of thick magnetorheological elastomers," *Journal of Intelligent Material Systems and Structures*, vol. 23, pp. 1033-1039, 2012.

[140] J.-H. Koo, A. Dawson, and H.-J. Jung, "Characterization of actuation properties of magnetorheological elastomers with embedded hard magnetic particles," *Journal of Intelligent Material Systems and Structures*, vol. 23, pp. 1049-1054, 2012.

[141] B. Ju, M. Yu, J. Fu, Q. Yang, X. Liu, and X. Zheng, "A novel porous magnetorheological elastomer: preparation and evaluation," *Smart Materials and Structures*, vol. 21, p. 035001, 2012.

[142] S.-H. Eem, H.-J. Jung, and J.-H. Koo, "Modeling of magneto-rheological elastomers for harmonic shear deformation," *IEEE Transactions on Magnetics*, vol. 48, pp. 3080-3083, 2012.

[143] X. Qiao, X. Lu, W. Li, J. Chen, X. Gong, T. Yang, *et al.*, "Microstructure and magnetorheological properties of the thermoplastic magnetorheological elastomer composites containing modified carbonyl iron particles and poly (styrene-b-ethylene-ethylenepropylene-b-styrene) matrix," *Smart Materials and Structures*, vol. 21, p. 115028, 2012.

[144] W. Li and M. Nakano, "Fabrication and characterization of PDMS based magnetorheological elastomers," *Smart Materials and Structures*, vol. 22, p. 055035, 2013.

[145] C. Collette, G. Kroll, G. Saive, V. Guillemier, and M. Avraam, "On magnetorheologic elastomers for vibration isolation, damping and stress reduction in mass-varying structures," *Journal of intelligent material systems and structures*, 2010.

[146] H. Deng and X. Gong, "Adaptive tuned vibration absorber based on magnetorheological elastomer," *Journal of intelligent material systems and structures*, vol. 18, pp. 1205-1210, 2007.

[147] H.-x. Deng and X.-l. Gong, "Application of magnetorheological elastomer to vibration absorber," *Communications in nonlinear science and numerical simulation*, vol. 13, pp. 1938-1947, 2008.

[148] A. A. Lerner and K. A. Cunefare, "Performance of MRE-based vibration absorbers," *Journal of Intelligent Material Systems and Structures,* 2007.

[149] X. Gong, J. Li, and L. Chen, "Study on a dynamic stiffness-tuning absorber with squeeze-strain enhanced magnetorheological elastomer," *Journal of Intelligent Material Systems and Structures,* 2009.

[150] X. Zhang and W. Li, "Adaptive tuned dynamic vibration absorbers working with MR elastomers," *Smart Structures and Systems,* vol. 5, pp. 517-529, 2009.

[151] Z. Xu, X. Gong, G. Liao, and X. Chen, "An active-damping-compensated magnetorheological elastomer adaptive tuned vibration absorber," *Journal of Intelligent Material Systems and Structures,* 2010.

[152] G. Liao, X. Gong, C. Kang, and S. Xuan, "The design of an active–adaptive tuned vibration absorber based on magnetorheological elastomer and its vibration attenuation performance," *Smart materials and structures,* vol. 20, p. 075015, 2011.

[153] Y.-K. Kim, J.-H. Koo, K.-S. Kim, and S. Kim, "Developing a real time controlled adaptive MRE-based tunable vibration absorber system for a linear cryogenic cooler," in *Advanced Intelligent Mechatronics (AIM), 2011 IEEE/ASME International Conference on*, 2011, pp. 287-290.

[154] R. Sinko, M. Karnes, J.-H. Koo, Y.-K. Kim, and K.-S. Kim, "Design and test of an adaptive vibration absorber based on magnetorheological elastomers and a hybrid electromagnet," *Journal of Intelligent Material Systems and Structures,* p. 1045389X12463461, 2012.

[155] S. Sun, Y. Chen, J. Yang, T. Tian, H. Deng, W. Li, *et al.*, "The development of an adaptive tuned magnetorheological elastomer absorber working in squeeze mode," *Smart Materials and Structures,* vol. 23, p. 075009, 2014.

[156] W. Li, K. Kostidis, X. Zhang, and Y. Zhou, "Development of a force sensor working with MR elastomers," in *2009 IEEE/ASME International Conference on Advanced Intelligent Mechatronics*, 2009, pp. 233-238.

[157] M. Yu and S. Wang, "The composite MRE embedded with a copper coil," *Smart Materials and structures,* vol. 19, p. 065023, 2010.

[158] H. Böse, R. Rabindranath, and J. Ehrlich, "Soft magnetorheological elastomers as new actuators for valves," *Journal of Intelligent Material Systems and Structures,* p. 1045389X11433498, 2012.

[159] B. Kavlicoglu, B. Wallis, H. Sahin, and Y. Liu, "Magnetorheological elastomer mount for shock and vibration isolation," in *SPIE Smart Structures and Materials+ Nondestructive Evaluation and Health Monitoring*, 2011, pp. 79770Y-79770Y-7.

[160] S. Kashima, F. Miyasaka, and K. Hirata, "Novel soft actuator using magnetorheological elastomer," *IEEE Transactions on Magnetics*, vol. 48, pp. 1649-1652, 2012.

[161] J. Li, Y. Li, W. Li, and B. Samali, "Development of adaptive seismic isolators for ultimate seismic protection of civil structures," in *SPIE Smart Structures and Materials+ Nondestructive Evaluation and Health Monitoring*, 2013, pp. 86920H-86920H-12.

[162] J. Fu, M. Yu, X. Dong, and L. Zhu, "Magnetorheological elastomer and its application on impact buffer," in *Journal of Physics: Conference Series*, 2013, p. 012032.

[163] X. Gong, X. Zhang, and P. Zhang, "Fabrication and characterization of isotropic magnetorheological elastomers," *Polymer testing*, vol. 24, pp. 669-676, 2005.

[164] X. Zhang and W. Li, "Adaptive tuned dynamic vibration absorbers working with MR elastomers," 2009.

[165] S. Opie and W. Yim, "Design and control of a real-time variable modulus vibration isolator," *Journal of Intelligent Material Systems and Structures*, p. 1045389X10389204, 2010.

[166] S.-H. Eem, H.-J. Jung, and J.-H. Koo, "Application of MR elastomers for improving seismic protection of base-isolated structures," *IEEE Transactions on Magnetics*, vol. 47, pp. 2901-2904, 2011.

[167] Y.-K. Kim, H.-I. Bae, J.-H. Koo, K.-S. Kim, and S. Kim, "Note: Real time control of a tunable vibration absorber based on magnetorheological elastomer for suppressing tonal vibrations," *Review of Scientific Instruments*, vol. 83, p. 046108, 2012.

[168] Z. Ying and Y. Ni, "Micro-vibration response of a stochastically excited sandwich beam with a magnetorheological elastomer core and mass," *Smart Materials and Structures*, vol. 18, p. 095005, 2009.

[169] B. Nayak, S. Dwivedy, and K. Murthy, "Multi-frequency excitation of magnetorheological elastomer-based sandwich beam with conductive skins," *International Journal of Non-Linear Mechanics,* vol. 47, pp. 448-460, 2012.

[170] K.-x. Wei, G. Meng, W.-m. Zhang, and S.-s. Zhu, "Experimental investigation on vibration characteristics of sandwich beams with magnetorheological elastomers cores," *Journal of Central South University of Technology,* vol. 15, pp. 239-242, 2008.

[171] G. Zhou and Q. Wang, "Magnetorheological elastomer-based smart sandwich beams with nonconductive skins," *Smart Materials and Structures,* vol. 14, p. 1001, 2005.

[172] G. Zhou and Q. Wang, "Study on the adjustable rigidity of magnetorheological-elastomer-based sandwich beams," *Smart materials and structures,* vol. 15, p. 59, 2005.

[173] G. Zhou and Q. Wang, "Use of magnetorheological elastomer in an adaptive sandwich beam with conductive skins. Part II: Dynamic properties," *International journal of Solids and Structures,* vol. 43, pp. 5403-5420, 2006.

[174] G. Zhou, K. Lin, and Q. Wang, "Finite element studies on field-dependent rigidities of sandwich beams with magnetorheological elastomer cores," *Smart materials and structures,* vol. 15, p. 787, 2006.

[175] S. Dwivedy, N. Mahendra, and K. Sahu, "Parametric instability regions of a soft and magnetorheological elastomer cored sandwich beam," *Journal of Sound and Vibration,* vol. 325, pp. 686-704, 2009.

[176] W. Choi, Y. Xiong, and R. Shenoi, "Vibration characteristics of sandwich beams with steel skins and magnetorheological elastomer cores," *Advances in Structural Engineering,* vol. 13, pp. 837-847, 2010.

[177] V. Lara-Prieto, R. Parkin, M. Jackson, V. Silberschmidt, and K. Zbigniew, "Vibration characteristics of MR cantilever sandwich beams: experimental study," *Smart Materials and structures,* vol. 19, p. 015005, 2009.

[178] D. Miedzinska, A. Boczkowska, and K. Zubko, "Numerical verification of three point bending experiment of magnetorheological elastomer (MRE) in magnetic field," in *Journal of Physics: Conference Series,* 2010, p. 012158.

[179] B. Nayak, S. Dwivedy, and K. Murthy, "Dynamic analysis of magnetorheological elastomer-based sandwich beam with conductive skins

under various boundary conditions," *Journal of Sound and Vibration*, vol. 330, pp. 1837-1859, 2011.

[180] J. Ginder, S. Clark, W. Schlotter, and M. Nichols, "Magnetostrictive phenomena in magnetorheological elastomers," *International Journal of Modern Physics B*, vol. 16, pp. 2412-2418, 2002.

[181] H.-J. Jung, S.-J. Lee, D.-D. Jang, I.-H. Kim, J.-H. Koo, and F. Khan, "Dynamic characterization of magneto-rheological elastomers in shear mode," *IEEE transactions on magnetics*, vol. 45, pp. 3930-3933, 2009.

[182] W. Li, G. Yao, G. Chen, S. Yeo, and F. Yap, "Testing and steady state modeling of a linear MR damper under sinusoidal loading," *Smart Materials and Structures*, vol. 9, p. 95, 2000.

[183] G. M. Kamath and N. M. Wereley, "A nonlinear viscoelastic-plastic model for electrorheological fluids," *Smart Materials and Structures*, vol. 6, p. 351, 1997.

[184] T. Long, S. Elliot, and M. Brennan, "Semi-active control using tunable vibration absorbers," in *INTER-NOISE and NOISE-CON Congress and Conference Proceedings*, 1995, pp. 709-712.

[185] A. Douay and N. Hagood, "Evaluation of optimal variable stiffness feedback control authority, stability, feasibility and implementability," in *Proceedings of Fourth International Conference on Adaptive Structures*, 1993.

[186] W. Li, X. Zhang, and H. Du, "Development and simulation evaluation of a magnetorheological elastomer isolator for seat vibration control," *Journal of Intelligent Material Systems and Structures*, p. 1045389X11435431, 2012.

[187] E. M. Lui, "Seismic Isolation for Earthquake Resistant Structures," *Journal of Structural Engineering*, vol. 127, pp. 1117-1118, 2001.

[188] J. Ramallo, E. Johnson, and B. Spencer Jr, "“Smart” base isolation systems," *Journal of Engineering Mechanics*, vol. 128, pp. 1088-1099, 2002.

[189] T. A. Morgan, *The use of innovative base isolation systems to achieve complex seismic performance objectives*: ProQuest, 2007.

[190] J. N. Yang and A. K. Agrawal, "Semi-active hybrid control systems for nonlinear buildings against near-field earthquakes," *Engineering Structures*, vol. 24, pp. 271-280, 2002.

[191] N. Wongprasert and M. Symans, "Experimental evaluation of adaptive elastomeric base-isolated structures using variable-orifice fluid dampers," *Journal of Structural Engineering,* vol. 131, pp. 867-877, 2005.

[192] P.-Y. Lin, P. Roschke, and C. Loh, "Hybrid base‐isolation with magnetorheological damper and fuzzy control," *Structural Control and Health Monitoring,* vol. 14, pp. 384-405, 2007.

[193] L.-Y. Lu and G.-L. Lin, "Fuzzy friction controllers for semi-active seismic isolation systems," *Journal of Intelligent Material Systems and Structures,* 2009.

[194] J. M. Kelly, "The role of damping in seismic isolation," *Earthquake engineering & structural dynamics,* vol. 28, pp. 3-20, 1999.

[195] I.-H. Hwang, J.-H. Lim, and J.-S. Lee, "A study on base isolation performance of magneto-sensitive rubbers," *Journal of the Earthquake Engineering Society of Korea,* vol. 10, pp. 77-84, 2006.

[196] M. Usman, S. Sung, D. Jang, H. Jung, and J. Koo, "Numerical investigation of smart base isolation system employing MR elastomer," in *Journal of Physics: Conference Series*, 2009, p. 012099.

[197] Y. Li and J. Li, "A highly adjustable base isolator utilizing magnetorheological elastomer: experimental testing and modeling," *Journal of Vibration and Acoustics,* vol. 137, p. 011009, 2015.

[198] Y. Yu, Y. Li, and J. Li, "Parameter identification of a new hysteretic model for magnetorheological elastomer base isolator using modified artificial fish swarm algorithm," *Proc. ISARC 2014 (Sydney)*, pp. 176-83, 2014.

[199] W. Holt, "Behavior of rubber under repeated stresses," *Rubber Chemistry and Technology,* vol. 5, pp. 79-89, 1932.

[200] L. Mullins, "Effect of stretching on the properties of rubber," *Rubber Chemistry and Technology,* vol. 21, pp. 281-300, 1948.

[201] L. Mullins and N. Tobin, "Theoretical model for the elastic behavior of filler-reinforced vulcanized rubbers," *Rubber Chemistry and Technology,* vol. 30, pp. 555-571, 1957.

[202] F. Bueche, "Molecular basis for the Mullins effect," *Journal of Applied Polymer Science,* vol. 4, pp. 107-114, 1960.

[203] D. Besdo and J. Ihlemann, "Properties of rubberlike materials under large deformations explained by self-organizing linkage patterns," *International Journal of Plasticity,* vol. 19, pp. 1001-1018, 2003.

[204] R. Sues, S. Mau, and Y.-K. Wen, "Systems identification of degrading hysteretic restoring forces," *Journal of engineering mechanics,* vol. 114, pp. 833-846, 1988.

[205] W. H. Robinson, "Lead‐rubber hysteretic bearings suitable for protecting structures during earthquakes," *Earthquake Engineering & Structural Dynamics,* vol. 10, pp. 593-604, 1982.

[206] K. Fuller, J. Gough, T. Pond, and H. Ahmadi, "High damping natural rubber seismic isolators," *Journal of Structural Control,* vol. 4, pp. 19-40, 1997.

[207] R. S. Mills, "Model Tests on Earthquake Simulators: Development and implementation of experimental procedures," 1979.

[208] R. S. Subramaniam, A. M. Reinhorn, M. A. Riley, and S. Nagarajaiah, "Hybrid control of structures using fuzzy logic," *Computer‐Aided Civil and Infrastructure Engineering,* vol. 11, pp. 1-17, 1996.

[209] L. Zhou, C.-C. Chang, and B. Spencer, "Intelligent technology-based control of motion and vibration using MR dampers," *Earthquake Engineering and Engineering Vibration,* vol. 1, pp. 100-110, 2002.

[210] H. Li, X. Sun, L. Wu, and H. Lam, "State and output feedback control of interval type-2 fuzzy systems with mismatched membership functions," *Fuzzy Systems, IEEE Transactions on,* vol. 23, pp. 1943-1957, 2015.

[211] Y. Li and J. Li, "Finite element design and analysis of adaptive base isolator utilizing laminated multiple magnetorheological elastomer layers," *Journal of Intelligent Material Systems and Structures,* p. 1045389X15580654, 2015.

[212] S. Sun, X. Deng, J. Yang, W. Li, H. Du, G. Alici, M. Nakano, "An adaptive tuned vibration absorber based on multilayered MR elastomers," Smart Materials and Structures, 24, 045045, 2015.

PUBLICATIONS

1. **J. Yang,** S. Sun, T. Tian, W. Li, H. Du, G. Alici, *et al*., "Development of a novel multi-layer MRE isolator for suppression of building vibrations under seismic events," Mechanical Systems and Signal Processing, vol. 70, pp. 811-820, 2016.

2. **J. Yang,** S.S. Sun, H, Du, W. H. Li, G, Alici, H. X. Deng, A novel magnetorheological elastomer isolator with negative changing stiffness for vibration reduction, Smart Materials and Structures, 23, 105023, 2014.

3. **J. Yang,** H.P. Du, W.H. Li, Y.C. Li, J.C. Li, S.S. Sun, and H.X. Deng, Experimental study and modeling of a novel magnetorheological elastomer isolator, Smart Materials and Structures, 22, 117001-117015, 2013.

4. **J. Yang,** S.S. Sun, W. Li, H. Du,M, Nakano, Development of a linear damper working with MRSTF, Journal of Intelligent Material Systems and Structures, p. 1045389X15577653, 2015.

5. **J. Yang,** S. S Sun, H Du, G Alici, T Yan and W Li, Fabrication and characterization of magneto-rheological shear-stiffened elastomers, Frontiers in materials, vol. 1, p. 1-6, 2014.

6. S.S Sun, H Deng, **J Yang**, W Li, H Du, G Alici, Performance evaluation and comparison of MRE absorbers working in shear and squeeze modes, Journal of Intelligent Material Systems and Structures, p. 1045389X14568819, 2015.

7. S.S Sun, H Deng, H Du, W Li, **J Yang**, G Liu and G Alici, A Compact Variable Stiffness and Damping Shock Absorber for Vehicle Suspension, IEEE/ASME Transactions on Mechatronics, 2015.

8. S.S. Sun, H.X. Deng, W.H. Li, Y.Q. Ni, J. Zhang, H.P. Du, G. Alici, **J. Yang**, Improving the critical speeds of high-speed train using magnetorheological technology, Smart Materials and Structures, 22, 115012-115026, 2013. (Cover article, Featured article, Highlight)

9. S.S. Sun, Y. Chen, **J. Yang**, T. F. Tian, H. X. Deng, W. H. Li, H, Du, G, Alici, The development of an adaptive tuned magnetorheological elastomer absorber working in squeeze mode, Smart Materials and Structures, 23, 075009, 2014.

10. S.S. Sun, H.X. Deng, **J. Yang**, W.H. Li, H. Du, G. Alici, M, Nakano. An adaptive tuned vibration absorber based on multilayered MR elastomers," Smart Materials and Structures, vol. 24, p. 045045, 2015.

11. S.S. Sun, **J. Yang**, H.X. Deng, H. Du, W.H. Li, G. Alici, and M. Nakano, Horizontal Vibration Reduction of a Seat Suspension Using Negative Changing Stiffness Magnetorheological Elastomer Isolators, International journal of vehicle design, 68(1-3), 104-118, 2015.

12. S.S. Sun, **J. Yang**, W. Li, H. Deng, H. Du, G. Alici, Development of a novel variable stiffness and damping magnetorheological fluid damper, Smart Materials and Structures, 24, 085021, 2015.

13. S.S. Sun, **J. Yang**, W.H. Li, H.X. Deng, H. Du, G. Alici, "Development of an MRE adaptive tuned vibration absorber with self-sensing capability," Smart Materials and Structures, 24, 095012, 2015.

14. Nugroho, P. Wahyu., W. Li, H. Du, G. Alici & **J. Yang** (2014). An adaptive neuro fuzzy hybrid control strategy for a semiactive suspension with magneto rheological damper. Advances in Mechanical Engineering, 2014 1-11.

15. **Jian Yang**, S.S. Sun, Weihua Li, and Masami Nakano, Development of a Novel Multi-Layer MRE Isolator, Eleventh International Conference on Flow Dynamics, Sendai, Japan, 2014.

16. **Jian Yang**, Shuaishuai Sun, Weihua Li, Haiping Du, Gursel Alici, Study on magnetorheological shear-stiffened elastomers, ERMR2014, Spain, 2014. (Abstract)

17. **Jian Yang**, Shuaishuai Sun, Tongfei Tian, Weihua Li, and Masami Nakano, Building Protection from Earthquakes using Stiffness Softening MRE Isolators, Twelfth International Conference on Flow Dynamics, Sendai, Japan, 2015.

18. Shuaishuai Sun, **Jian Yang**, Haiping Du, and Weihua Li, Development of a Novel Variable Stiffness and Damping Shock Absorber for Vehicle Suspension Application, Twelfth International Conference on Flow Dynamics, Sendai, Japan, 2015.

19. Shuaishuai Sun, **Jian Yang**, Weihua Li, and Masami Nakano, Development of a Tuned Mass Damper Working with MR Elastomers, Twelfth International Conference on Flow Dynamics, Sendai, Japan, 2015.

20. Shuaishuai Sun, **Jian Yang**, Weihua Li, and Masami Nakano, Development of a Compact Variable Stiffness and Damping Isolator, Twelfth International Conference on Flow Dynamics, Sendai, Japan, 2015.